EXPLORING THE EFFECTS OF FIBER ANGLE AND STACKING SEQUENCE

ON THE STATIC STRENGTH AND ACOUSTIC EMISSION SIGNATURE

OF EPOXY-FIBERGLASS COMPOSITES IN MARINE ENVIRONMENTS

by

Jake Douglas Nunemaker

A thesis submitted in partial fulfillment
of the requirements for the degree

of

Master of Science

in

Mechanical Engineering

MONTANA STATE UNIVERSITY
Bozeman, Montana

January 2017

ACKNOWLEDGEMENTS

iii

TABLE OF CONTENTS

TABLE OF CONTENTS – CONTINUED

v

LIST OF TABLES

LIST OF FIGURES

LIST OF FIGURES – CONTINUED

LIST OF FIGURES – CONTINUED

NOMENCLATURE

W	Watts
Wh	Watt-hours
V	Volume
ϕ	Volume fraction
θ	Angle between fibers and loading direction
E	Young's modulus
G	Shear modulus
F	Strength
m	Mass
ρ	Density
ν	Poisson's ratio
J	Diffusive flux
D	Diffusivity
C	Concentration
M	Moisture content
NDT	Non-destructive testing
NDI	Non-destructive inspection
S_0	Zero order symmetric wave node
A_0	Zero order anti-symmetric wave node

Subscripts

c	Composite
f	Fiber
m	Matrix
i	Initial
∞	Maximum saturation
1,2,3	Natural material axes: 1 – longitudinal to fiber, 2,3 – transverse to fiber
x,y,z	Axes of the coordinate system
t	Tensile

ABSTRACT

Marine Hydro-Kinetic (MHK) devices encompass promising new technologies designed to harness energy from ocean currents and tides. However, there are unique challenges to successful implementation of MHK devices. Material selection and characterization are crucial steps in the design process as the marine environment can be extremely detrimental to many materials systems. Epoxy-fiberglass composites, the premier material in wind turbine blades are being studied for use in MHK due to desirable price and durability. Preliminary research has shown a significant drop in ultimate strength due to moisture absorption in unidirectional laminates. This research extends these studies by exploring these effects on balanced and unbalanced off-axis fiber angles for a common epoxy-fiberglass material system. Ply by ply analysis is completed to explore the efficacy of a strength reduction prediction method for off-axis laminates. It also extends the study to include acoustic emission analysis to further investigate the material degradation at a micromechanical level. Partial saturation strength reduction in symmetric laminates is also studied.

INTRODUCTION

Marine Hydro-Kinetic Energy

In the last few decades, the production of energy has become an important topic. Fossil fuels provided past societies with an abundance of energy. However, with increasing energy usage and the downsides of fossil fuels becoming more evident, scientists and engineers have begun to look elsewhere for energy production. The goal of "green energy" is to decrease pollution and create more renewable methods of energy production. These more environmentally conscious production methods include wind turbines, nuclear power, solar and hydro-kinetic power. Each one of these systems brought a tremendous amount of technology to support them. While green energy has made significant progress in recent years, there are still many challenges to overcome as well. These technologies frequently have key downsides too; nuclear reactor meltdowns, effects on wildlife populations and inconsistency in power generation are a few examples.

Of these new energies, hydro kinetic energy is one of the oldest. Greek civilizations began using water wheels to grind flour over 2000 years ago. This practice remained prevalent throughout history. The modern hydro turbine was first conceived in the mid-1700s by Forest de Belidor, a French military engineer. Hydroelectric power plants were first put into practice in the 1920s by the US Army Corps of Engineers. Throughout the 20th century, an expansion of hydroelectric power began long before other green energies came to fruition. Although an old practice, river based hydroelectric power hasn't been without its faults. Environmentally, it can be very taxing on the river system if managed incorrectly and has a significant effect on fish population and their spawning patterns.

However, in the last 10 – 15 years, a new vision for water driven electricity was born. Instead of using an entire river, engineers have looked towards the thousands of miles of coastline and predictable tidal wave patterns. This new type of energy has been given the moniker Marine Hydro-Kinetic Energy (MHK).

Figure 1. Areas near US coasts that possess high velocity ocean currents where energy extraction devices could be installed[1].

MHK offers tremendous possible energy production due to the amount of coastal area available to harness energy from. Approximately 50% of the population lives near the coast as well minimizing the distance the energy needs to be transported. With an abundance of accessible area, it will also be significantly easier to mitigate the environmental impacts seen in river based power plants.

Within the development of MHK technology, four different sub-types have been targeted for extraction: wave, tidal streams, ocean currents and ocean thermal gradients.

---

[1] US Water Power Program.

Each of these include unique design considerations and installation locations. Differentiation between these different energy potentials can be subtle. It is important to define some terminology to be able to tell the difference between these techniques. A wave is the movement of the surface of the water, or what is seen crashing against the beach. Tide is the rise and fall of large bodies of water caused by the gravitational pull of the moon. Ocean currents comprise of large masses of water that move in one direction. These currents are caused by discrepancies in the density or temperature of water over a large distance.
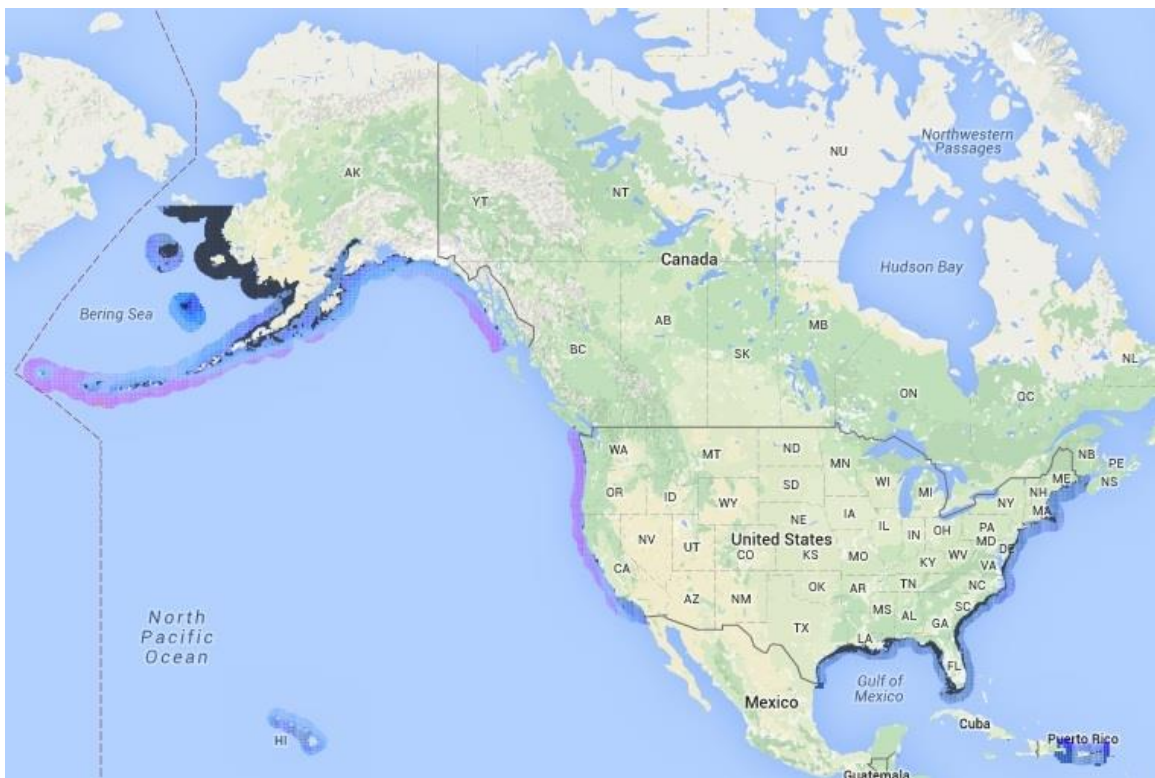
Figure 2. Areas of high wave activity where extraction devices could be installed to produce electricity for US homes[2].

---

[2] US Water Power Program.

The U.S. Water Power Program, through the Department of Energy has compiled research on the potential power from these different types of extraction [1]. In the context of renewable energy, power is how much energy is being produced at an instant, measured in Watts (W). However, as these types of production are inconsistent, it becomes more useful to talk about the amount of energy produced over a period of time. This is measured in a watt-hour (Wh), or the equivalent to one Watt of energy production for one hour. This provides a better unit to compare renewable energy sources as they are not always producing the same amount of power. Solar panels only produce energy while the sun is shining on them, and rivers produce differing amounts of energy based on the flow rate of the river. Listing these extraction methods by the amount of energy produced by year is a common way to compare the different methods. In Table 1, technical energy production metrics are presented for various types of marine hydro-kinetic devices.

Table 1. Technical resource potential for different MHK energy extraction methods.

Resource	Technical Resource Potential
Waves	898 – 1229 TWh/year
Tidal Streams	222 – 334 TWh/year
Ocean Currents	45 – 163 TWh/year[3]

The technical resource potential for these devices represents a portion of the theoretical energy in the system. These numbers exclude other constraints such as economic, environmental and regulatory considerations that are difficult to speculate on. As the industry evolves, these other factors and their effects on the resource potential will need to be evaluated further. According to the Department of Energy, approximately 90,000 average homes in the United States could be powered with 1 TWh/year [1]. As seen above,

---

[3] TWh = 10^12 Wh/year

Marine Hydrokinetic Energy (MHK) offers a great potential for renewable energy. Even considering the excluded factors conservatively, these energy sources have the capability of providing clean energy to millions of homes across the country. With predictable and continuous tidal patterns, MHK can also provide more consistent power output than the more variable wind and solar energies.

MHK is promising due to the amount of coastline available to harness tidal energy. As these systems are designed, it becomes paramount to have accurate mechanical strength values for the materials being used in construction. Similar to the wind energy industry, the most common material studied for MHK applications are fiberglass-epoxy composites. Offering good strength and stiffness values for the cost, it follows naturally to study these materials as a primary structural material for underwater turbines as well.

THEORETICAL BACKGROUND

<u>Composite Materials</u>

In the development of MHK systems, one of the prominent design constraints is the material they are made of. The saltwater environment and inconsistent loading presents a difficult application for many classes of materials. Corrosion properties become very important to consider as well as the structures must be submerged in saltwater for their entire design lifetimes. Another concern is weight of the structure as these systems need to be able to be suspended with ease underwater. One material that is frequently studied for these applications are composites.

Composite materials provide greater flexibility in design than other material types. Formed from two or more different constituent materials, it is possible to tailor the mechanical properties of the structure to specific loading directions, fatigue patterns, corrosive environments and other design criterion. Typically, these materials are made from reinforcements held together with a matrix material. One of the simplest examples of this composites is steel rebar reinforced concrete. The rebar provides stiffness and strength in the direction of the steel while the concrete holds them in place and oriented correctly while also providing compression strength. When multiple layers (plies) are included in the manufacture, different angles per ply can be chosen providing strength in multiple directions.
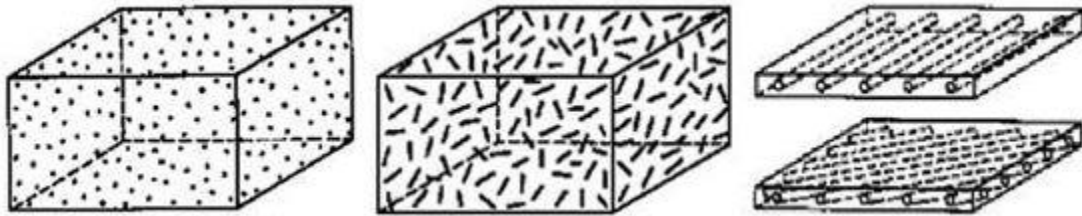
Figure 3. Examples of composite materials and varying reinforcement types. From left to right: particle reinforcements, short fibers, unidirectional fibers.

Epoxy Fiberglass Composites

This same concept has been applied in smaller applications as well. Since the 1930s glass manufacturers have known how to produce glass strands from a melt. As this process was refined the strands became more uniform and they began being used as reinforcements in composite materials. In the renewable energy industry, glass fiber reinforced composites are the most common material utilized in construction of wind turbine blades and other energy extraction devices. Glass fibers offer good stiffness and strength at a much cheaper cost than carbon fibers. These fibers are then arranged in various ways depending on their application.

In the manufacture of fiber composites, the fiber material typically comes in a woven mat to keep the individual fibers constrained. Structures that see most of their loads in one directions, most of the fibers might be aligned in one direction with a small amount of fibers being used to stitch these together to hold them in place. Fiber mats that are labeled as unidirectional frequently have as much as 8 – 10 % of their fibers oriented perpendicular to the principal orientation to hold the remaining fibers together during manufacture. This type of fiber architecture would technically classify as a "pseudo-unidirectional" but would commonly be considered unidirectional within the industry. In other applications, many

different loads are seen by the structure requiring there to be fibers aligned in multiple directions. In these applications, woven mats over fibers are commonly used. Mats that have two primary directions are called "biax" for two axes. Mats with three primary directions are given the moniker "triax" etc. Figure 4. An example of a woven mat. In this type of mat there are two principal directions (0° and 90°). The mat is woven with fiber tows which are made from many individual fibers. is an example of a biax woven mat as there are two primary directions of fibers.
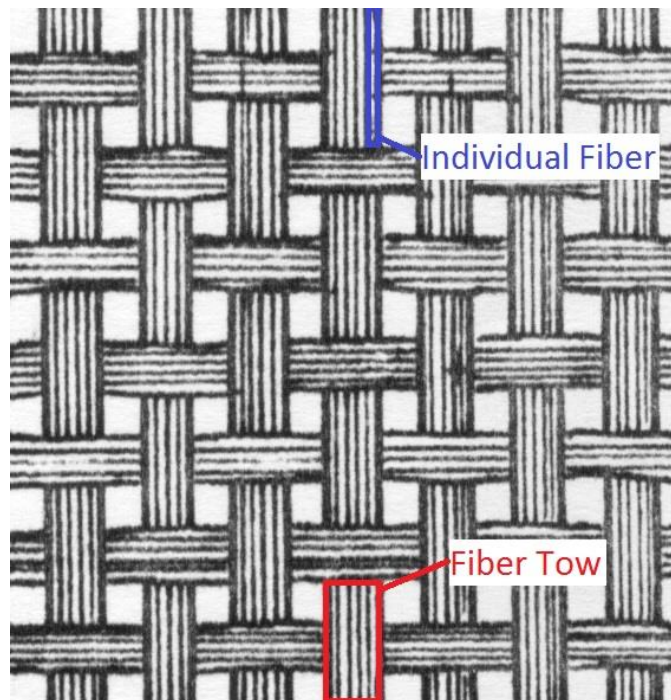
Figure 4. An example of a woven mat. In this type of mat there are two principal directions (0° and 90°). The mat is woven with fiber tows which are made from many individual fibers.

The other key constituent material in a composite system is the matrix. The matrix hold the fibers in the desired orientation and provided stability in compressive loading. There are several matrix materials that are common within the industry. In general, there are two classifications of matrix materials: thermosets and thermoplastics. Thermoplastic

materials have a curing process that is reversible as no chemical bonding takes place. Thermosets on the other hands, have two parts that chemically cross-link during the curing process. In general, thermoset resins produce a stronger material as a direct result of the cross-linking. One of the most frequently used and studied thermosets is epoxy resin systems. Epoxy offers a good bond to the fibers as well as increased fatigue life over other resin systems. However, this comes at a cost in MHK applications, epoxy resins are particularly susceptible to environmental effects and degrade faster than other resins.

<u>Composites Manufacturing</u>

The manufacture of composites is a complex operation with many different considerations. In composite manufacturing, it is important to get a good bond between the resin and the fiber and minimize the amount of resin used. One of the simplest methods of production is a hand layup. In this process, the fibers are manually oriented in the desired position and the resin is forced into the fiber mat by hand. Resin material is poured onto the fibers and rollers are used to press the resin into the fibers. While this method is the simplest and often the cheapest, it is very unreliable and has many problems associated with it. It is very difficult to get a consistent amount of resin throughout the material. This can manifest itself in an inconsistent thickness and adhesion between the matrix and the fibers. Another disadvantage is porosity; as the fibers are exposed to the air prior to manufacture, large air pockets are often present in the resultant material. These air pockets make the material much more prone to premature failure as it gives existing damage easy pathways to travel throughout the material and there is a decreased load transfer between the fiber and the matrix.

Another process more commonly used is resin transfer molding (RTM). In this method, resin is forced through the fibers driven by a positive pressure from the resin reservoir. This method produces much better composites than hand layups as the process of pressing the resin through the fibers can force most the air out of the material resulting in less porosity. Given an even flow across the material, it is also much easier to achieve a more consistent thickness and infusion. However, this process does nothing to minimize the thickness of the composite. As the fibers carry most of the longitudinal load, minimizing the amount of resin used significantly increases the strength of the overall material.

Vacuum assisted resin transfer molding (VARTM) is a variation of RTM that produces thinner and more consistent material through the introduction of a vacuum. Two ports are open on the mold prior to infusion. One of these is the inlet for resin material, the other a port for a vacuum to be applied. A heavy plastic is used to seal the fiber material to the mold and when the vacuum is applied, negative gage pressure pulls the fiber material against the mold creating less free space for the resin to fill. The vacuum also helps drive the flow of the resin through the material. This is one of the most common methods of producing composite materials as it results in a very consistent infusion while minimizing the resin that is used. The materials used for research presented later in this study were manufactured using the VARTM method. The Montana State University Composites Group has consistently used this manufacturing method over the last two decades to produce test samples. A diagram of the VARTM process with the different materials used in production can be seen below in Figure 5.
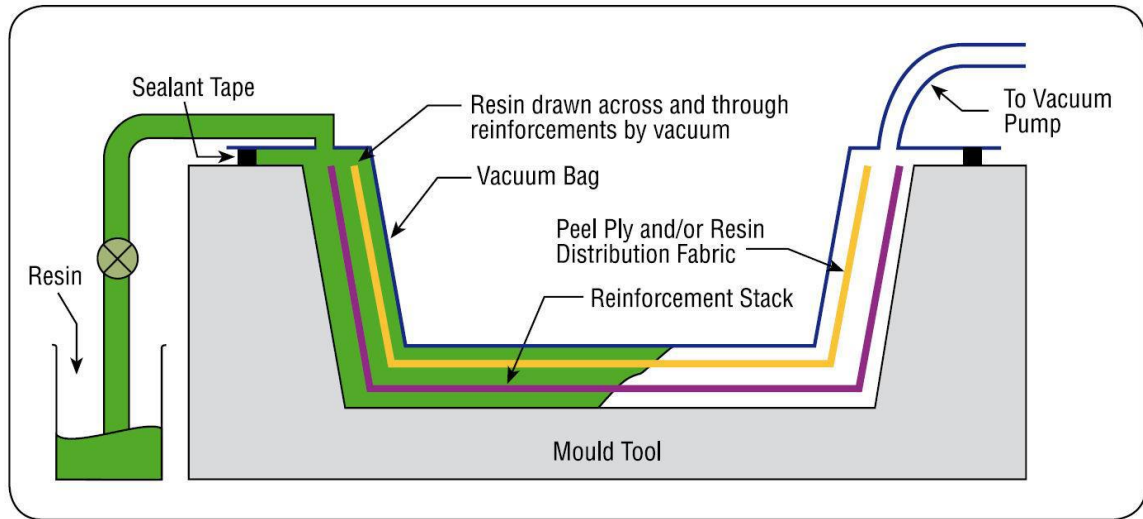
Figure 5. VARTM manufacturing process[4].

The VARTM process produces material with high volume fractions (ϕ_f), which in turn results in higher strengths. Fiber volume fraction is a measure of the volume of fibers relative to the overall volume of the material. It is calculated per equation 1 below, where V_c is the volume of the composite and V_f is the volume of the fibers.

$$\phi_f = \frac{V_f}{V_c} \tag{1}$$

In practice, measuring volume fraction is done by a matrix burn off. A sample of material is placed in an oven at a temperature where the resin will burn off but not the fibers. Using the densities of the two materials and the change in weight, an accurate measurement of volume fraction can be completed.

The direction in which resin is infused into the fibers is another advantage to the VARTM process. With a hand layup, the resin must be forced into the mat transverse to the fiber. This orientation is not conducive to flow and can cause significant porosity in the

---

[4] http://www.gurit.com/files/documents/vac-consv2pdf.pdf

composite. However, with VARTM, the infusion is parallel to the direction of the fibers. This results in significantly less air gets trapped behind the fibers producing less porosity and increasing the strength of the overall composite.

This method does present a problem when manufacturing samples that have plies in both the 0º and 90º orientation. A simple linear orientation of the two ports causes some layers to be infused transverse to their principal direction. In these cases, it is beneficial to use spiral tubing along two sides of the plate allowing resin to flow diagonally across the coupon. This drives flow in both directions, achieving a much more uniform volume fraction. It also helps avoid porosity on the backside of the 90º fibers.

Failure Mechanisms in Composites

The failure mechanisms in composites are difficult to study due to the complexity of the microstructure. The existence of multiple constituent materials allows for several different types of failures to exist within a composite material. Damage within the composite can occur in any of the constituent materials or at the interface between them. As the fibers are typically much stronger and stiffer than their surrounding material, the transfer of load between them and the matrix is very important. When these bonds begin to fail, the load must be transferred through other parts of material. It is common for composites to see significant damage within the microstructure long before final failure of the material occurs.
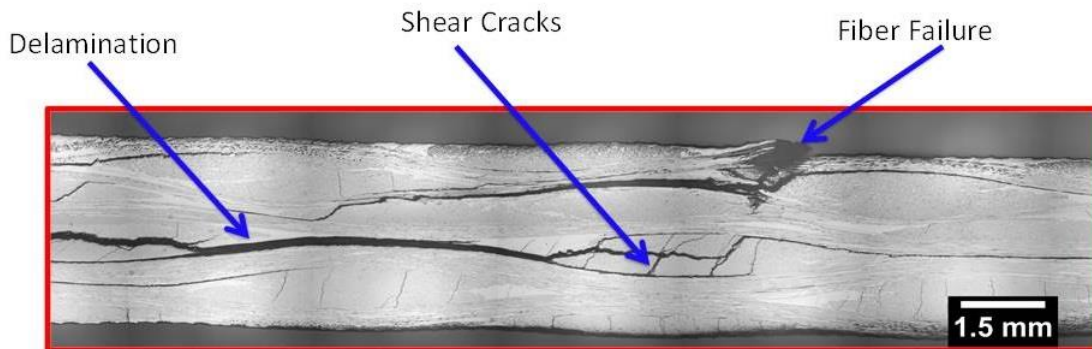
Figure 6. Examples of damage types seen within composites materials[5].

Failure mechanisms in composites have been studied and presented in recent literature. Research by Cantwell and Morton concluded that matrix and interphase failures occurred at lower stresses and strains than fiber failures [2]. These events exhibited release of fracture energy as well. Kim and Nairn added observations on interfacial debonding and fiber fracture for many different materials [3]. However, the research is far from having concrete theoretical models commonly seen in other material systems. One reason for this uncertainty is the amount of different material options available within the industry.

As mentioned above, one of the first damage mechanisms seen in testing is cracking of the matrix material. Thermoset resin systems are brittle in comparison to their thermoplastic counterparts. As they transfer the increased load from fiber tows, cracks will form in regions of high strain energy. These matrix cracks are low energy events and are typically seen throughout testing as load is continuously redistributed throughout the specimen. Individual matrix cracks are rarely catastrophic as the fibers inhibit a consistent

[5] Hart

crack path. The existence of large voids can provide matrix cracks with easy propagation paths.
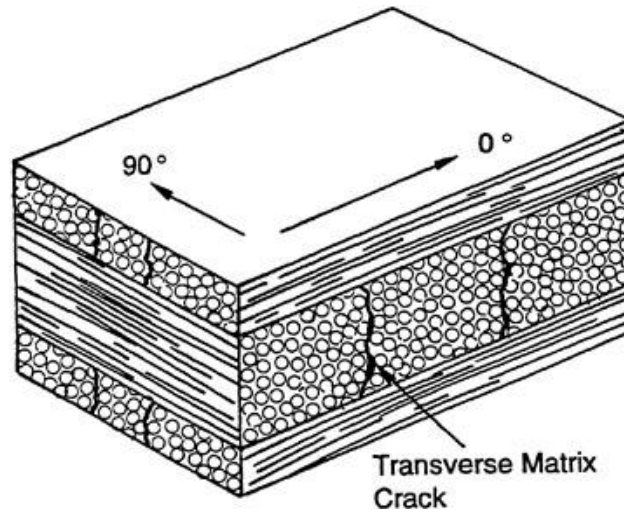
Figure 7. Matrix cracking in fiber reinforced composites. Note the tortuous pathway the crack takes through the fibers[6].

The bonds between fibers and the matrix are the primary pathway for the load to be distributed throughout the structure. As matrix cracks begin to degrade this interface, the load must be redistributed, further stressing the interface. There are two different interfacial failures that are typically seen, fiber/matrix pullout and fiber/matrix debond. Fiber/matrix pullout is a shear stress dominated failure that results in the fiber slipping along the matrix and shearing away from it. Fiber/matrix debond is a normal stress dominated interface failure resulting in the fiber being pulled away from the matrix normal to the interface.

---

[6] National Research Council
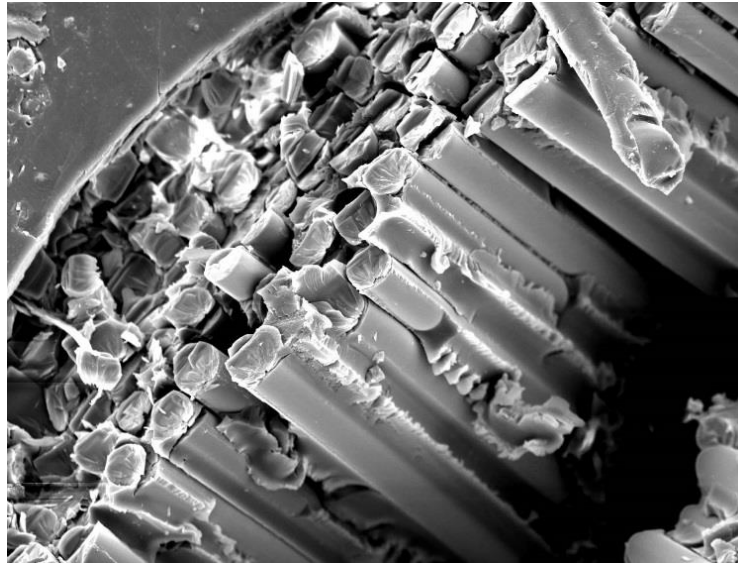
Figure 8. SEM image of fiber/matrix pullout failure surfaces[7].

Pullouts and debonds can occur at the same time depending on the specific loading conditions and many times the failure of the interface is a combination of the two. They are very difficult failures to differentiate and are often grouped into one category encompassing all interphase damage mechanisms. Post testing microscopic imaging shows very similar failure surfaces for both damage types. Fiber failure is much easier to identify as glass fibers are brittle and fail catastrophically when they are overloaded. This is not a common failure to see in the testing of composite materials as they are typically the strongest material within the material and the other constituents fail before the fibers reach their ultimate strength. Each of these types of damage exist at the microstructure level and contribute to the failure of the overall material. These mechanisms will be studied more in depth later in this study as they will be classified using acoustic emission analysis.

---

[7] John Summerscales
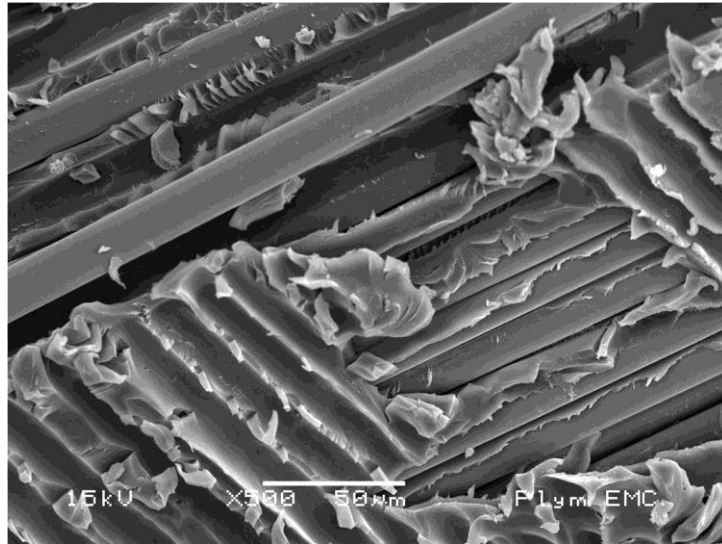
Figure 9. Debond failure between the fiber and matrix[8].

Diffusion

In order to study the possibilities of using composite materials in marine environments, it becomes important to understand the mechanics of diffusion in fiber reinforced polymers. Diffusion in its simplest form is the movement of molecules or atoms from a region of high concentration to a region of low concentration. This is a common phenomenon seen throughout daily life. When a drop of food coloring is added to a glass of water, the movement of the color molecules can be seen throughout the volume of water. The original drop of food coloring has a high concentration of color molecules while the water does not. Over time, they diffuse into the water towards a steady state or an equal concentration throughout the water.

[8] John Summerscales
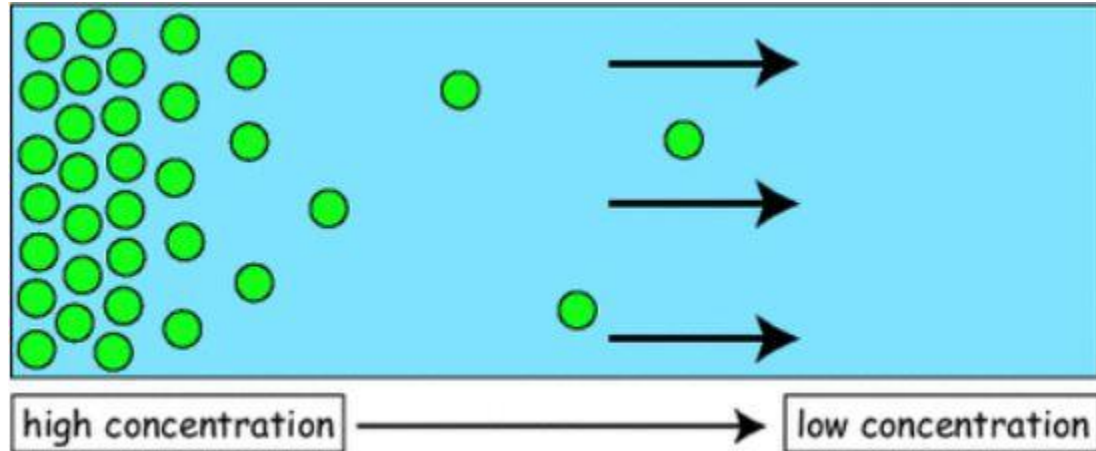
Figure 10. Diagram of simple diffusion. Over time the solution will approach a steady state where all molecules are equally spread out[9].

The study of diffusion in composite materials has an extra layer of complexity as each constituent material can possess different diffusion characteristics. For this specific study, the two constituent materials in question are the epoxy resin system and the fiberglass reinforcements. In other published literature, fiberglass has been found to absorb a negligible amount of moisture [4-6]. This greatly simplifies the analysis of the overall composite as the resin is the only constituent to evaluate in regards to water diffusion. It has been seen in other published literature that epoxy polymers follow similarly to diffusion in porous media [4].

This phenomenon has been studied extensively and is classified by a pair of laws developed by Adolf Fick in 1855. Fick was a German-born physician and physiologist that is most known for his contributions in diffusion modeling. He continued his study of movement of liquid in the field of medicine as he was the first person to measure cardiac output in 1870.

---

[9] Kyle Yeung

Fick's First Law

Before Fick's first law can be presented, a few terms must be explained. Flux (J) is the mathematical representation of how fast a material is diffusing; it can be thought of as the rate at which diffusion is occurring. Diffusivity (D) is a measure of how easily fluids can spread within a material. Materials with a lower diffusivity are more resistant to diffusion. For some materials, e.g. isotropic materials, the direction of travel isn't important in measuring how easily something can diffuse. However, this is not true with composites. Composites by default are not considered isotropic materials and therefore diffusivity changes depending on the direction in which flow is occurring. Concentration (C) is a measure of the amount of a material present at a specific location within the material.

Fick's first law relates these above terms. Specifically, it states that the diffusive flux is proportional to the diffusivity times the concentration gradient (spatial derivative of the concentration).

$$J_i = -D_{ij} \frac{\partial C}{\partial x_j} \tag{2}$$

Where:

J_i = The moisture flux term

D_{ij} = The mass diffusivity tensor

C = The moisture concentration

x_j = The spatial coordinate of interest

The above equation simplifies greatly when only one direction is considered. The mass diffusivity tensor is replaced by a single constant representing diffusivity in the direction desired and the concentration gradient becomes a single spatial derivative. The

inclusion of the off diagonal terms in the D_{ij} tensor complicates diffusion studies greatly and is frequently neglected. An example of one dimensional diffusion can be seen above in Figure 10.

Fick's Second Law

Fick's second law follows as a natural extension from his first. Through a combination of his first law and the conservation of mass it relates how the concentration of the diffusing substance changes with time. The concentration of mass states that the concentration of the diffusing substance must change by the same amount of substance that is entering the control volume. This is represented mathematically below:

$$\frac{\partial C}{\partial t} + \frac{\partial}{\partial x_i} J_i = 0 \tag{3}$$

Combining this Fick's first law as an expression for J_i, the following equality can be achieved:

$$\frac{\partial C}{\partial t} = \frac{\partial}{\partial x_i}\left(D_{ij}\frac{\partial C}{\partial x_j}\right) \tag{4}$$

A partial differential equation, 1st order in time and 2nd order in time, this equation relates the change in concentration in time to the change in concentration across space through the diffusivity tensor described above. For a homogenous material with off diagonal diffusivity terms ignored, this can be reduced to:

$$\frac{\partial C}{\partial t} = D_{ii}\frac{\partial^2 C}{\partial x_i^2} \tag{5}$$

1-Dimensional Solution

For the research presented in this paper, it was decided to simplify the above equations and consider diffusion in the analysis of the composite coupons as one

dimensional. The primary factor for this decision is the eventual application that these materials will see. The design and construction of MHK devices has followed that of wind turbine blades. These structures are typically made with a light core on the inside surrounded with composite material for added strength and stiffness. An example of this can be seen below in Figure 11.
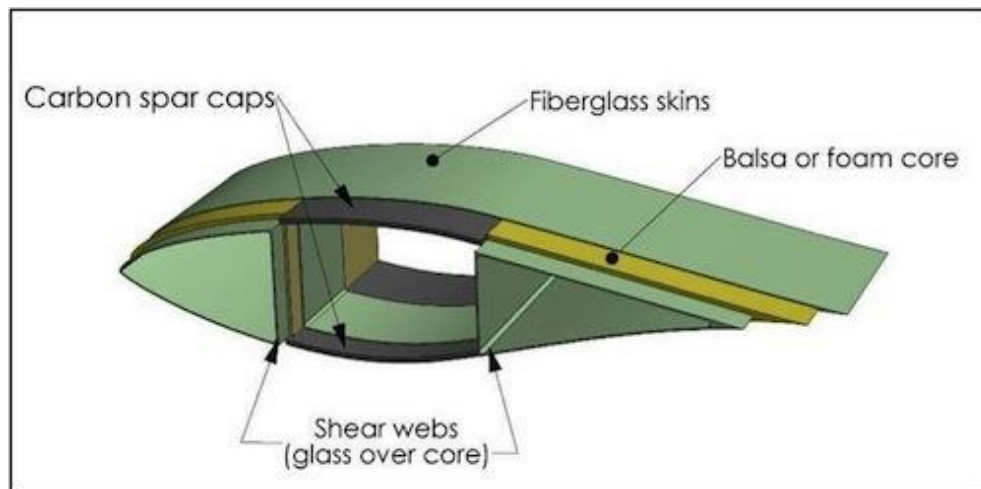
Figure 11. Cut away of a wind turbine blade. The construction method seen above is extremely common in the wind industry and it is likely that MHK construction will follow similar patterns.

Assuming a similar construction method for MHK energy extraction devices, diffusion will be primarily in one direction as there will be large "flat" surfaces exposed to the water protecting the inner structure of the blade. A more detailed diagram with this assumption can be seen below in Figure 12.
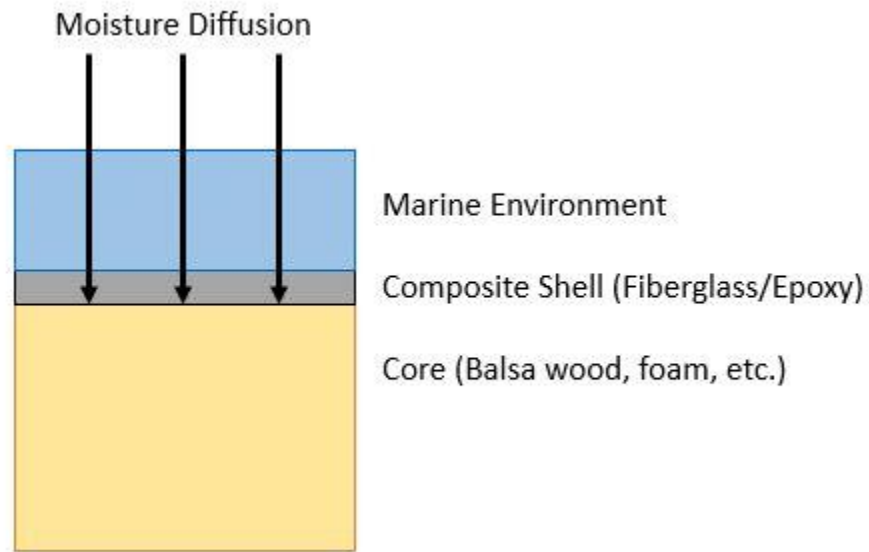
Figure 12. Stacking sequence involved in composite structure construction and the moisture penetration path.

With the assumption of 1-dimensional diffusion behavior, it becomes trivial to solve equation 5 above for concentration with respect to time. This allows a generalized curve for concentration to be plotted. The moisture curve presented below in Figure 13 will be utilized throughout the rest of this study. Periodic weight gain measurements were taken for conditioned samples to verify that the material behaved as expressed in Figure 13.
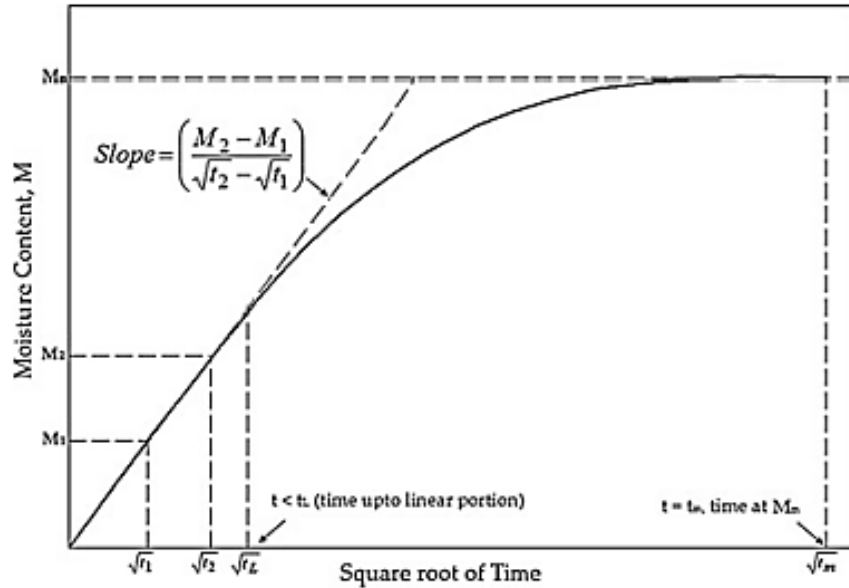
Figure 13. Generalized moisture curve for Fickian diffusion in 1-dimension.

In this application, concentration is analogous to moisture content. Moisture content is a measure of how much liquid (water in the case of MHK structure) has been diffused into the structure. It is a comparison of the weight of the conditioned composite to the weight of the dry composite and is calculated as follows:

$$M(t) = \frac{m_t - m_i}{m_i} \tag{6}$$

For the assumption of 1-dimensional diffusion to remain valid the coupons had to be designed to mimic this behavior. This will be covered in more detail later in the experimental procedures section.

Diffusion in Composites

While the 1-dimension solution of Equation 5 can be used for composite materials, the lack of homogeneity adds complexity to the analysis. As discussed above fiberglass and epoxy have very different diffusion properties. In practice, the fiberglass has a negligible maximum moisture content ($M_{\infty f}$) while studies have shown that most epoxy resin systems

will absorb up between 2.5 – 3% moisture. This is denoted by $M_{\infty m}$. As these materials are combined, the material properties of the composite must be calculated rather than using the individual constituent properties. The theoretical maximum moisture content of the composite ($M_{\infty c}$) can be calculated as follows:

$$M_{\infty c} = \phi_m M_{\infty m} \frac{\rho_m}{\rho_c} \tag{7}$$

where ϕ_m represents the matrix volume fraction. ρ_m and ρ_c are the densities of the matrix and composite respectively. The density of the composite can be calculated from the constituent densities as follows:

$$\rho_c = \rho_f \phi_f + \rho_m \phi_m \tag{8}$$

Using the above equations, the theoretical maximum moisture content of the coupon can be calculated and compared to the experimental values. Good agreement in the two moisture contents are seen throughout the research presented later.

<u>Strength Reduction</u>

The absorption of water into the material structure is detrimental to the strength of the material. This phenomenon has been shown several times in published literature and in past research conducted at MSU[5, 7]. The research presented is an extension of previous research and will attempt to classify these strength reductions further with the addition of new analysis techniques.

The complexity of composite materials is not limited to the diffusion. The stiffness and strength are governed by large sets of tabular equations. These equations consider fiber orientation and thickness per ply to calculate a total stiffness and strength in the global

coordinate system. In the simplest form, this material property tensor is reduced to 5 independent material properties. At its most complicated in a reasonable application, a fully anisotropic solid, there may be as many as 21 independent constants.

Previous research for diffusion has focused on simple cases, where all the fibers are aligned in one or two directions (usually 0 or 90 degrees to maintain another layer of simplicity). The failure mechanisms that show up in 0 degree coupons are much different than the ones present in 90 degree coupons. While valuable research, there is little information for other ply angles or combinations of ply angles. As it is expected that the inclusion of the water effects only a handful of these failure mechanisms, the effects of moisture absorptions should vary depending on the construction of the sample. Examples of the strength reduction in unidirectional composites can be seen below in Figure 14 and Figure 15 research was conducted at MSU and provided a starting point for the work presented herein.
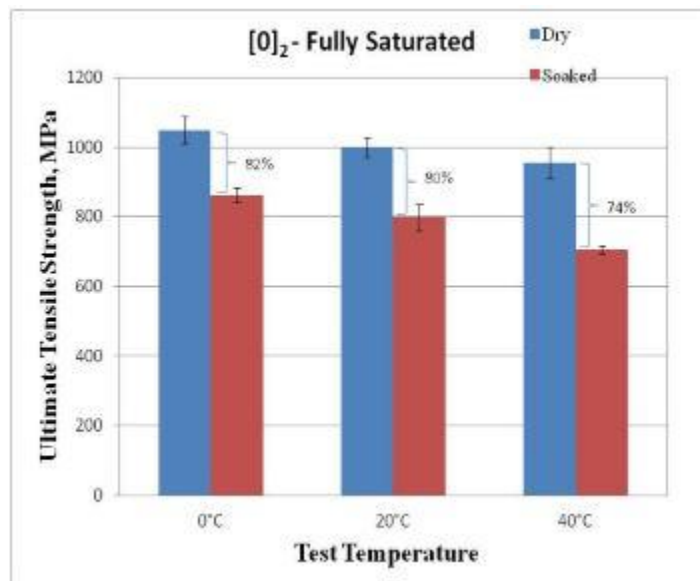
Figure 14. Fully saturated epoxy tensile sample with 0.86 % Wt. Gain, $V_f = 0.56$, Cured at 70C and soaked at 40C. [8]
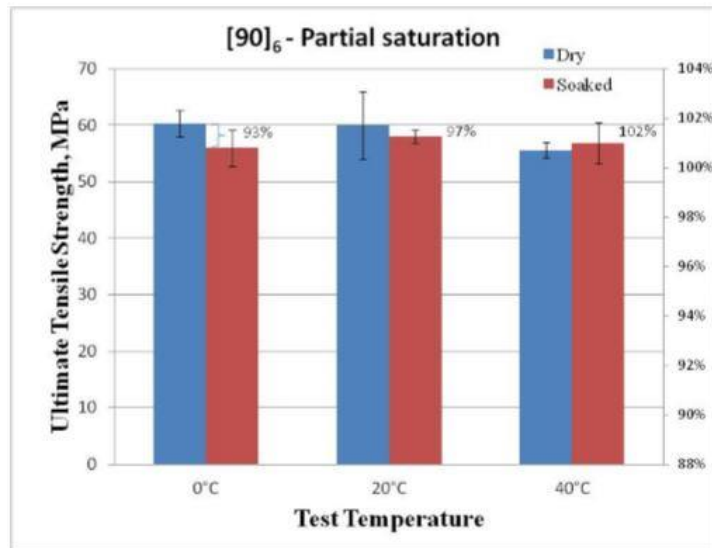
Figure 15. Partially saturated epoxy sample with 0.47 % Wt. Gain, V_f = 0.56, Cured at 70C and soaked at 40C.

Two different studies will be presented in this research. Both attempt to provide some insight into how moisture absorption degrades the overall material. As discussed above, the different failure mechanisms seen within composites are dependent on the internal stress state of the material. Changing the layup can significantly alter the internal stress states making certain damage mechanisms more prevalent than others.

Effects of Fiber Angle and Moisture Diffusion

The first half of the study will focus on the effects of diffusion on the static strength and acoustic emission signatures given different fiber angles. Six different layups were chosen to study as they provided a broad spectrum of internal stress states to analyze. Specifically, unbalanced off-axis and balanced antisymmetric laminates were studied.

In a unidirectional off-axis composite (fibers are primarily aligned in one direction) the stress distribution and thus the failure mechanisms are generally uniform throughout

the thickness of the sample. However, as the angle between the principal load and the orientation of the fibers changes, the internal stress state seen in the material changes considerably. With the fibers aligned along the axis of principal load (0°), the load is primarily carried in the fibers as they are in their optimal orientation and can provide their full strength. This contrasts with samples with only 90 degree fibers. The fibers provide very little strength to the overall composite as they are oriented perpendicular to the principal load. In this case, the limiting factor becomes how well the fibers are bonded to the matrix as the failure occurs when one the two are pulled apart.

When the fiber angle is varied between 0° and 90°, the stress state becomes much more complicated as the stiffness of the coupon does not align with either principal axes of the load. In this case, the bonds between the fiber and matrix are subjected to a combination of tension and shear. The amount of each type of stress changes throughout the range of angles, reaching a maximum shear at 45°.

In a balanced coupon, there are an equal number of plies with the opposite angle as that of the positive angle. For example, in a 2 ply balanced coupon there would be one +X and one –X ply, denoted by [±X]. Samples with this construction provide a unique stress state as well. The net stiffness of the sample is in the primary direction of the load (0°) but the individual plies have increased stiffness in different direction. There is a significant amount of shear stress present between the two plies as each one wants to rotate against the other one. As the angle X is increased, the amount of shear is increased and the amount of tension being carried by the fibers is decreased.

Effects of Stacking Sequence and Moisture Diffusion

The second study that will be presented varies stacking sequence and studies the effects of partial moisture saturation on static strength. Under the assumption of Fickian diffusion, the concentration of water is variable within the sample during the soaking process. This phenomenon was studied analytically in research completed by Stoffels [7]. The result of this study, a cross section showing variable moisture content, can be seen below in Figure 16. The extension of this conclusion is that the strength reduction of the material will be variable when the sample is not fully saturated.
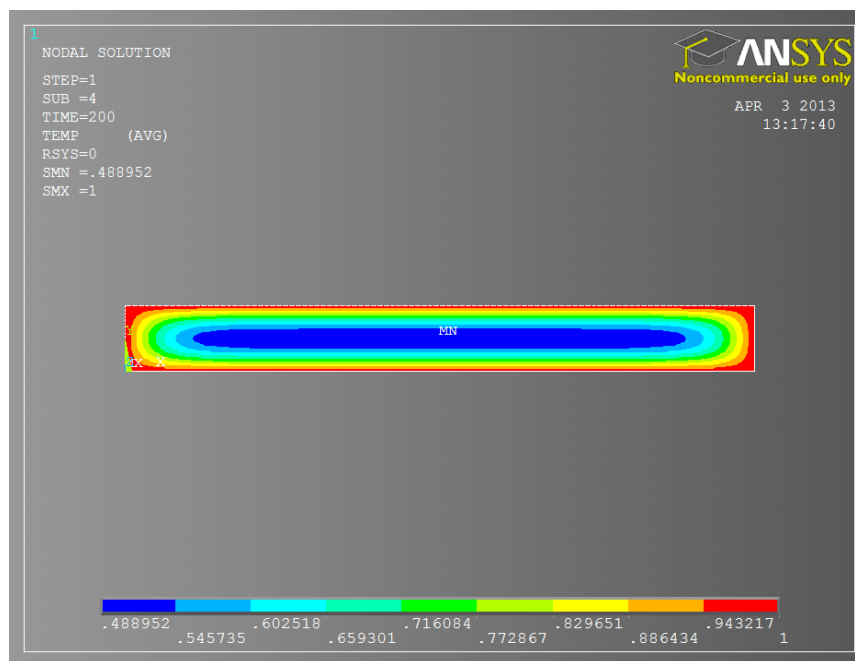
Figure 16. Saturation profile throughout the two-dimensional cross section at time = 200 hours. Note: minimum saturation ratio value of 0.488952.

As discussed above, 0° and 90° plies have very different properties when subjected to tensile loads. When these two fiber angles are combined and tested in a static tensile test, the 0° plies carry most the load while the 90° plies provide lateral stiffness. It follows that

when tested in a static tensile test, the moisture effects on the 0º plies are more important to the integrity of the overall material.

Combining these two concepts, it is then assumed that the stacking sequence of the sample is pertinent to the strength throughout the saturation process. In a traditional design scenario, plies with high longitudinal stiffness are placed on the outside of the material to maximize flexural stiffness. In the design of MHK systems, these plies would be the first subjected to moisture effects possibly negating the advantages of increased flexural stiffness. Looking specifically at an unconditioned 4-ply layup consisting of two 0º and two 90º plies, the position of the plies does not affect the tensile strength. Assuming an equal distribution of water, the different stacking sequences would have identical tensile strengths at full saturations as well. However, the difference in these two layups becomes important when there is a partial saturation within the coupon. As there is a concentration gradient between the two surfaces, each ply will have a different amount of moisture within it. As most of the strength is from the 0º plies, the samples with the 0º plies on the inside will degrade much slower than those with the 0º plies on the outside.

<u>Acoustic Emission Testing</u>

Non-destructive testing (NDT) and non-destructive inspection (NDI) cover many technologies that are finding new applications in academic settings and already see wide acceptance in industry. These technologies allow the user to analyze the material in question without altering the overall structure. There are several industries that rely on these techniques for design and inspection of their products. NDI is utilized regularly in the aircraft industry during routine inspections. Cracks in primary structure can be

discovered through the skin panels allowing for faster inspections into hard to reach areas. NDI techniques are also utilized during testing, providing unique insight into how the material is failing. These techniques are typically considered a subsection of NDT labeled as 'in-situ" analysis. Acoustic Emission (AE) analysis is one of these methods and was used during all mechanical tests presented throughout this research.

<u>Wave Theory</u>

To understand the analysis methods of AE testing, it is necessary to understand the fundamentals of elastic wave release and propagation. As a structure is loaded, energy is being stored within the system. As the fibers and matrix are strained, the amount of energy increases until failure occurs. In brittle materials, microstructure failure typically occurs very fast and results in catastrophic failure for the entire structure. In contrast, epoxy fiberglass materials can build up significant damage at the microstructure level without resulting in catastrophic failure due to the complexity of the material system. Each of the failure mechanisms outlined above can contribute to this. As these failures occur, the load is transferred to other parts of the structure away from the damage. This resettling of load occurs incredibly fast and results in an elastic wave being propagated throughout the material.

Elastic wave theory has been studied extensively throughout literature. In 1917 Lamb successfully decomposed the wave equation into components applicable to plate geometry [9]. For a zero-order Lamb wave these two components denote the symmetric (S_0) and anti-symmetric wave (A_0) modes. They are more commonly referred to as the extensional and flexural wave modes. Extensional wave modes are those that expand and

contract the plate symmetrically across the mid-plane of the plate. Flexural wave modes displace the material asymmetrically perpendicular to the direction of the wave. Examples of these two wave modes can be seen in Figure 17.
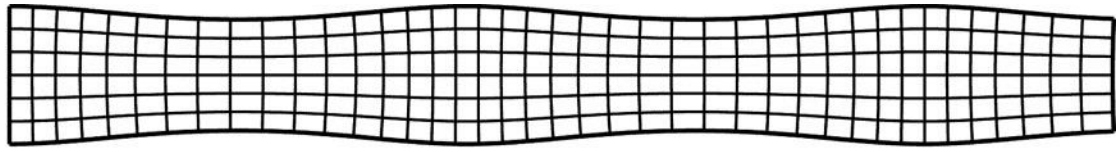
(a) S_0-mode
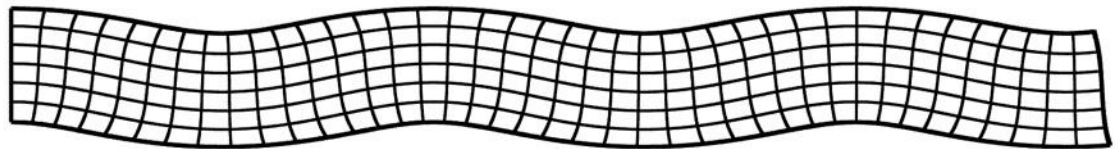
(b) A_0-mode

Figure 17. Distinct wave modes for a zero-order lamb wave. S0 and A0 represent the extensional and flexural modes respectively.

However, the above solutions describe wave modes of a homogenous, infinite plate, one of the simplest forms to analyze. As these equations are then applied to composite materials, many added complexities need to be considered. First off, composite materials are inherently not homogenous as they are made of multiple constituent materials. As the waves that are released during damage propagate through the material, they are met with boundaries where one material ends and one material starts. The two different materials can have differing wave propagation properties which can significantly alter the waveform as it crosses the boundary. The boundaries can also provide a reflective quality as the wave must pass from one material to the next resulting in smaller reflections within the material [10]. The reflections seen from material mismatch complicate the wave analysis

significantly as the reflections can interfere with the initial signal. The AE timing parameters that will be discussed later are used in attempt to limit the amount of reflections recorded by the sensors.

Lamb's equations also assume an infinite plate for their development. In real world applications, it is not feasible to test an infinite plate. Experimental limits require that test specimens have an edge to them which further deviates from Lamb's initial theories. These edges of the test specimens also create boundaries for the initial elastic wave to reflect off [11].

Wave Speed

Wave propagation within composite materials very difficult to fully define analytically. However, a few assumptions can be made which significantly simplify the analysis. The first assumption made in this research is that the material can be described as a homogeneous orthotropic material. This is an assumption classically used throughout composites research where orthotropic material properties are derived using laminate plate theory. Laminate plate theory, presented by Barbero [12] uses ply by ply equations to derive a global stiffness matrix for the overall material. The material can then be treated as if it was homogenous with the material properties calculated.

This is especially useful for AE wave speed calculations as it has been shown that the extensional and flexural wave speeds are proportional to the tensile and bending stiffness of the material, respectively. These equations can be seen below.

$$c_e = \sqrt{\frac{A_{11}}{\rho h}} \tag{9}$$

$$c_f = \sqrt[4]{\frac{D_{11}}{\rho h}} * \sqrt{\omega} \qquad (10)$$

Where ρ represents material density, h is the thickness and ω is the frequency of the wave [13]. Analyzing the above equations, it can be noted that the extensional wave speed is not dependent on the frequency, also known as non-dispersive. The flexural wave speed is dispersive and is proportional to the square root of the frequency. The increased root of the flexural wave generally dictates that the flexural wave has a slower wave speed. A typical waveform with the two signals is shown below in Figure 18.
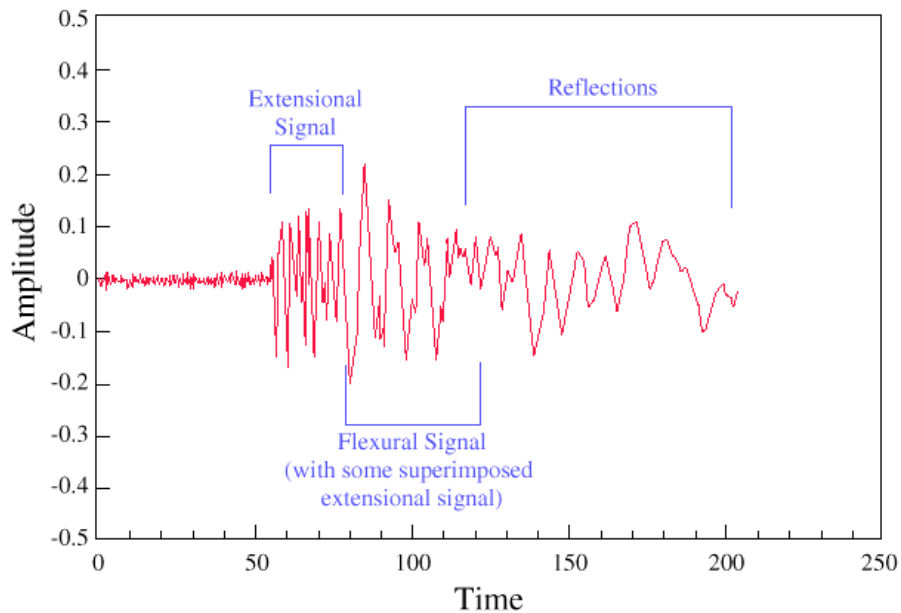
Figure 18. A typical AE signal with both an extensional and flexural component. Reflections caused by material boundaries can be seen at the end of the signal.

The above figure is important for AE analysis as it is important to differentiate between the two types of signals in the classification of damage mechanisms. Current AE research tends to focus on the extensional signal as the indicator of the type of damage, due

to its non-dispersive nature. There is a possibility that both signals may be of importance to the classification of damage but this research will not be covered within this paper.

<u>Acoustic Emission Hardware</u>

Understanding the hardware and its limitations is integral to the success of Acoustic Emission testing. As the signals are extremely complex and varied, different hardware setups are often required to maintain quality data. This is evidenced in the wide variety of sensors that are available for purchase and implementation. In general, the hardware of an AE system can be broken into two parts: sensors and recorder.

AE sensors are manufactured to maintain clear signal acquisition while also protecting the sensitive piezoelectric crystal from wear or damage. Typically, these sensors come encased in a metal jacket to protect the sensitive pieces. A wear plate typically constructed with a hard ceramic is used in direct contact with the piezoelectric crystal. A typical configuration can be seen below in Figure 19.
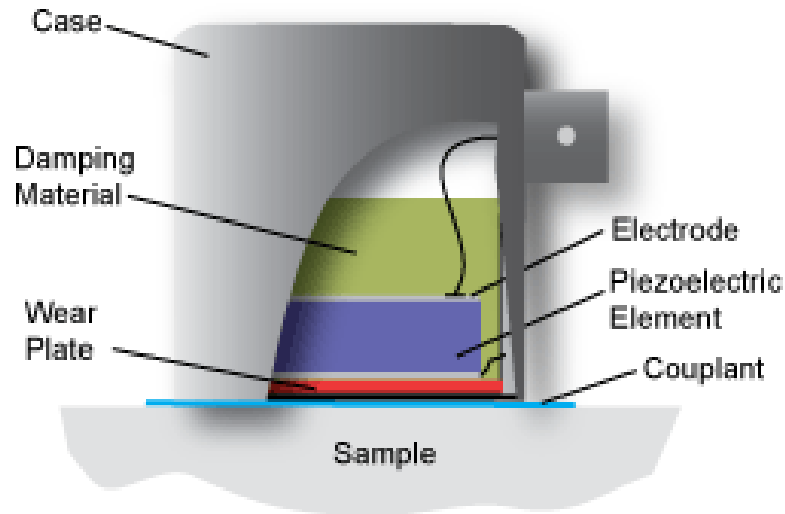
Figure 19. Standard AE sensor utilizing piezoelectric data acquisition[10].

While most sensors are constructed as above, the sensitivity of the piezoelectric crystal can be tailored for many different applications. Typically, sensors that house only one crystal are specifically tuned for a certain frequency range that is expected to be prevalent. The increased sensitivity at a specific range is useful for applications where only certain frequencies are expected or only certain frequencies are important. However, in the investigatory manner that AE sensors are used in for composites, a wideband sensor is often more applicable. Wideband sensors have less sensitivity at specific ranges but have a more consistent range of frequencies they are sensitive to. The downside of wideband sensors is that the crystals are smaller so the sensitivity is decreased. Choosing the correct sensor for a given application is a difficult process and often the use of multiple different sensors can provide the highest quality of data. The sensitivity diagrams for the sensors used in this study can be seen in Appendix A.

---

[10] https://www.nde-ed.org

The second piece of hardware pertinent to AE testing is the PCI board responsible for interpreting the signal and storing it. The PCI board can be a limiting factor depending on the sampling frequency available as it is necessary to record according to the Nyquist rate. Typical AE signals have a broad range and can reach frequencies of 1 MHz. For epoxy fiberglass composites, it has been seen in past research that fiber breakage events can result in frequencies above 400 kHz [14-16].

Peak Frequency Analysis

There have been many methods presented throughout literature that attempt at classifying damage based on different AE metrics. These metrics can be derived from both the time and frequency domain of the signal. Time based AE metrics are those that are derived or calculated directly from the voltage-time output of the sensor. Frequency based metrics are calculated through post processing methods to dissect the time signal into its respective frequency components. The research presented in this paper will focus on the frequency based AE metrics. The simplest method for frequency analysis is the Fast Fourier Transform (FFT).

As the released elastic wave travels throughout the material it will reflect off material boundaries and the edges of the sample. The reflections can constructively and destructively interfere with the initial elastic wave complicating the signal that is received by the AE sensor. FFT analysis of the waveform can help to dissect the waveform into components to determine which components are the more important. An example of FFT decomposition can be seen below in Figure 20 and Figure 21.
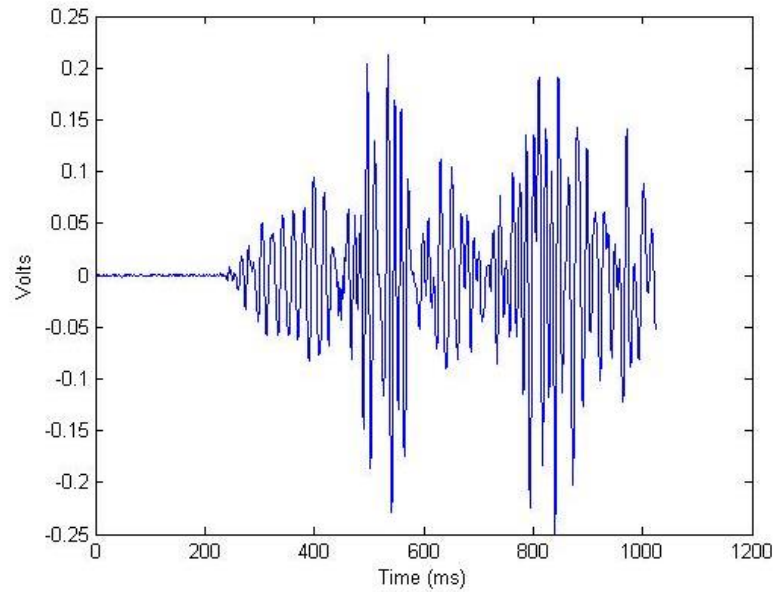
Figure 20. A representative AE signal in the time domain.
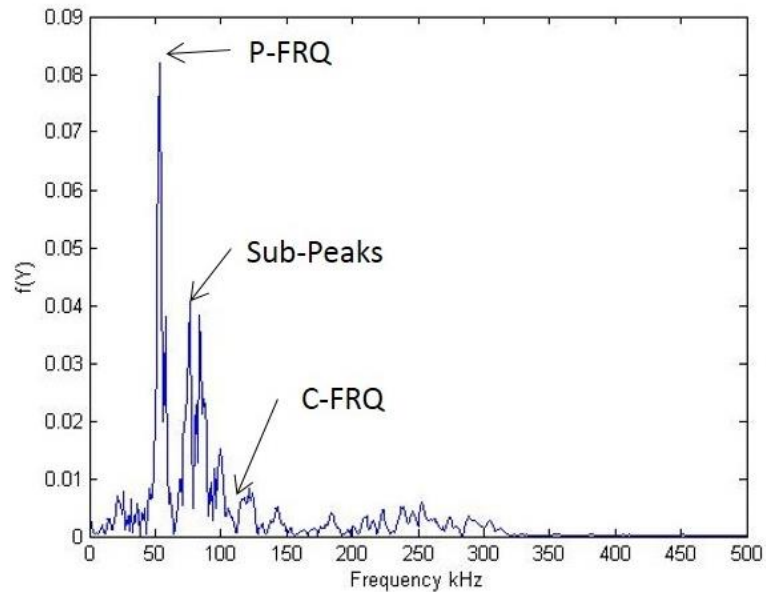
Figure 21. An AE signal decomposed using an FFT analysis. The FFT analysis shows which frequencies are most prevalent in the underlying signal. The Peak Frequency (P-FRQ) can then be used to classify the waveform.

One of the current methods for identifying and classifying damage in a material is

through the analysis of the peak frequency of a signal. The individual signals are analyzed

with a FFT to decompose the wave into its respective frequencies and their intensity. The strongest frequency is then labeled as the peak frequency, and is used to describe the "damage event."

Peak frequency has been studied extensively in past literature. Early on within AE testing on composite materials, researchers noted that a relatively small number of "bands" of frequencies would be present within the test results. Some of the early researchers studying peak frequency in fiberglass/epoxy composites include Suzuki, deGroot, Ramirez-Jimenez and Bohse. These researchers used a combination of materials and inspection methods to classify specific damage mechanisms to specific [14-17]. Their work provided the basis for Michael Schuster in which he developed a set of discrete frequency bins typically seen in the material systems studied at MSU [18]. His summary and visualization of their work can be seen below in Figure 22.
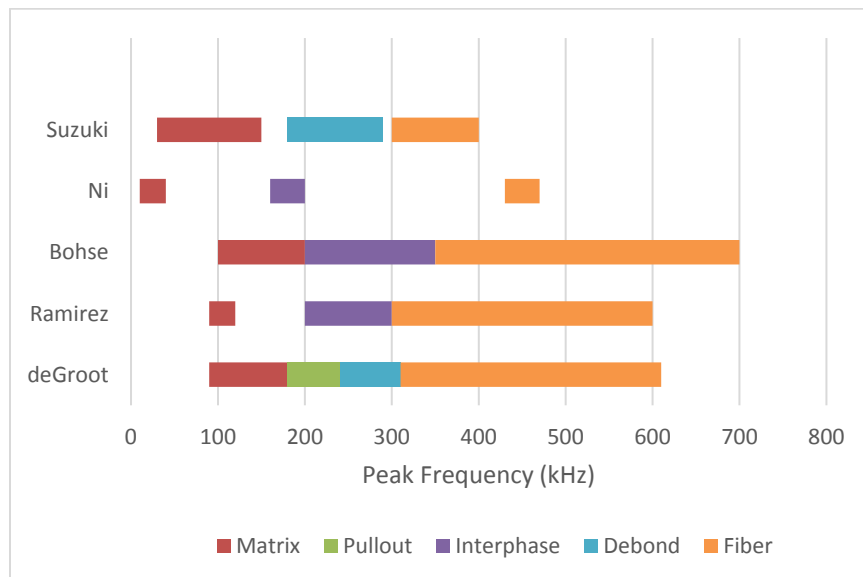
Figure 22. A summary of prior research in peak frequency analysis for fiberglass/epoxy composites.

Utilizing the above research as well as observations during his own research on the specific material studied at MSU, Schuster came up with the following discrete bins which will be used in this research as well. Events that fall into the 50 – 120 kHz range will be classified as matrix cracking. Interphase damage types will be split into two ranges, 120 – 180 kHz representing fiber/matrix pullout while 180 – 300 kHz will represent fiber/matrix debond. Events with a peak frequency greater than 300 kHz will be classified as a fiber failure. Peak frequency analysis with a combination of dry and soaked samples will provide insight into the effects of moisture absorption on the failure mechanisms on composites.

The goal has always been to correlate these common frequencies to specific damage mechanisms within the material, often at the microstructure level. Attempts at developing an all-encompassing set of frequencies has been frivolous. The discrete bins that these frequencies can be grouped into changes based on fiber architecture, fiber type, lay-up, stacking sequence, etc. There are an immense number of variables in the study of AE signatures for composite materials which has stymied researchers in the quest for one answer. New methods are emerging utilizing Artificial Neural Networks (ANN) to cluster data by automated methods. They often result in complicated clustering techniques that are difficult to complete in real time and provide very little information as to what type of damage is occurring. They also require an immense computing power and time to be complete. These ANN's can differentiate the data to a level a human researcher doesn't have the capability, they also see changes as the material structure changes. Ultimately, it doesn't appear that ANN's have any advantage in developing one set of rules over simpler analysis methods such as peak frequency.

EXPERIMENTAL PROCEDURES

Coupon Manufacture

All test specimens used in this research were manufactured by the Montana State University Composites Research Group. The research completed by this group has helped maintain the MSU/SNL/DOE database for the last 25 years. This database is meant to provide designers with research quality testing data for a variety of conditions and materials. The materials studied are specific to the renewable energy industry and wind energy developers.

Vacuum Assisted Resin Transfer Molding

Test specimens were manufactured using vacuum assisted resin transfer molding (VARTM). The VARTM process requires a significant amount of setup and sacrificial material but produces consistently high quality test coupons. Research presented in this work was manufactured using material studied extensively throughout the database, providing an extensive amount of data to compare to. Layups were chosen to help study the effects of water submersion at different thicknesses and fiber angles. The two fiber systems discussed below are very similar. Unfortunately, Vectorply changed the fiber weight of their E-LT system in the middle of the research. However, the change was minimal and assumed negligible.

To produce static tensile coupons, a large rectangular plate was produced on an aluminum mold and individual coupons were cut from the plate. The mold used measured 36" by 24" and was made from 1/2" aluminum. Two 3/16" ports were drilled through the

mold at the locations shown below in Figure 23. The mold was conditioned with Loctite 770-NC Frekote mold release to make the process of removing the plate easier. The process for applying the mold release can be seen on the manufacturer specifications sheet in Appendix A. The two ports were installed with shark tooth quick connection fittings to easily connect to the plastic injection tubing. One of these ports was connected to the reservoir of resin and the other to the vacuum.
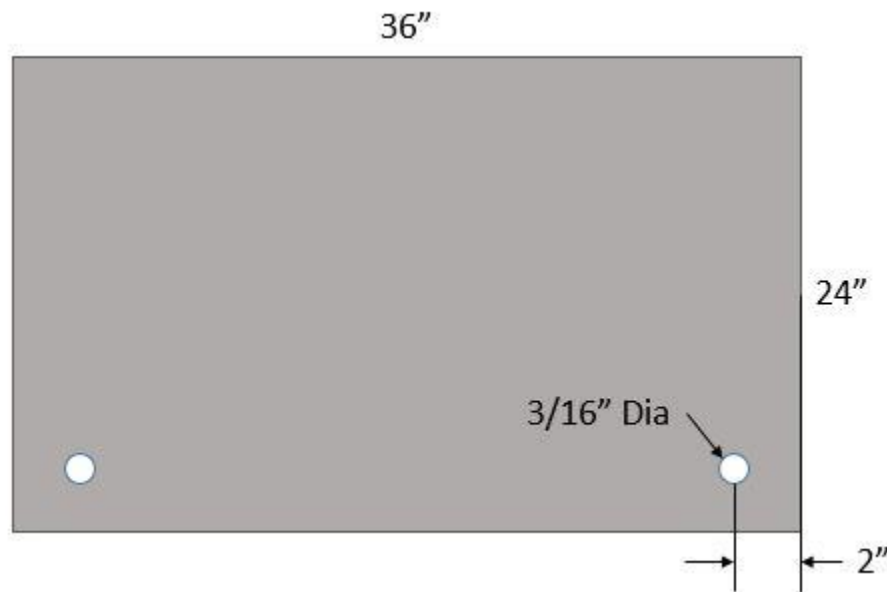
Figure 23. Schematic for aluminum mold used for manufacture of coupons.

After the mold release was applied, tacky tape was run around the outside of the plate leaving the top layer of paper intact. This tape would later be used to seal the constituents within the vacuum bag. It was important to place the tape on the mold first to minimize the possibility of a stray fiber being trapped under the tape. In this case, the vacuum would not be able to be maintained and the infusion would result in a lower volume fraction and strength. Careful consideration was taken to ensure a good seal was achieved throughout the process.

A layer of peel ply was then placed on the mold. Manufactured by Airtech, the peel ply provided a sacrificial layer between the mold and the fibers making it easier to remove the plate without damaging the fibers. The fibers were then aligned in their desired orientation. When applicable, the backing was placed together. For the 4-ply samples, the backings were all placed towards the inside of the plate. Another layer of peel ply was placed on top of the fibers. Finally, a layer of flow media manufactured by Airtech was placed on top of the peel ply. The flow media is a sheet of plastic mesh with a diamond pattern. When the vacuum bag was compressed into the material, the resin can flow easier along the long direction of the diamonds than the short direction. This helps get a consistent fiber volume fraction along the length of the plate.

The above stacking sequence was then sealed with vacuum bag material manufactured by Airtech. After the bag material is initially sealed, careful inspection was completed to find areas where errant fibers bridged across the tape. If any were found, extra tacky tape would be applied under the bag to complete the seal. After this initial inspection, the infusion port was sealed off with a clamp and the vacuum was pulled. The vacuum port was then sealed off with another clamp. After 15 minutes completely sealed off, the vacuum bag was inspected to verify that there were no leaks in the system. Even a small leak during this time would result in the vacuum bag loosening significantly. If a leak was present, extra tacky tape was placed along the seal.

The resin reservoir was then connected to the infusion port and the vacuum port was released allowing the resin to flow through the material towards the vacuum side. The flow rate was limited for the initial 50% of the infusion to slow down the infusion process

and reduce the amount of porosity seen near the infusion port. After the infusion front slowed down considerably, the restriction was taken off and the resin was left to infuse the remainder of the plate. After the infusion was completed, both ports were sealed off and the plate was left on the mold for the first part of the curing cycle outlined below.

Fiber Systems

Two fiber systems were utilized for the research presented in this paper: Vectorply E-LT 3800 and Vectorply E-LT 3900. Both systems are unidirectional fiber systems utilizing E-Glass fibers woven into a mat. They both have 91% of their fibers in the 0° orientation, with 9% in the 90° orientation. Stitching accounts for less than 1% of aerial weight. Vectorply is known for high quality fabric utilized in the wind industry and was chosen for study as it provides great mechanical properties in the fiber orientation with enough reinforcing fibers to ease the manufacturing process. It was also chosen because there is a wide variety of aerial weights available with very similar fiber architectures available. After validating research is completed, the research in this paper should provide a basis for other aerial weights with a similar fiber architecture. The switch in fiber systems occurred between the two sections of research. Effects of fiber angle and moisture diffusion was completed using Vectorply E-LT 3900. Effects of stacking sequence and moisture absorption was completed using Vectorply E-LT 3800. More detailed information on the fiber systems can be seen in Appendix A.

Resin System

The resin system chosen was a two-part epoxy from Momentive developed for the wind industry, EpikoteTM RIMR 135 and hardener EpicureTM RIMH 1366. This resin

system is commonly used in research at MSU as it provides good overall properties and some of the best fatigue properties for these applications. A detailed list of mechanical properties for this resin can be found in Appendix A.

The post cure cycle specified by the manufacturer called for 24 hours at room temperature (23 C) and 12 hours at 70 C. The location of infusion was consistently beneath that of the specifications so an extra heating element was added to maintain the aluminum plate at the recommended temperature. This heating element was placed underneath the aluminum mold and the temperature was monitored with a thermocouple. After the initial curing cycle, the composite was then removed from the plate and placed into a curing oven for the remaining 12 hours.

Post Infusion

All specimens were then cut to 300mm by 30mm from the plates manufactured. The sizing was selected as it provided an approximate representation of 1-D diffusion, enough facial area to mount the AE sensors and an overall strength low enough to be tested with equipment at MSU. The samples had loading grip tabs attached where the samples would be gripped by the load frame. Before the tabs were attached, the ends of the sample were sanded lightly to produce a good surface for the tabs to bond to. They were sanded for approximately 10 – 15 seconds on each side to verify that the fibers were not damaged during this process. The tabs were made from G10 and were manufactured to 64 x 32 mm. They were attached with 3M Scotch-Weld DP460 epoxy [Appendix A]. The tabs were held to the coupon with large binder clips while the adhesive cured. The clips were then removed

24 hours later and the tab surfaces were sanded to produce two parallel surfaces to be gripped by the load frame.

<u>Test Design</u>

There were several layups chosen to be studied. As the goal of the research was to investigate the effects of moisture absorption on the static strength and AE signatures, layups were chosen that would provide a breadth of situations to analyze. As can be seen in the background section, it is known through previous research that the moisture absorption has serious implications on the integrity of material. However, the extent of the effects is not known for all scenarios.

For the first section, layups were chosen to study the effect of moisture absorption at varying fiber angles. Six different 2-ply layups were chosen; three balanced and three unbalanced. The different stacking sequences tested were $[15]_2$, $[30]_2$, $[45]_2$, $[\pm15]$, $[\pm30]$, $[\pm45]$. It is suspected that the inclusion of moisture is affecting the material at the micromechanical level. The selection of layups chosen above provides a wide variety of internal stress states. The balanced coupons were to produce a significant amount of shear between the two plies. As the fiber angles are increased, the inter-ply shear stress would increase as well. The unbalanced coupons were designed to produce the opposite effect. As both plies are in the same direction, there will be a negligible amount of inter-ply shearing stress. The internal stress state of these coupons instead focuses on the bonds between the fibers and matrix. As the fiber angle is increased the amount of normal force on the bonds increases and the shearing stress decreases. In the case of a $[0]_2$ sample, the only normal force pulling the fibers apart laterally within the sample is the contraction seen from

Poisson's effect. However, in the case of [15]$_2$ samples, a portion of the tensile load is translated into a normal force on the bond.

The second section of research focused on how the effects of moisture absorption changed with the stacking sequence. As previous research has shown that the moisture diffusion follows Fickian diffusion principles, the amount of water at a specific point within the sample is dependent on both time and location. Given the assumption that the inclusion of moisture is affecting the material at the microstructural level, it follows that the stacking sequence should be very important during the diffusion process. The second set of samples were designed to test this hypothesis. For these coupons, it was chosen to produce samples that had the same tensile strength before diffusion but would have different strengths during the diffusion process. The two layups that were chosen were [0/90]$_s$ and [90/0]$_s$. Both layups have the same theoretical tensile strength as they both have the same amount of fibers in the tensile direction. In both coupon sets, the 0 degree plies provide the majority of the stiffness and strength in the tensile direction while the 90 degree plies provide lateral stability. However, as these coupons are subjected to a water environment and diffusion begins, the difference in stacking sequences will affect which plies are degraded first.

<u>Water Submersion</u>

The coupons were conditioned in a variety of ways. For the first round of tests, the samples were soaked in synthetic sea water manufactured to conform to ASTM D1141. The manufactured salt water and coupons were kept in sealed plastic containers and conditioned at 50C. The increased temperature significantly hastened the diffusion rate allowing for thicker samples to be tested in shorter time. This phenomenon is referred to

as the Arrhenius relationship and is a well-known effect of temperature. Research on accelerated aging was referenced that concluded that the increased temperature was negligible for M_∞ and the strength reduction of the composites [4].

For the second round of tests, the samples were conditioned in distilled water at 50 C. The decision to switch to distilled water stemmed from problems with the salt skewing the weight gain measurements. It was noticed in the first round of tests that salt would build up on the surfaces of the samples. This salt would have to be washed off before the weights could be recorded, significantly complicating the process and introducing possible error. Prior research at MSU has explored the difference between saltwater and distilled water for weight gain and the difference in strength reduction and maximum moisture content is negligible for these material systems.

Weight measurements were taken periodically throughout the soaking process using a scale accurate to 0.0001g. To get a consistent measurement, the samples were removed from the water and placed on paper towels and allowed to dry for 10 minutes. They were then flipped onto the opposite side on a fresh set of paper towels. This process ensured that no surface moisture would skew the weight gain measurements. Other testing was done to verify that this time was not enough for the water to significantly diffuse out.

The mass of the samples was then compared to the original weight of the sample to calculate the percent weight gain. This calculation can be seen below in equation 11. M_c, m_c and m_i represent the weight percentage or moisture content, the current mass and the initial mass respectively.

$$M_c = \frac{(m_c - m_i)}{m_i} \tag{11}$$

For the first round of samples, the salt build up was not washed off until the final weight measurement. When full saturation was reached, signified by the weight gain curve leveling off asymptotically, the salt was then washed off and the samples were weighed again to get a more accurate moisture uptake percentage.

Test Procedures

All samples were tested in static tensile loading specifications as per ASTM D3039. Tests were completed on an Instron 8562 100 kN servo-electric load frame in static tension tests. All tests were completed in environmental conditions of 23 C and 20% - 40% humidity. The hydraulic grips were pressurized to approximately 3000 psi throughout all tests. Strain was collected during the tests using an Instron 2620-824 extensometer with a gage section of 12.7mm and a rage of ±40% strain. Load and strain data were output from the load frame to the AE system and recorded through the AE software. The load was zeroed prior to the specimen being loaded into the grips to calibrate against the self-weight of the actuator head. Loading rates of 0.05"/min to 0.06"/min were chosen for the tests depending on the layup.

Test Matrices

For the first section of testing, fiber angle and moisture absorption were varied. In these tests, only two conditioning steps were studied: fully saturated and dry. The test matrix for this section can be seen below in Table 2.

Table 2. Lists of tests completed to study the effects of moisture absorption on various off-axis laminates.

Layup	Fabric	# of Tests	Load Rate	Conditioning
$[15]_2$	E-LT 3900	6	.05"/min	3 Dry, 3 Saturated
$[30]_2$	E-LT 3900	6	.05"/min	3 Dry, 3 Saturated
$[45]_2$	E-LT 3900	6	.05"/min	3 Dry, 3 Saturated
$[\pm15]$	E-LT 3900	6	.05"/min	3 Dry, 3 Saturated
$[\pm30]$	E-LT 3900	6	.05"/min	3 Dry, 3 Saturated
$[\pm45]$	E-LT 3900	6	.05"/min	3 Dry, 3 Saturated

For the second section, stacking sequence and moisture absorption were varied. It was chosen to study the effects of moisture absorption throughout the saturation process to explore partial degradation effects. Times were chosen that would represent various levels of moisture saturation evenly distributed between 0.0% moisture and M_∞. As the diffusion process is much faster at the beginning, the times selected ended up being weighted towards the beginning of the saturation process. The testing matrix can be seen below in Table 3.

Table 3. List of tests completed in order to study the effects moisture absorption on various stacking sequences.

Layup	Fabric	# of Tests	Load Rate	Conditioning
$[0/90]_s$	E-LT 3800	5	.06"/min	0.0% Moisture
$[0/90]_s$	E-LT 3800	5	.06"/min	0.2% Moisture
$[0/90]_s$	E-LT 3800	5	.06"/min	0.5% Moisture
$[0/90]_s$	E-LT 3800	5	.06"/min	0.7% Moisture
$[0/90]_s$	E-LT 3800	5	.06"/min	Fully Saturated
$[90/0]_s$	E-LT 3800	5	.06"/min	0.0% Moisture
$[90/0]_s$	E-LT 3800	5	.06"/min	0.2% Moisture
$[90/0]_s$	E-LT 3800	5	.06"/min	0.5% Moisture
$[90/0]_s$	E-LT 3800	5	.06"/min	0.7% Moisture
$[90/0]_s$	E-LT 3800	5	.06"/min	Fully Saturated

AE Procedures

Acoustic emission testing was utilized for all tests. The system used was a Mistras PCI-8 owned and operated by the composites research group at MSU. WD and WDI sensors from Physical Acoustics were used. These sensors are the same piezo crystal setup however the WDI has an internal amplifier with a gain of 40 dB and the WD is ran through an external amplifier with the same gain. Both the WD and the WDI are wideband sensors with frequency ranges between 50 and 400 kHz. Vacuum grease was used as a couplant between the sensor and the specimen.

Two sensors were used in a linear array for all tests. The sensors were placed 128 mm apart, each 64 mm from the center of the coupon. The sensors were held in place by caps and rubber bands. The acoustic emission parameters were set so that waveforms that originated outside of the sensors were not recorded. It was decided to eliminate these events as it is hard to differentiate the difference between test damage and damage initiated by the grip pressure. The specific timing parameters used in the AE software can be seen in Appendix C.

Prior to each test, the Acoustic Property Matrix Generator (APMG) was ran to verify that the sensor was working properly. This utility within the AE software sent out a signal from one sensor and read it from the other. The time of flight between the two sensors was then reported as well as the relative amplitude of the signals between the two sensors. As the location between the two sensors was already input into the system, the wave speed could then be calculated from the time of flight. In addition to the APMG, a pencil lead break test was completed for each sample. A pencil lead break test allowed the user to

verify the accuracy of the location calculations happening within the AE system. Pencil lead was broken in three different places along the length of the coupon. Measuring from sensor one to sensor two as length L; pencil lead was broken at 0.25L, 0.50L and 0.75L. These locations were then compared to the output location on the AE software.

AE Post Processing

The AE system stores the individual waveforms as part of the large data file generated during a test. Data analysis was completed partially within the AE system and partially using external MatLab scripts developed at MSU. The AE software analyzes the waveforms using an FFT and outputs several characteristics of the waveform. As discussed above, the characteristic of interest for this research is the peak frequency. The AE system also outputs test data at the moment the waveform is recorded allowing frequency data to be matched up with mechanical data.

A set of MatLab scripts were developed to automate the data analysis methods. The main purpose of the scripts was to allow the user to truncate the data file at a specific time. During mechanical testing, the final failure of the composite produces a large quantity of noise and events that is difficult for the sensors to differentiate. For this reason, all tests were truncated at max load as the goal of the AE analysis was to study the damage happening at a microstructural level prior to final failure. After truncation, the MatLab scripts then separated the events into the respective bins as outline above in the background section of this work. From there, the user could work with the data in various ways. Plotting functions could be called directly from MatLab. The data was then exported to excel for further analysis.

RESULTS

Overview

All samples manufactured for testing were inspected to verify quality and consistency. Volume fraction was measured with a burn off for each manufactured plate. The recorded volume fractions for each plate were consistent throughout each test set. Static ultimate strength results will be presented in MPa, with standard deviation error bars added to show variation in the data. For AE results, frequency will be plotted against time or strain where applicable. The percentages of each damage category will also be presented. Standard deviation error bars are added to the bin percentage charts to show the variation in the data.

Visual Inspection of Damage

When the saturated samples were removed from conditioning, damage was already visible. The damage appeared as regions of opaqueness parallel to the direction of the fibers. The damage was often visible at multiple places along the length of the coupon. Examples of the damage can be seen below in Figure 24 and Figure 25. Once these samples were subjected to tensile loading, the damage would propagate further along the fiber angle. A few samples were removed from testing and the damage was inspected using optical microscopy. Cross sections through the areas of opaqueness were cut and various levels magnification were used. Unfortunately, the damage was not obviously visible at a microscopic level. Future work will include SEM analysis as the capability is available.

Figure 24. Coupon 2442-5 and the damage seen after the coupon was removed from the saltwater bath.

Figure 25. Coupon 2444-11 and the damage after the coupon was removed from the saltwater bath.

Off-Axis Strength Reduction

Moisture Absorption

For the study of off-axis strength reduction, six different layups were tested: $[15]_2$, $[30]_2$, $[45]_2$, $[\pm15]$, $[\pm30]$, and $[\pm45]$. Samples were manufactured from four different plates. Witness samples for each of these plates was placed in saltwater and measured periodically to document the absorption process. The resulting absorption curves can be seen below in Figure 26. The samples exhibited Fickian diffusion characteristics as expected. As the sample weights were measured it was noticed that there was significant salt buildup on the surface. The salt was not washed off prior to weight measurements until full saturation as it was difficult to verify that a consistent washing occurred. There was also a concern that the washing would induce additional diffusion further skewing the data. As the moisture curve leveled off to a consistent weight gain at 1000 hours, it was concluded that moisture absorption had ceased. The samples were conditioned for another 500 hours to ensure the samples were at full saturation. A thorough washing was then completed eliminating the salt buildup. This last weight measurement is representative of the amount of water absorbed into the material without the added weight of the salt build up.
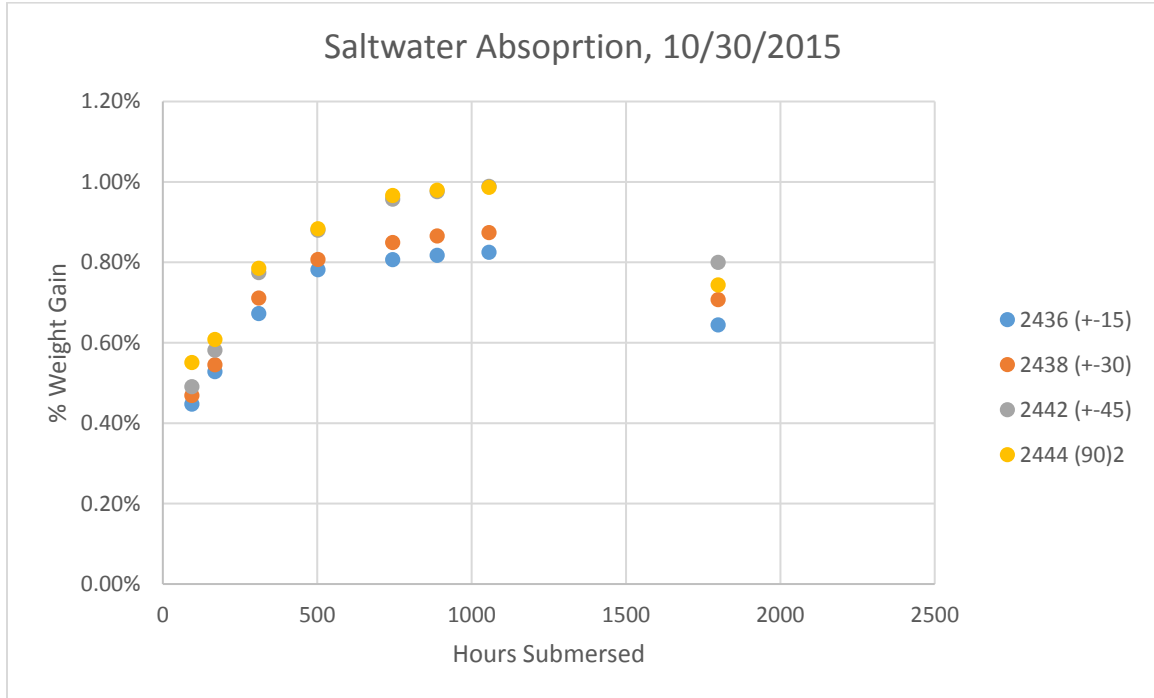
Figure 26. Moisture absorption for off-axis samples to study the effects of fiber angle and moisture diffusion on static strength and AE signatures.

Static Strength Reduction

Three samples of each layup were tested to static failure in both dry and saturated conditions. The average strength values for each layup in dry/saturated conditions can be seen below in Figure 27.
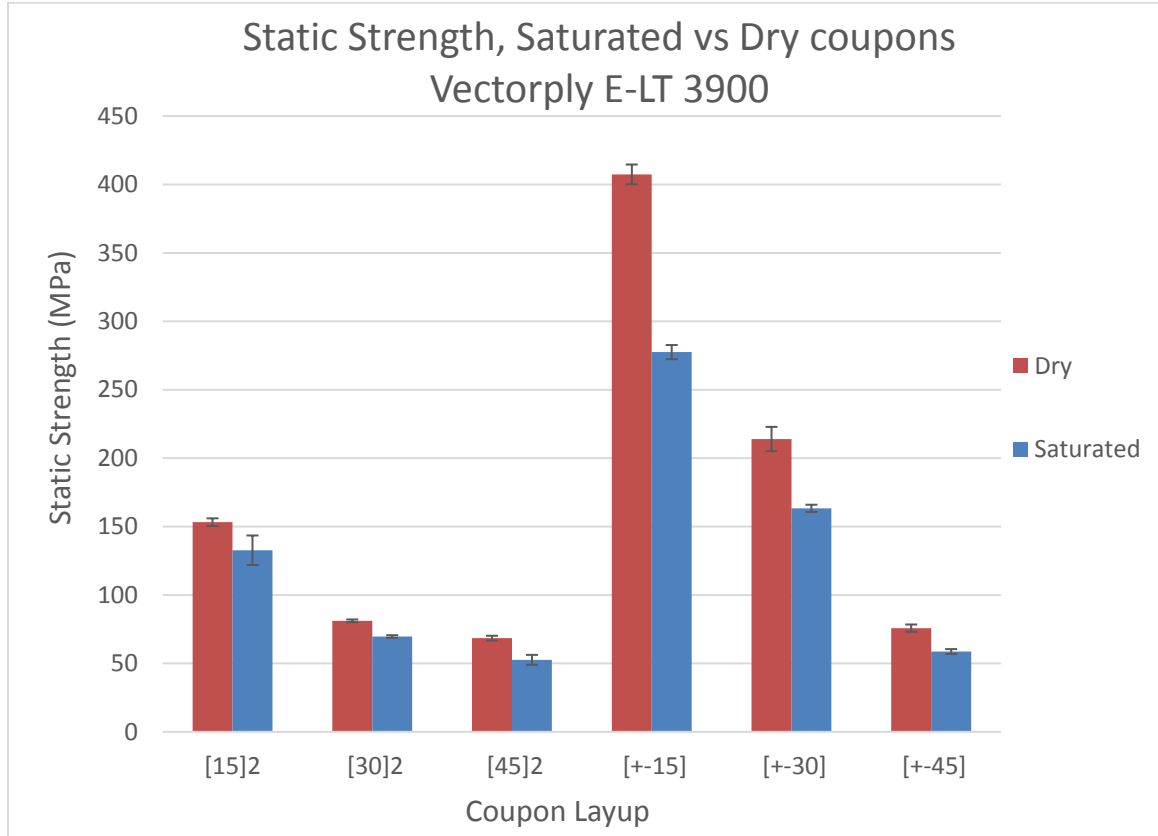
Figure 27. Static strength for both dry and saturated coupons at various fiber angles. Consistent failures occurred for all layups and conditions.

The static strengths of the dry laminates are in line with expected results from previous research at MSU. The strength reductions in the off-axis laminates are similar to those seen in unidirectional laminates. Interestingly, the inclusion of water affected the strength of the balanced coupons more than the unbalanced coupons. Strength in the [45]2 samples was reduced by 23% while the [±15] samples were degraded by 32%. The standard deviation error bars show little variation in the strengths of the layups at each condition.

Analysis Model

As discussed earlier, epoxy-fiberglass materials are being considered for implementation in marine environments. In these situations, material characterization

becomes paramount. Mechanical designers require accurate material properties to complete successful designs for MHK devices. The research presented throughout this paper has a direct effect on these designs as the material properties are significantly altered by the moisture absorption. However, the strength reductions of specific layups testing must be able to be extended to a larger structure. This is accomplished using a mechanical model.

There have been many mechanical models developed for composite materials as they have seen wider implementation throughout industry. Unfortunately, due to the inherent material complexity many of these models fall short. Often the models correctly predict behavior at specific fiber angles but fail at others. This is typically due to the difference in failure modes at other angles. Models also tend to struggle predicting strengths in woven lamina as the transverse fibers complicate the derivation of material properties.

In general, mechanical models for composites fall into three categories: bulk material models, ply level models and micromechanical models. Bulk material models, the simplest of the three calculate equivalent strengths and moduli in each direction and then treat the material as if it was homogenous with the resultant properties. These models have several shortcomings, the primary being the inability to calculate the stresses between plies. They often work well for simple structures and for basic design, but for failure analysis they leave out interply interactions. These interply interactions are critical for the transfer of load between plies and without them a large design consideration in composites is ignored.

The next level of analysis are ply level models, also known as lamina level analysis. Instead of treating the entire structure as a homogenous material, ply level models calculate strengths and moduli in each direction per ply. Stresses and strains can then be calculated on a local ply basis given external loading. These models can then be extended to include failure analysis. Failure analysis methods provide a way to predict when specific plies fail given their local stress. Simple method within this category include Max Stress and Max Strain, while more complicated models like Tsai-Wu and Tsai-Hill include interaction terms. Ply by ply analysis models provide much more flexibility, however they are still plagued by inaccuracies and inability to predict across a wide range of fiber angles and architectures.

Micromechanical analysis models provide even greater detail. These models often model individual fibers or fiber bundles in an FEA format. Micromechanics models have the capability of providing some of the most in depth analysis techniques, but require a large amount of input data and processing power that is often infeasible for composite designers.

Model Parameters

For this research, it was chosen to use lamina based analysis as these models have the most applicability to industry designers. In lamina analysis, the lamina are generally assumed to be transversely isotropic materials. This reduces the number of required elastic constants for the lamina to five. The required elastic constants are the longitudinal modulus (E_1), transverse modulus (E_2), shear modulus (G_{12}) and two Poisson's ratios (ν_{12} and ν_{23}). In addition to the elastic constants, strengths of the material are required to fully define the

lamina. In tensile applications, typically the longitudinal tensile strength (F_{1t}), transverse tensile strength (F_{2t}) and shear strength (F_6) are required.

For the analysis of the current work, two material property sets were required: one for dry material, and one for fully saturated material. Currently the analysis does not include partial saturation however this work is underway. To determine the material properties for the model, several baseline tests were completed. To determine E_1 and F_1, $[0]_2$ coupons were tested in static tensile loading conditions. In this orientation, the longitudinal properties can be extracted from the stress-strain curve and the ultimate strength of the sample. Similarly, $[90]_2$ coupons are used to derive E_2 and F_2. Shear properties G_{12} and F_6 are determined from a simulated shear test per ASTM Standard D3518 [Appendix B]. A summary of the model parameters used for dry material can be seen below in Table 4. The test data that was used to derive these material properties can be seen in Appendix B.

Table 4. Model input parameters for unconditioned E-LT 3800.

E-LT 3800 Unconditioned		
F_{1t}	1133	MPa
F_{2t}	57	MPa
F_6	49.2	MPa
E_1	40.2	GPa
E_2	15.9	GPa
v_{12}	0.27	
G_{12}	3.54	GPa
v_{23}	0.35	

Saturated input parameters were derived from another set of data as the baseline coupons were still undergoing moisture saturation. In previous research at MSU [19], strength reduction due to moisture absorption was studied using the same resin used in the current research. The fabric used in the prior research was slightly different, however, both

fabrics had a similar architecture and the volume fractions in both sets were similar as well. It was assumed that the percentage strength reductions seen in the previous research extends to the current material properties as well. For samples at full saturation, 0.86% moisture, F_{1t} decreased by 20% while E_1 only decreased by 2%. F_{2t}, derived from $[90]_6$ samples decreased by 3% at 1000 hours saturation. It is important to note that the $[90]_6$ tests were not completed at full saturation, but 0.46% moisture. This discrepancy was assumed irrelevant though as the controlling strength seen later in the analysis was the shear strength, F_6 across all layups and the F_2 only dropped 3% at more than halfway to full saturation.

Shear strength, F_6 is difficult value to define as it is difficult to achieve pure shear in a fiber-reinforced polymer. There are several testing methods that have been developed for determining F_6 in these materials, although each has its disadvantage. In the dry input parameters above, ASTM standard D3518 for simulated shear tests was used to determine a value for F_6. In this method, samples of $[\pm 45]$ are tested and the stress at 5% strain is used as F_6. As seen earlier in the results section, $[\pm 45]$ samples saw a 22% reduction in strength. This reduction was applied to the F_6 value derived from the simulated shear test to round out the mechanical properties for saturated E-LT 3800.

Table 5. Model input parameters for saturated E-LT 3800.

E-LT 3800 Saturated		
F_{1t}	906.4	MPa
F_{2t}	55	MPa
F_6	38.4	MPa
E_1	39.4	GPa
E_2	15.1	GPa
v_{12}	0.27	
G_{12}	3.54	GPa
v_{23}	0.35	

Ply Stresses

Using the above material properties, the local stresses for each ply were calculated per laminate plate theory as outlined by Barbero [12]. The variety of fiber angles within the laminates tested resulted in a unique set of internal stress states. The laminates primarily featured transverse tension and shear stresses. The local longitudinal tensile stress was not significant in respect to the strength for any of the laminates discussed. For comparison of the laminates, the ratio of shear stress to transverse tensile stress was calculated and can be seen below in Table 6. The stress ratio details the prevalence of one stress to the other, allowing for strength reduction analysis to be related back to the internal stress state of the material.

Table 6. Lamina shear / transverse stress ratio per laminate.

	$\dfrac{\sigma_6}{\sigma_2}$
$[15]_2$	3.73
$[30]_2$	1.73
$[45]_2$	1.00
$[\pm15]$	2.20
$[\pm30]$	1.30
$[\pm45]$	0.95

As seen above, the shear stress was the dominant stress for four of the six laminates. However, as the fiber angle reached 45 degrees, both shear and transverse tension stress reached similar magnitudes. The stress ratios for the balanced coupons show less variation than in the unbalanced coupons.

Interacting Failure Criterion

Utilizing the above stress ratios, it becomes apparent that there is significant interaction in stresses within the lamina. It is important to consider these interactions when extending unidirectional strength values to off-axis laminates. This rules out failure criterion such as Max Strain and Max Stress as they do not include interactions of stresses. There are several criterion that do include interactions, each taking a slightly different approach to the interactions. Tsai-Wu failure criterion includes all lamina stresses into one equation, with a mix of linear and quadratic terms. Interacting failure criterion, presented by Barbero is a modification to Tsai-Wu that separates fiber dominated failures from matrix dominated failures. For the development of the model in this paper, interacting failure criterion was chosen for the analysis. The separation of fiber and matrix dominated failure lends itself to off-axis analysis as there will likely be negligible fiber dominated failure. This also allows matrix dominated failure to be studied individually. The results of the failure model can be seen below in Figure 28 and Figure 29 compared to the experimental results. Interacting failure criterion incorrectly predicts the experimental results across all laminates. In the balanced samples, the percentage difference between the experimental results and the failure criterion varied between 18% and 81%. The unbalanced samples saw even greater difference, varying between 78% and 115%. Clearly laminate plate theory and interacting failure criterion do not adequately describe the laminates. There are several possible reasons for these discrepancies. First off, laminate plate theory assumes a perfectly unidirectional lamina, while the fibers used in the construction of the laminates studied were in the form of a stitched mat. The inclusion of 9% backing strands complicates analysis as these strands produce varying amounts of strength depending on fiber angle.
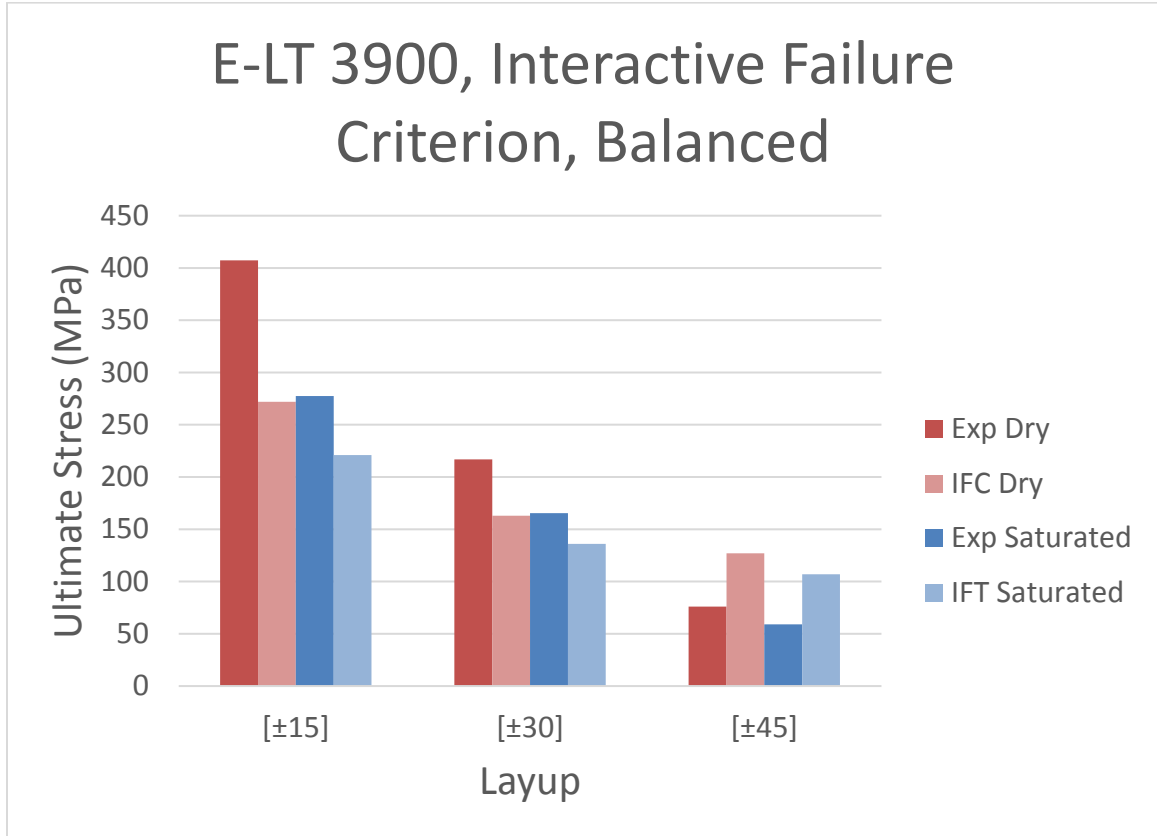
Figure 28. Strength, Interactive Failure Criterion (IFC) vs Experimental Results (Exp) for balanced laminates.

Another possible source of error is the value for shear strength F_6. Shear strength is a difficult value to define as it is very difficult to test a material in pure shear. Also, the strain to failure for shear stress is often considerably larger than other failure modes which complicates the analysis. Per ASTM D3518, the shear stress at 5% strain is used as the shear strength. However, 5% strain is not achievable in these laminates so the shear strength of the lamina may not be indicative of the shear strength of the laminate. Laminate plate theory and interacting failure criterion do not have the capability of considering this discrepancy. A micromechanical model with material property inputs for both resin and

individual fibers would be needed to adequately describe this phenomenon. However for the current scope of this work, that is not feasible.
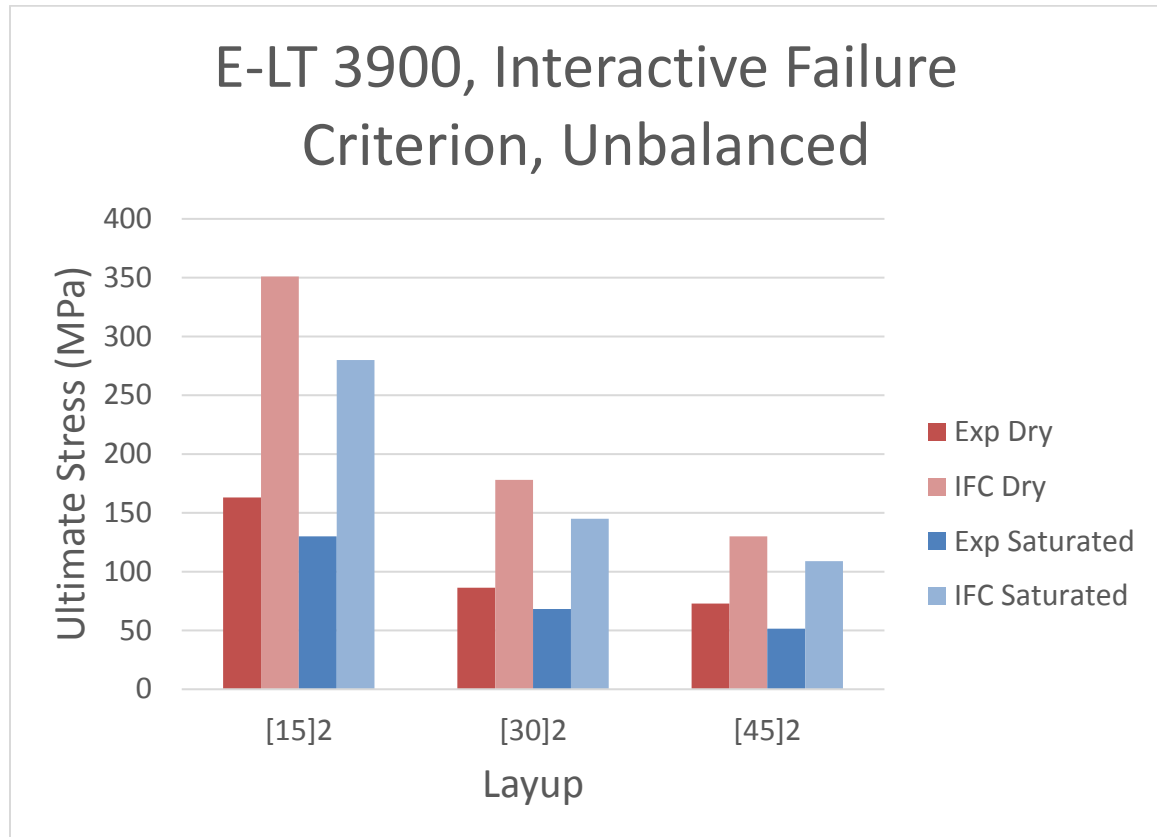
Figure 29. Strength, Interactive Failure Criterion (IFC) vs Experimental Results (Exp) for unbalanced laminates.

AE Analysis

AE analysis was performed on the tests presented above to further study the effects of moisture inclusion. The waveforms were analyzed utilizing an FFT and the peak frequency of the events was recorded. The events were then collected into the discrete damage bins discussed earlier, each representing a different failure mechanism. As the purpose of the research was to investigate the difference in failure mechanisms between dry and saturated samples, the percentage of different damage bins will be presented for

the two conditions. Using the percentage of events in each bin provides a better comparison between tests as the number of individual events can change drastically. Below in Figure 30 - Figure 35, the AE results of each laminate set are displayed. Each set keeps the same format which shows the bin percentages summarized on the left chart for each condition. Standard deviation error bars are added to show the variation of the data. On the right side of the page, frequency distribution plotted again stress is showed for one test of each condition. These charts are important as they show the progression of damage as opposed to a snapshot at the end of the test.

The bin percentage charts show very similar results across the different laminates. All laminates showed a decrease in events classified as fiber/matrix debond and an increase in matrix cracking. For saturated samples, the percentage of matrix cracking events exceeded 70% for all three sample sets while percentages for the dry samples varied from 34.4% to 42.0%. The percentage of fiber/matrix pullout (bin 2) events remained relatively consistent throughout all balanced layups with a slight decrease after moisture saturation. For saturated samples, the percentage of events classified as fiber/matrix pullout varied from 1.9% to 2.1% while the dry samples had a range from 3.8% to 9.4%. Fiber failure was negligible for all laminates tested as expected.
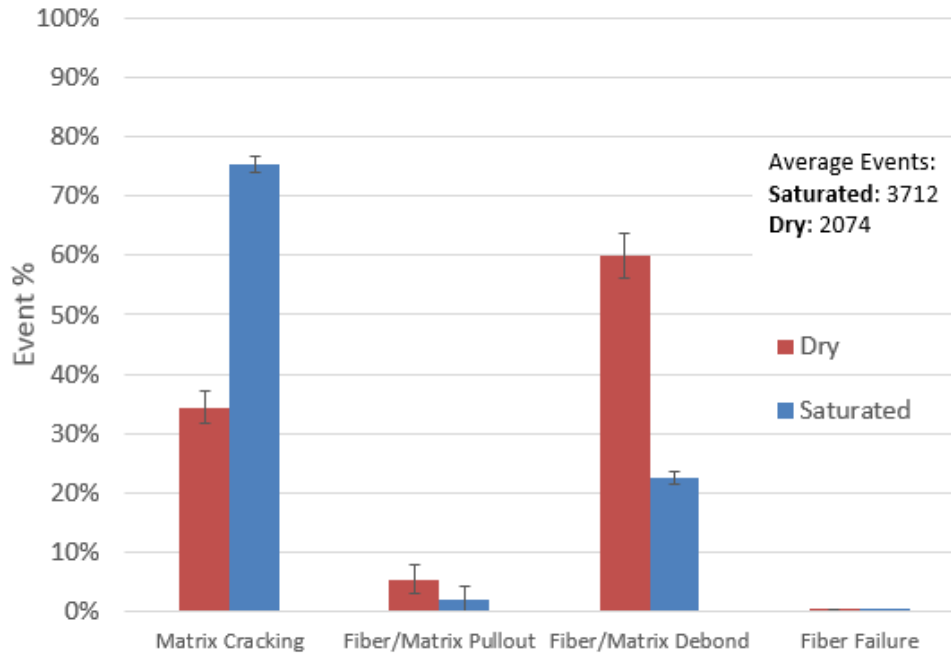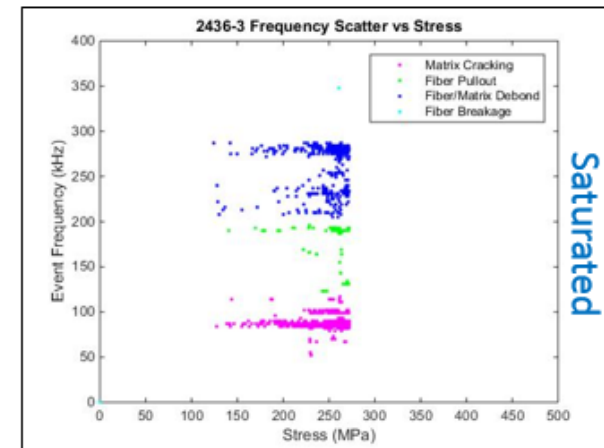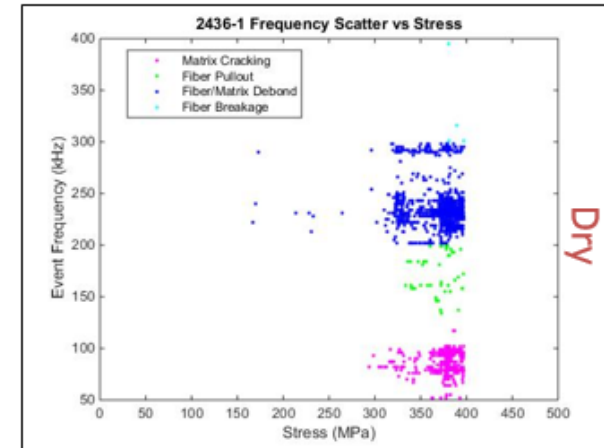
Figure 30. Percentage of damage mechanisms for [±15] samples. Frequency scatter plots are shown to the right, showing the development of damage throughout the test.
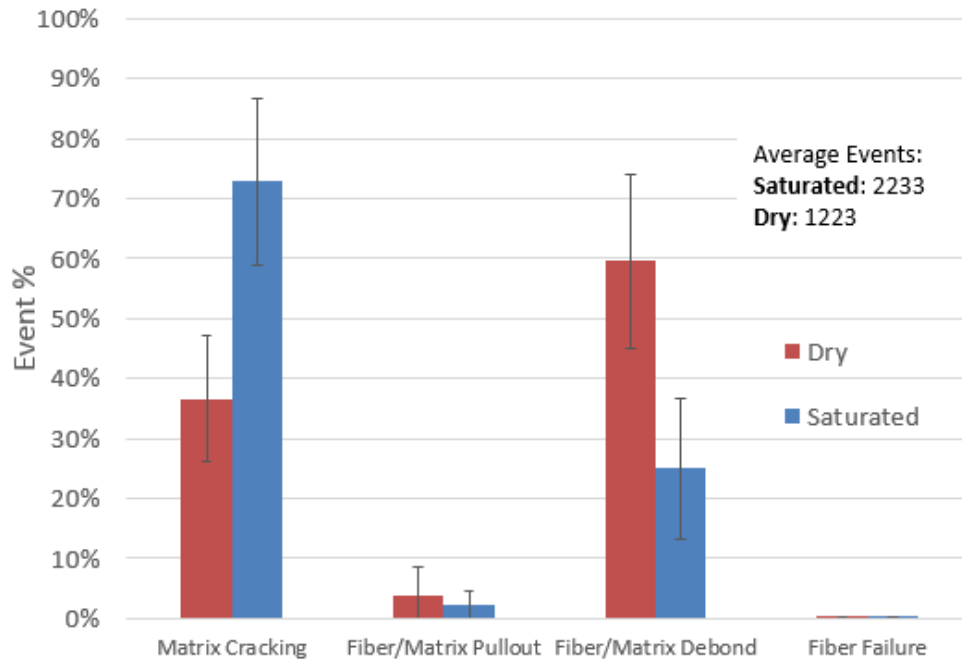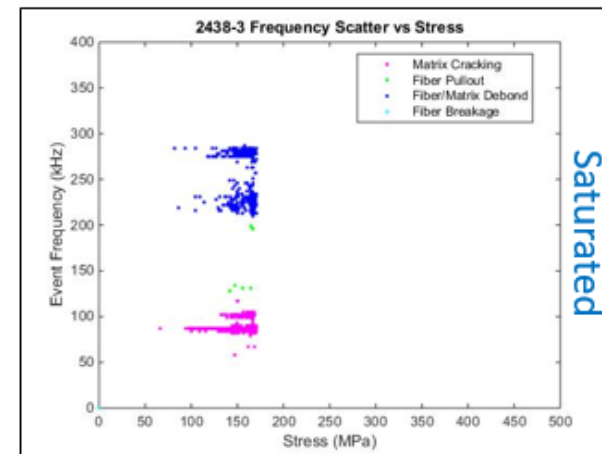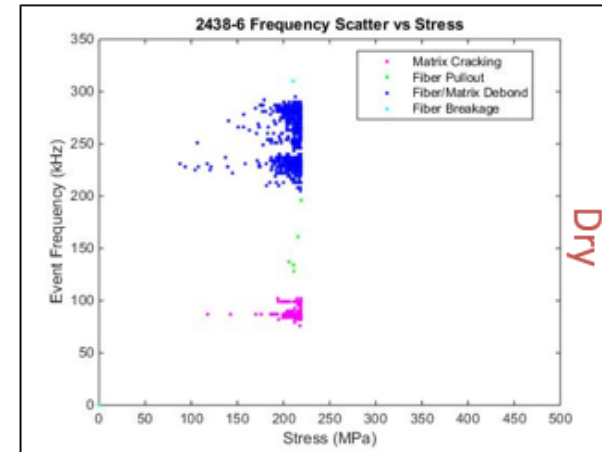
Figure 31. Percentage of damage mechanisms for [±30] samples. Frequency scatter plots are shown to the right, showing the development of damage throughout the test.
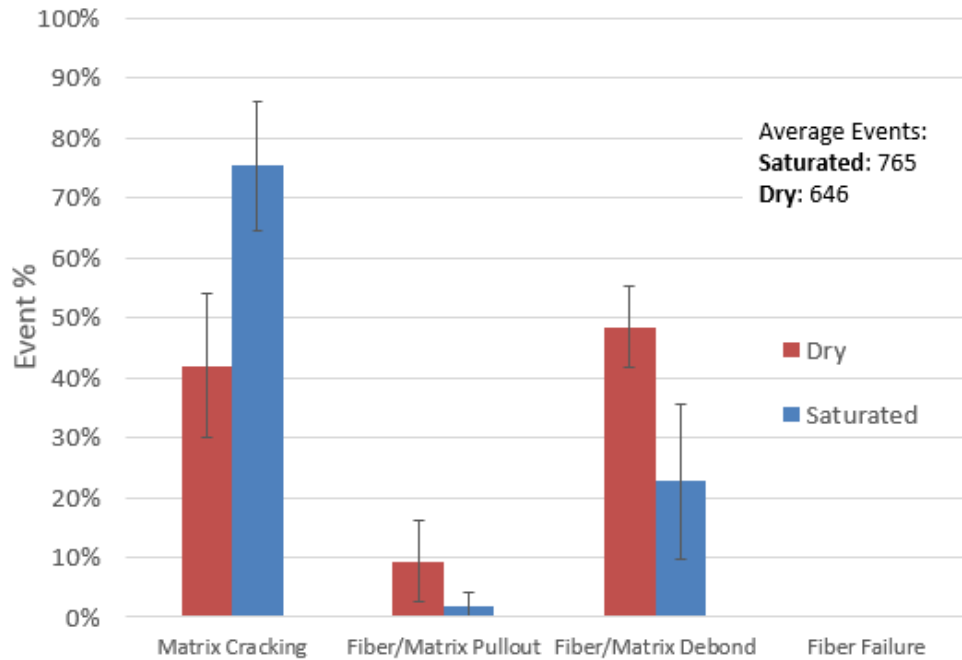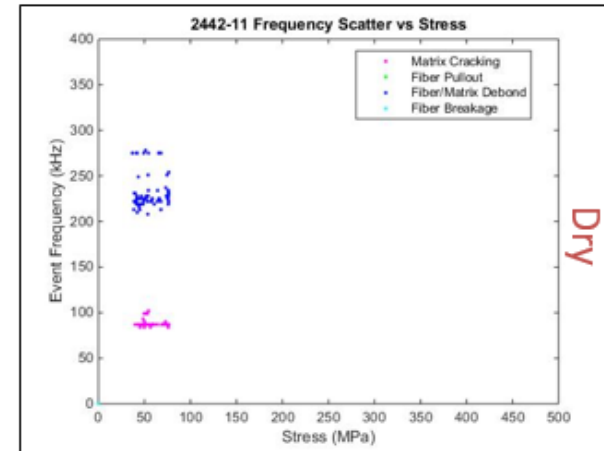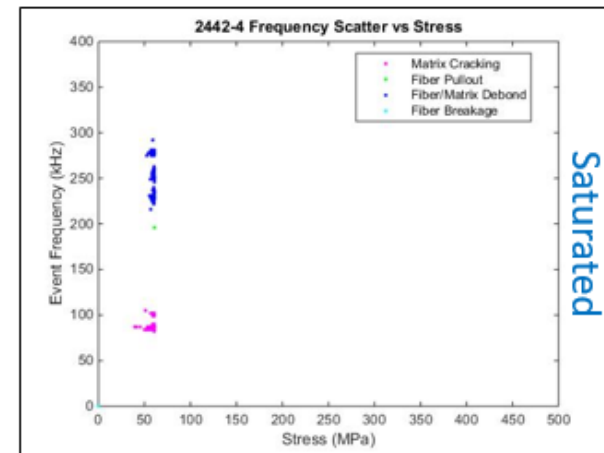
Figure 32. Percentage of damage mechanisms for [±45] samples. Frequency scatter plots are shown to the right, showing the development of damage throughout the test.
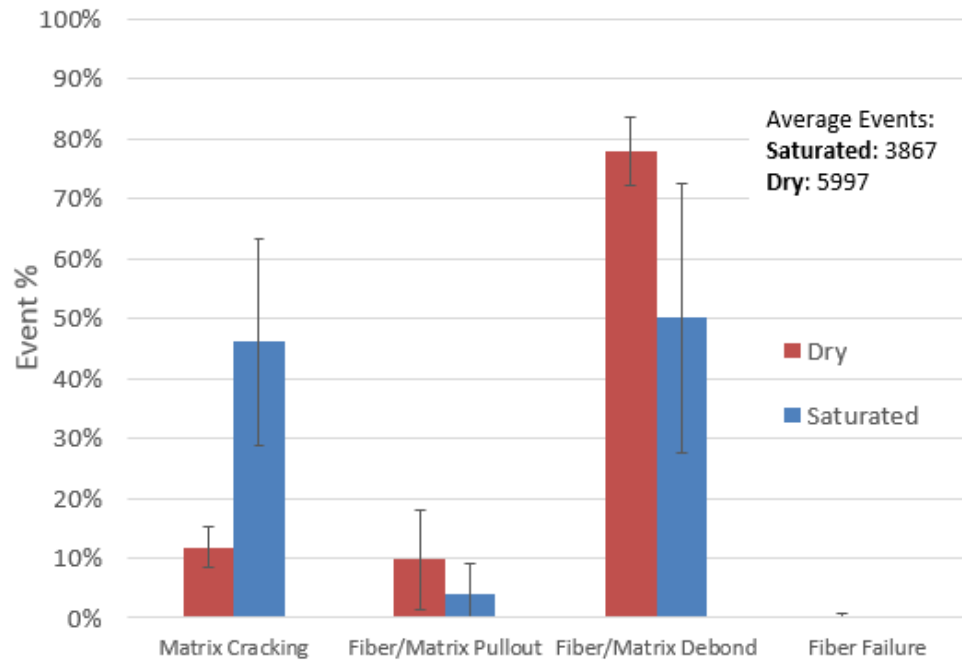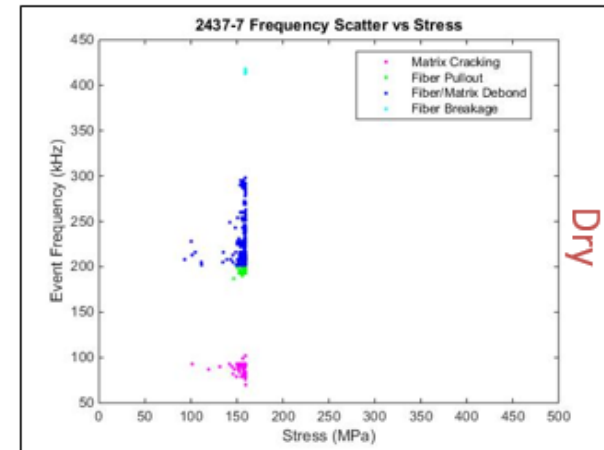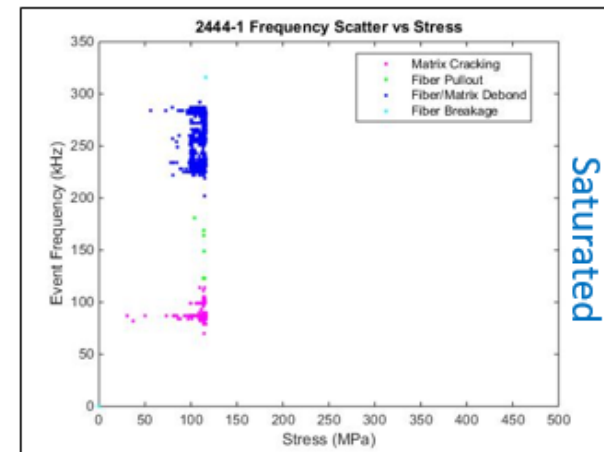
Figure 33. Percentage of damage mechanisms for [15]₂ samples. Frequency scatter plots are shown to the right, showing the development of damage throughout the test.
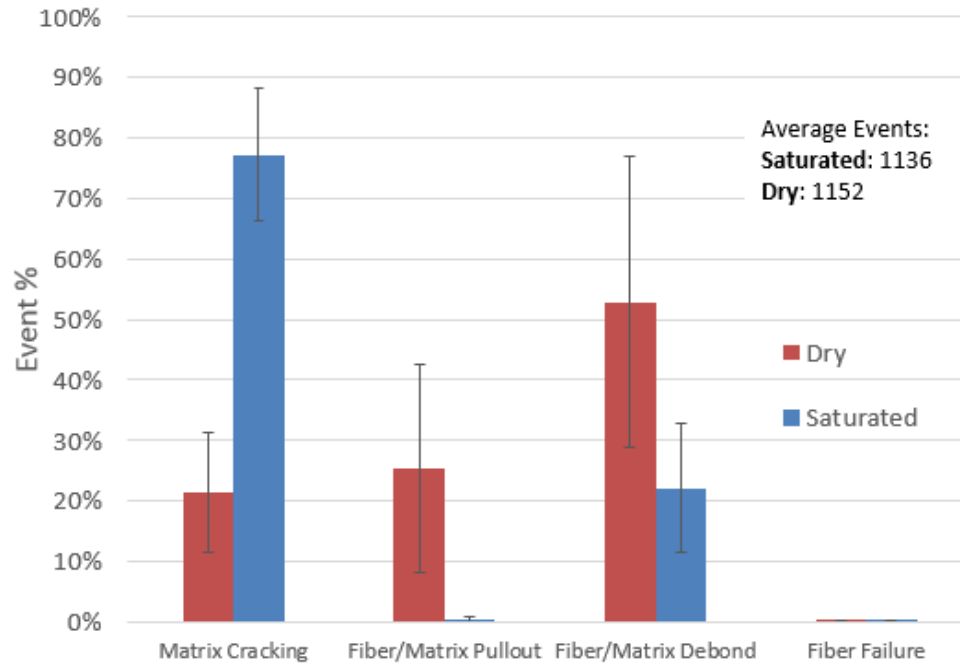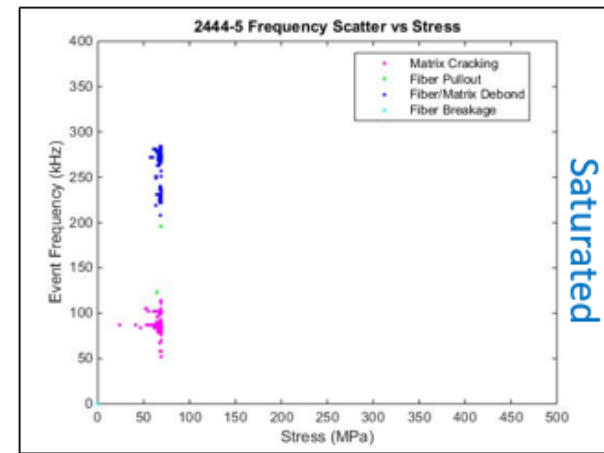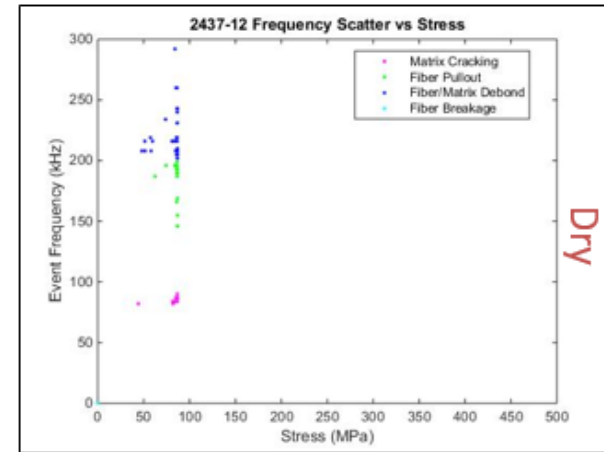
Figure 34. Percentage of damage mechanisms for [30]₂ samples. Frequency scatter plots are shown to the right, showing the development of damage throughout the test.
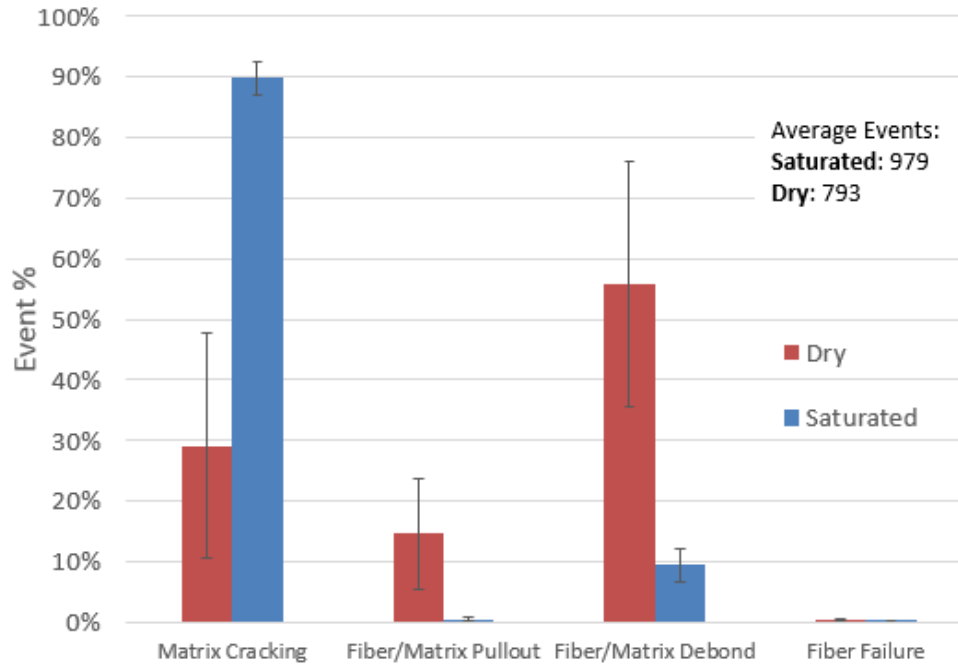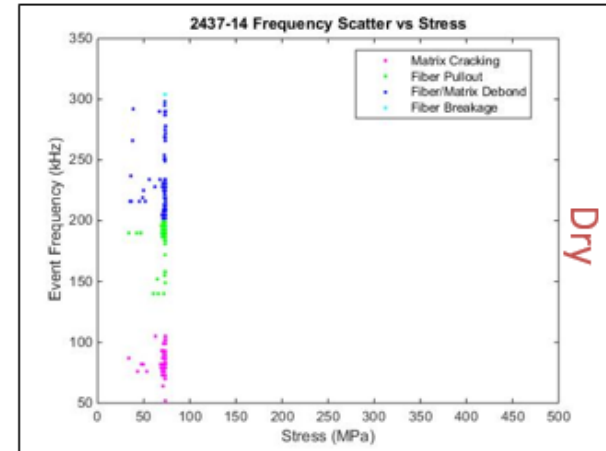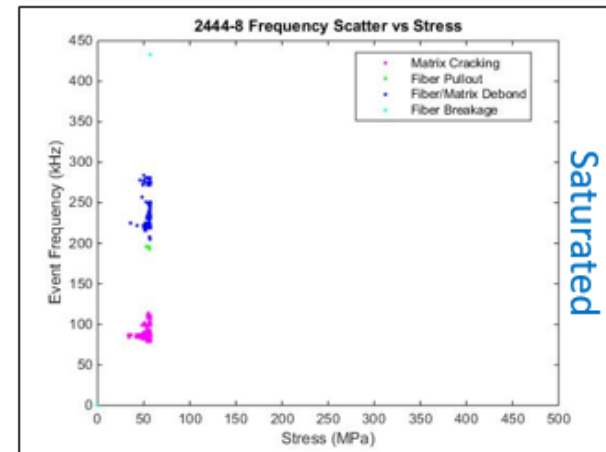
Figure 35. Percentage of damage mechanisms for [45]₂ samples. Frequency scatter plots are shown to the right, showing the development of damage throughout the test.

The AE results provide further insight at a micromechanical level into the specific effects of the moisture absorption. All laminates tested had a decreased amount of fiber/matrix debond damage events and an increase in matrix events post saturation. The increase of matrix cracking events may indicate that the saturated matrix material is failing prior to the bonds of the unconditioned samples. This also appears evident when the AE events are plotted against stress. It can then be seen when damage mechanism bins become prevalent during the test.
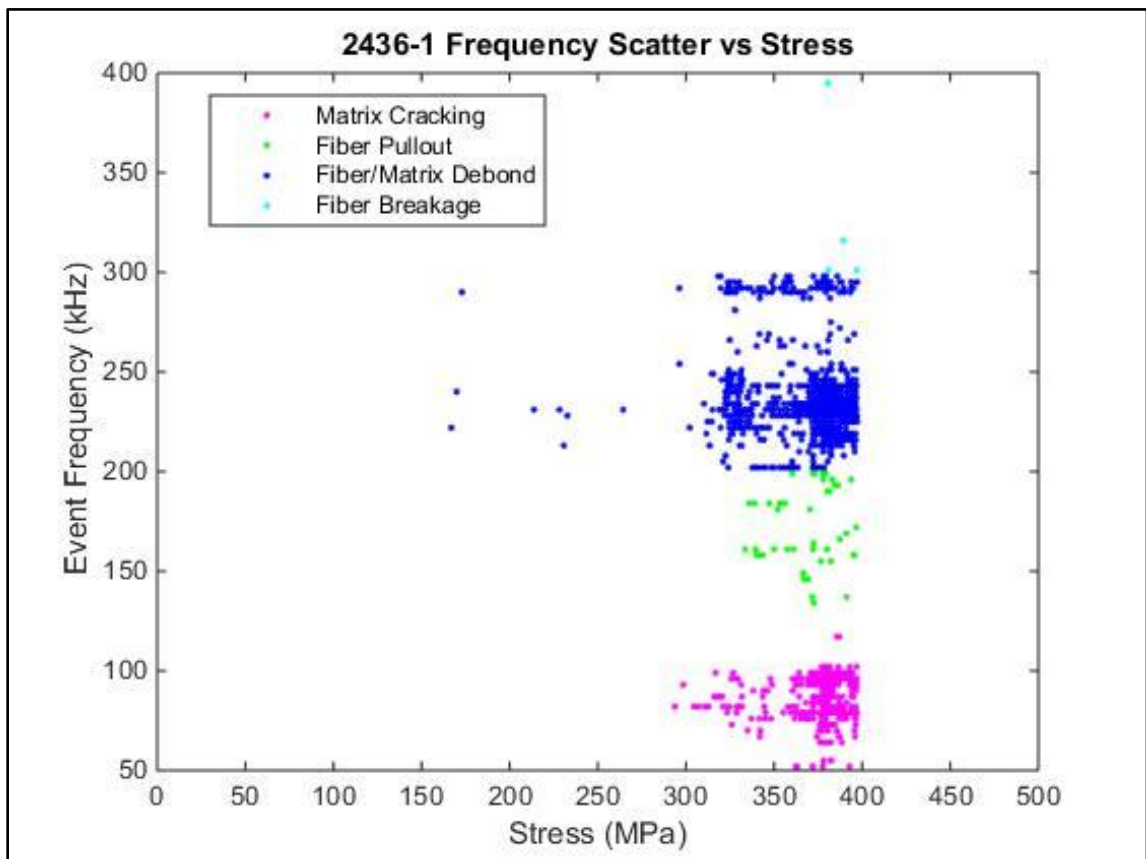
Figure 36. Frequency distribution plotted against stress for a dry [±15] sample.

Figure 36 shows the damage events plotted by frequency at the load they occurred at. There is a build-up of events occurring in bin 3 (fiber/matrix debond; blue) prior to

failure but the events in bin 1 (matrix cracking; pink) occur much closer to failure. This

contrasts with the events diagram for the saturated sample seen below in Figure 37.
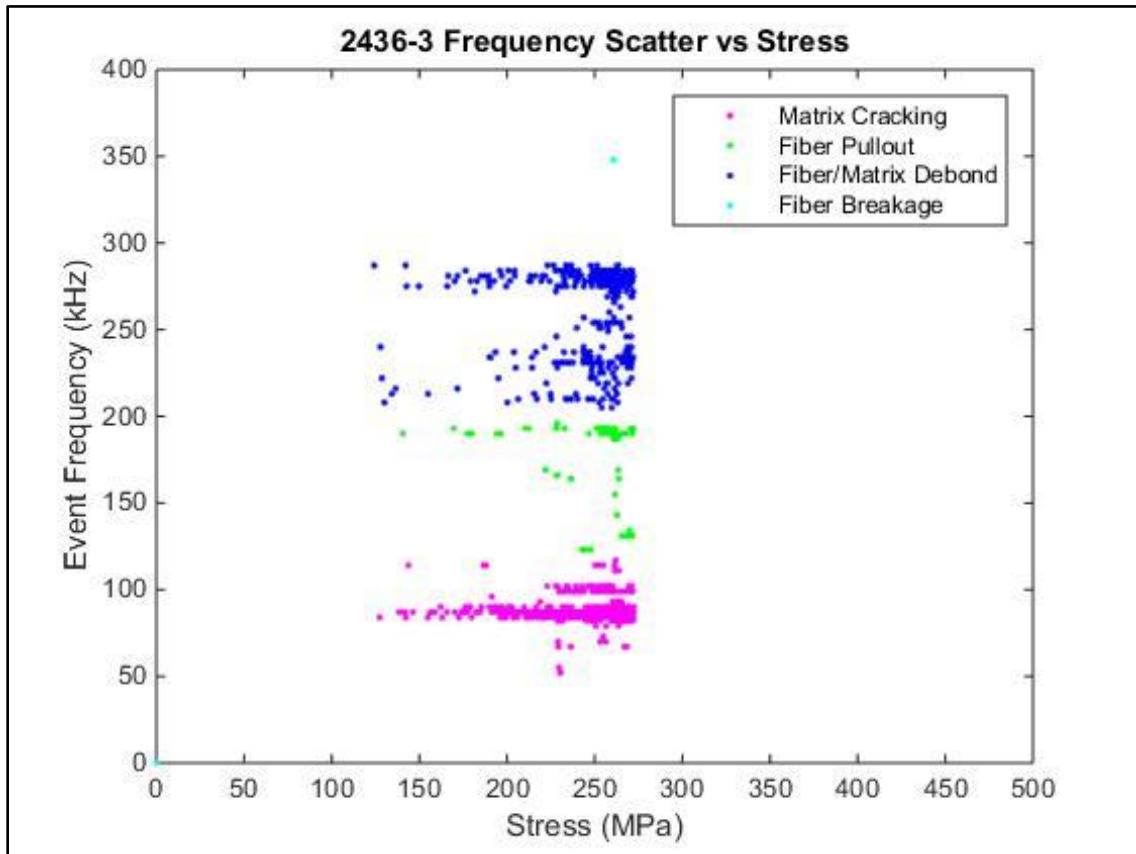
Figure 37. Frequency distribution plotted against stress for a saturated [±15] sample.

For the saturated sample, the matrix cracking events begin to occur much earlier

prior to failure. In this case, the matrix cracking begins prior to the fiber/matrix interface

failures. This indicates that the matrix failing prematurely, may be overloading areas of

fiber/matrix interface causing further damage to the microstructure of the material. This

effect would result in a premature failure as seen throughout mechanical testing. It is also

evident from this chart that the matrix cracking bin is far more prevalent than fiber/matrix

debond. These results are consistent throughout all laminates tested and can be seen

throughout all scatter diagrams shown in Figure 30 - Figure 35.

Partial Saturation Strength Reduction

Static Strength

Five samples of each layup outlined above were tested for each time step. Both layups tested had very similar static strengths in the control set. As the samples were subjected to the marine environment, the strength of both layups decreased throughout time. The strength of the samples vs time and vs saturation percentage can be seen below in Figure 38 - Figure 39.
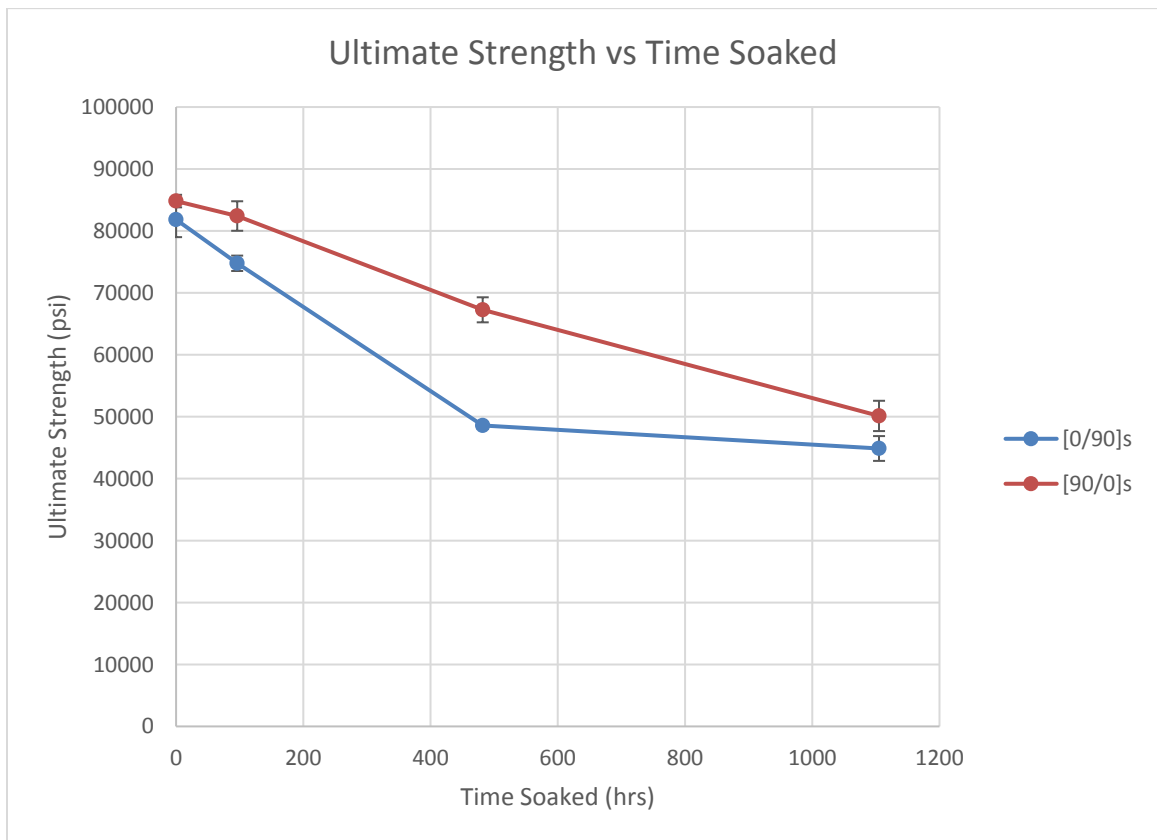
Figure 38. Ultimate strength vs time soaked for [0/90]s and [90/0]s coupons. Note: five tests performed for each layup at each time step.
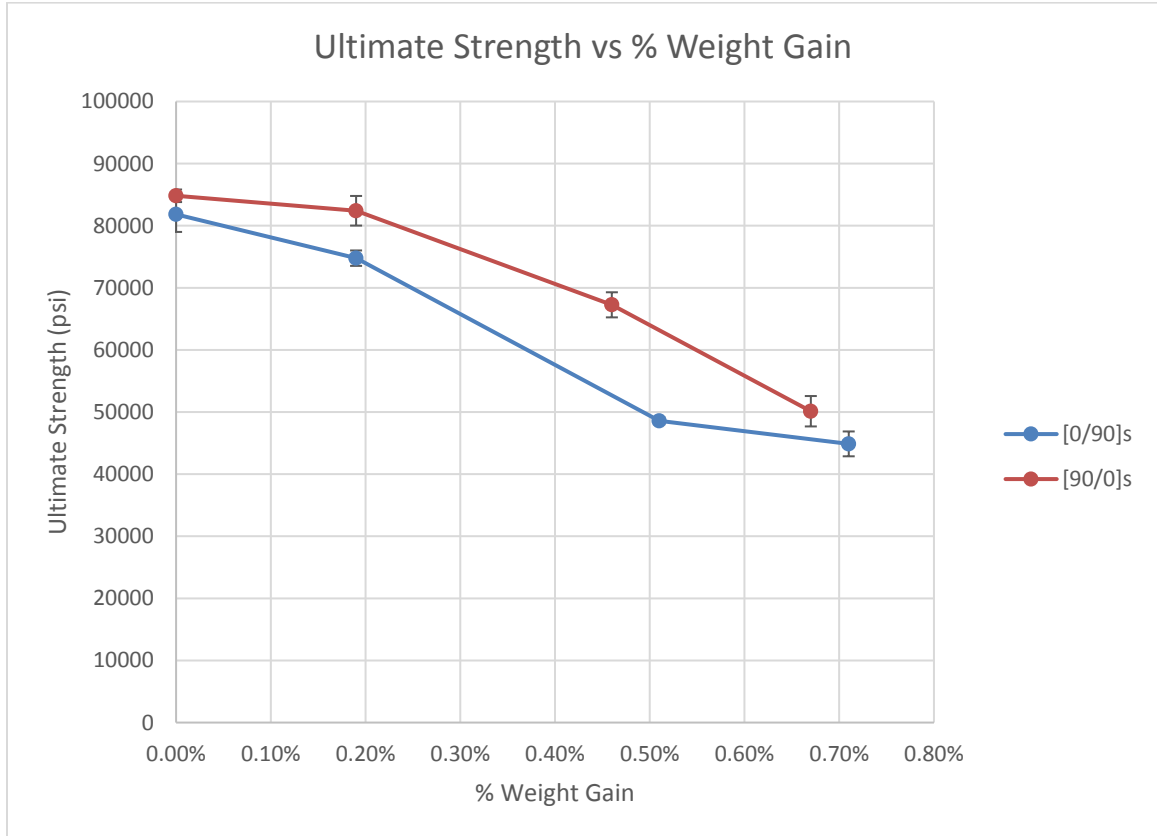
Figure 39. Ultimate strength vs % weight gain for [0/90]$_s$ and [90/0]$_s$ coupons. Note: five tests performed for each layup at each time step.

As expected, the [0/90]$_s$ samples saw a larger decrease in the first part of the moisture saturation curve than the [90/0]$_s$ samples as the primary load bearing plies were subjected to the moisture first. The full saturation data points are not in the charts as they have not been able to be completed yet. The samples are still undergoing conditioning and are expected to be complete in a couple months. The trend for the 0.6% and 0.8% moisture sample sets shows that the samples are approaching the same value again as expected.

As discussed above, this is a simple extension of the Fickian diffusion laws but it has the potential to be very important to MHK designers. In traditional composite design, the stiff plies are placed on the outside to maximize the bending strength they provide to

the structure. The results above provide another provide another consideration as it may be beneficial to design structure with sacrificial layers on the outside. These layers would protect the load bearing plies from significant degradation for a significant amount of time. Moisture detection methods could be installed as well allowing repairs to the surface to be completed prior to the primary plies being damaged.

<u>AE Data</u>

Acoustic emission testing was utilized in the analysis of the tests to explore the specific mechanisms affecting the strength degradation. Unfortunately, the data collected did not add any value to the discussion due to unforeseen circumstances. The stacking sequence of the layup influences the acoustic emission signature significantly. This was supported by the results in this study as the number of events in each bin was significantly different for the two layups in the control set. The $[90/0]_s$ samples exhibited primarily matrix cracking while the $[0/90]_s$ samples had a more varied signature. The summary of the control samples can be seen below in Figure 40.
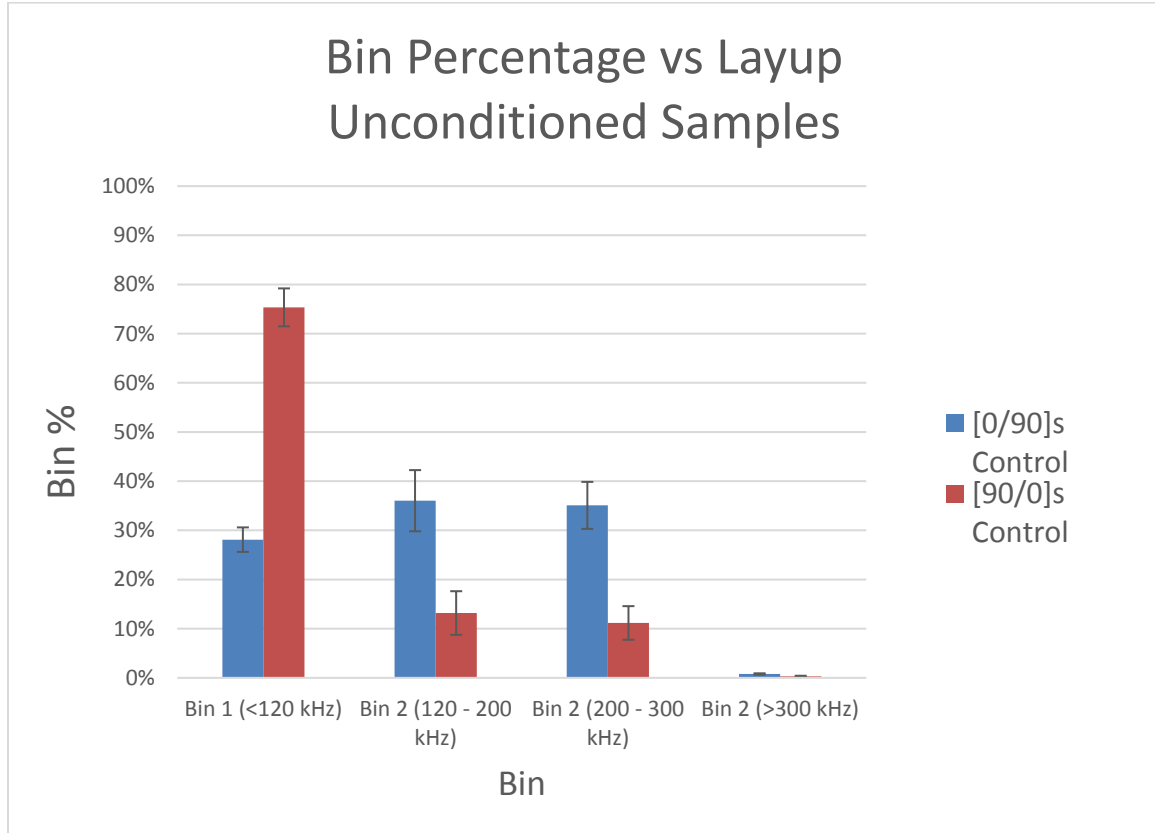
Figure 40. Bin percentages for both layups in the control set.

As seen above, there is a significant difference between the two layups tested, even within the unconditioned control samples. The question arises as to whether this effect is caused by a difference in the failure of the material, or how the elastic waves are perceived by the sensors. As both layups have the same theoretical strength in the tensile direction, it is assumed that this effect is due to the AE signals. During testing of these samples, the 90 degree plies build up a lot of damage prior to final failure of the coupon. This damage begins occurring at approximately 0.4% strain. It is likely that the 90 degree plies being in direct contact with sensors is skewing the number of events towards matrix cracking. The sensors are picking up the damage in the transverse plies first due to the proximity and then

shutting out the other damage occurring further within the material. Further examples of this effect can be seen below in Figure 41 and Figure 42.

Unfortunately, this effect causes the AE data for the two layups to not be able to be compared. The relative change in the percentage of the events in each bin was sought after in these tests. As the control samples do not show similarity, conclusions cannot be drawn from the changes in each layup at this time. Future work will explore this effect as the reasons for it are currently unknown.
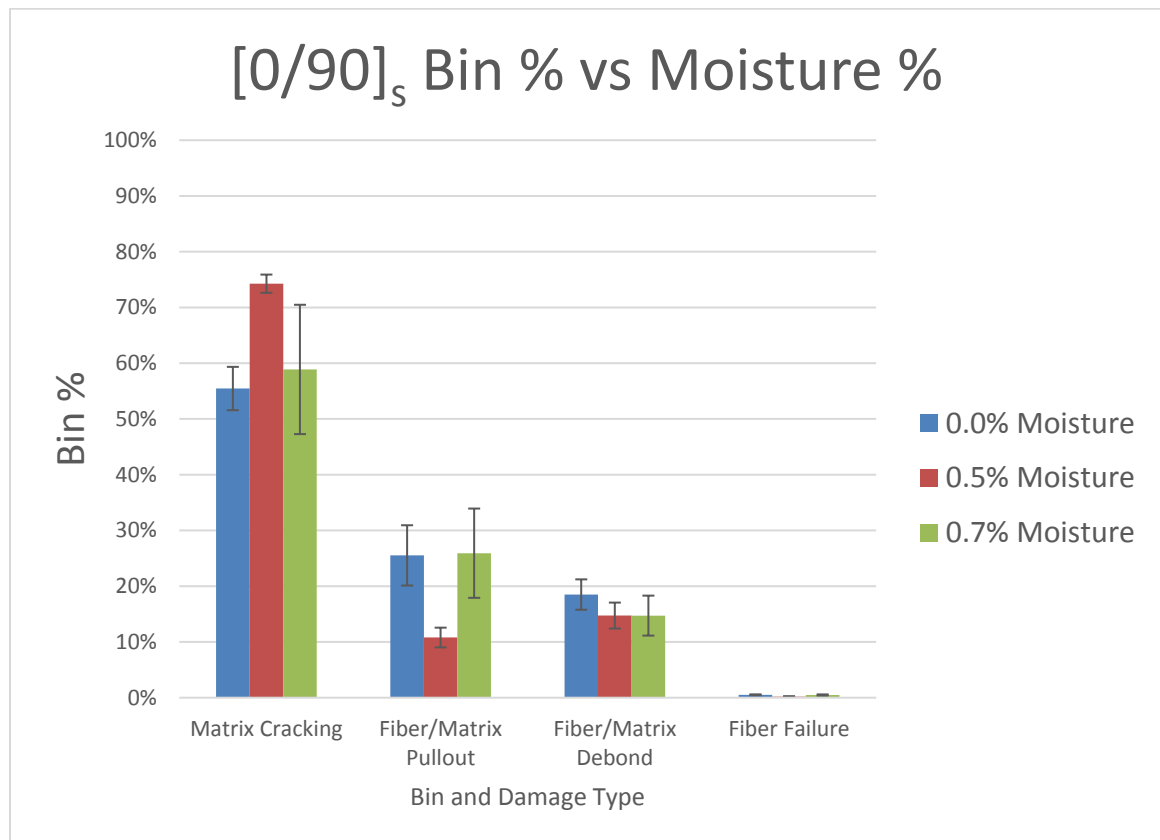
Figure 41. Percentage of AE events in each bin for [0/90]$_s$ samples, varying moisture percentage.
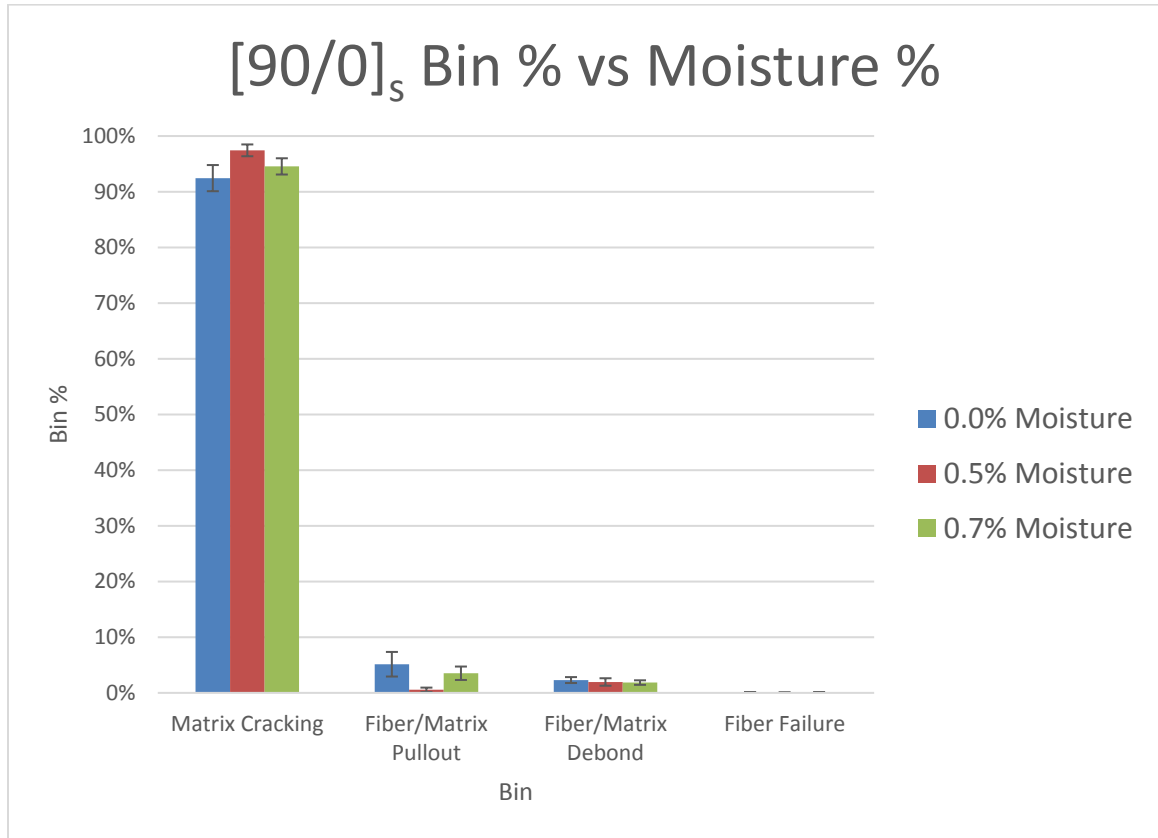
Figure 42. Percentage of AE events in each bin for [90/0]ₛ samples, varying moisture percentage.

CONCLUSIONS

Strength reductions seen in off-axis epoxy/fiberglass laminates were consistent and in line with previous unidirectional results. The six laminates tested provided a breadth of strength values at fiber angles not normally tested. Both the unconditioned and saturated ultimate strengths are directly applicable to industry. Preliminary MHK designs will need accurate strength values for both conditions to ensure proper durability throughout device lifetime. This research also began to expand test data into mechanical analysis with a broad application to potentially minimize future mechanical testing required. However, interactive failure criterion did not adequately describe the failure stresses seen in the experimental results. The inconsistencies were present in the prediction of the unconditioned samples and are indicative of deficiencies in off-axis prediction methods. The amount that each lamina strength value is contributing to the laminate strength is unknown and makes further classification of strength reduction difficult.

Further analysis was completed to understand the strength reductions on a micromechanical level. Acoustic emission analysis was performed and provided a unique insight into a potential change in damage progression due from moisture inclusion. Matrix cracking damage events, picked up by the AE system began to accumulate at earlier points prior to failure in saturated samples. In unconditioned samples, fiber/matrix debond damage events start happening before or at a similar time to matrix cracking. The change in damage progression within the laminate due to the inclusion of moisture complicates the mechanical analysis as well. The extent to which each lamina strength is contributing to the laminate strength likely changes in addition to the change in damage progression. This

information combined with the mechanical analysis points towards interply matrix regions as a key area for future study. This region of matrix material is often subjected to large shear stresses in off-axis laminates.

Partial saturation testing was successful in extending the importance of stacking sequence on the evolution of strength reduction. This idea is novel in composites design as the primary load bearing plies are typically placed on the outside of a laminate. The research presented above challenges this principal. In situations where damage to the outside of the MHK device occurs, it may be beneficial to have sacrificial layers exposed to the marine environment to protect the primary plies.

Acoustic emission analysis of partial saturation testing was inconclusive. The difference in the two layups resulted in the frequency bin percentages varying significantly between the control sets. Analysis was not able to be completed into how damage mechanisms evolved throughout absorption as this effect outweighed any other trends. However, it did reveal the effects of stacking sequence on the peak frequency of events, which will be investigated further in future work.

<u>Future Work</u>

A clear path forward for the study of off-axis laminates is evident. Static strength reduction values for off-axis laminates provides designers with a great baseline of data. The next step would be to expand this data to include other material systems and layups. It will also be important to expand the data to include fatigue strength reduction to ensure proper design. Data collected in this research points towards the shear strength of the matrix. There are several techniques available to study this effect in greater detail.

Iosipescu shear testing (ASTM Standard D5379) is designed to test materials in shear loading. It utilizes a double v-notched sample loaded in bending producing a shear stress between the two notches. This method could be used for the analysis of neat resin samples at absorption intervals. The study of fracture toughness in neat resin samples is also an area of study to be completed in future work. Various testing methods could be employed to study the effects of absorption on the toughness. These studies will result in a more complete understanding of how the constituent materials are affected by moisture saturation. Additional further work into the classification of damage mechanisms and how they extend to the laminate strength in dry and saturated conditions will also be important.

Further work into the development of partial saturation strengths involves determining the strength curves for individual lamina. These curves would then be input parameters for a laminate based analysis model with the goal of being able to predict the partial saturation of the entire laminate. Further development of diffusion models in composites materials would provide greater accuracy for strength reduction models.

REFERENCES CITED

[1]   D. o. E. DOE. (2015). *Quadrennial Technology Review*. Available: http://energy.gov/sites/prod/files/2015/09/f26/Quadrennial-Technology-Review-2015_0.pdf

[2]   W. J. Cantwell and J. Morton, "THE SIGNIFICANCE OF DAMAGE AND DEFECTS AND THEIR DETECTION IN COMPOSITE-MATERIALS - A REVIEW," (in English), *Journal of Strain Analysis for Engineering Design,* Review vol. 27, no. 1, pp. 29-42, Jan 1992.

[3]   B. W. Kim and J. A. Nairn, "Observations of fiber fracture and interfacial debonding phenomena using the fragmentation test in single fiber composites," *Journal of Composite Materials,* vol. 36, no. 15, pp. 1825-1858, 2002 2002.

[4]   C. H. Shen and G. S. Springer, "MOISTURE ABSORPTION AND DESORPTION OF COMPOSITE-MATERIALS," *Journal of Composite Materials,* vol. 10, no. JAN, pp. 2-20, 1976 1976.

[5]   W. L. Bradley and T. S. Grant, "THE EFFECT OF THE MOISTURE ABSORPTION ON THE INTERFACIAL STRENGTH OF POLYMERIC MATRIX COMPOSITES," (in English), *Journal of Materials Science,* Article vol. 30, no. 21, pp. 5537-5542, Nov 1995.

[6]   G. Marom and L. J. Broutman, "MOISTURE IN EPOXY-RESIN COMPOSITES," *Journal of Adhesion,* vol. 12, no. 2, pp. 153-164, 1981 1981.

[7]   M. Stoffels, "EFFECTS OF EXTERNALLY APPLIED TENSILE STRESSES ON THE MOISTURE DIFFUSIONCHARACTERISTICS OF EPOXY GLASS COMPOSITES."

[8]   D. Miller, "Evaluating performance of composite materials for MHK applications," *ASME 2011 International Mechanical Engineering Congress and Exposition, IMECE 2011,* vol. 8, pp. 47 - 51, 2011.

[9]   H. Lamb, "On waves in an elastic plate," *Proceedings of the Royal Society of London Series a-Containing Papers of a Mathematical and Physical Character,* vol. 93, no. 648, pp. 114-128, Mar 1917.

[10]   J. J. Scholey, P. D. Wilcox, M. R. Wisnom, and M. I. Friswell, "Quantitative experimental measurements of matrix cracking and delamination using acoustic emission," *Composites Part a-Applied Science and Manufacturing,* vol. 41, no. 5, pp. 612-623, May 2010.

[11]   L. Wang and F. G. Yuan, "Group velocity and characteristic wave curves of Lamb waves in composites: Modeling and experiments," *Composites Science and Technology,* vol. 67, no. 7-8, pp. 1370-1384, Jun 2007.

[12]   E. J. Barbero, *Introduction to Composite Materials Design*, 2nd ed. CRC Press, 2011.

[13]   M. R. Gorman, "ACOUSTIC-EMISSION IN 2-D CARBON-CARBON COUPONS IN TENSION," (in English), *Journal of Composite Materials,* Article vol. 25, no. 6, pp. 703-714, Jun 1991.

[14]   J. Bohse, "Acoustic emission characteristics of micro-failure processes in polymer blends and composites," *Composites Science and Technology,* vol. 60, no. 8, pp. 1213-1226, 2000 2000.

[15]   C. R. Ramirez-Jimenez, N. Papadakis, N. Reynolds, T. H. Gan, P. Purnell, and M. Pharaoh, "Identification of failure modes in glass/polypropylene composites by means of the primary frequency content of the acoustic emission event," *Composites Science and Technology,* vol. 64, no. 12, pp. 1819-1827, Sep 2004.

[16]   P. J. deGroot, P. A. M. Wijnen, and R. B. F. Janssen, "Real-time frequency determination of acoustic emission for different fracture mechanisms in carbon epoxy composites," (in English), *Composites Science and Technology,* Article vol. 55, no. 4, pp. 405-412, 1995.

[17]   M. Suzuki, H. Nakanishi, M. Iwamoto, and E. Jinen, "Application of Static Fracture Mechanisms to Fatigue Fracture Behavior of Class A-SMC Composite," in *Proc. 4th Japan-US Conf on Composite Materials*, 1988, pp. pp. 297-306.

[18]   M. Schuster, "Characterization and Energy Analysis of Fiber Reinforced Polymer Composites by Acoustic Emission Analysis," MS, Mechanical Engineering, Montana State University, 2014.

[19]   D. Miller, M. J. F., S. D. D., H.-S. B. A., and G. D. Todd, "Performance of composite materials subjected to salt water environments," *Collection of Technical Papers - AIAA/ASME/ASCE/AHS/ASC Structures, Structural Dynamics and Materials Conference,* 2012.

APPENDICES

APPENDIX A

APPENDIX A: Product Information

✳VECTORPLY®

Performance Composite Reinforcements
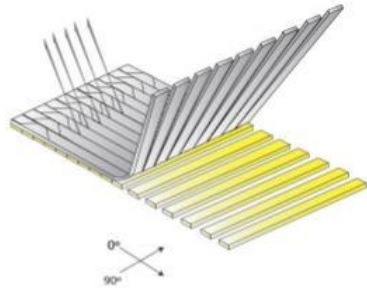
E-LT 3800-10

Fiber Type: E-Glass
Architecture: 0º/90º Biaxial

Total Weight: 37.26 oz/sq.yd / 1263 g/sq.m

Roll Specifications			Fiber Architecture Data	
Roll Width:	Roll Weight:	Roll Length:	0 º :	33.55 oz/sq.yd / 1138 g/sq.m
50 in. / 1270 mm	220 lbs / 100 kg	68 yd / 62 m	90 º :	3.36 oz/sq.yd / 114 g/sq.m
			Chopped Mat:	N/A
			Polyester Stitching:	0.35 oz/sq.yd / 12 g/sq.m

* Packaging: Bag

Vectorply Corporation
3500 Lakewood Drive Phenix City, AL 36867
tel. 334-291-7704 fax. 334-291-7743

<u>Disclaimer:</u>

The customer is solely responsible for determining the performance and fitness for a particular use of any product produced by customer utilizing a reinforcement fabric or material produced or manufactured by Vectorply Corp. Specifications of reinforcements may change without notice.

REV: 3/13/2015

VECTORPLY
Performance Composite Reinforcements
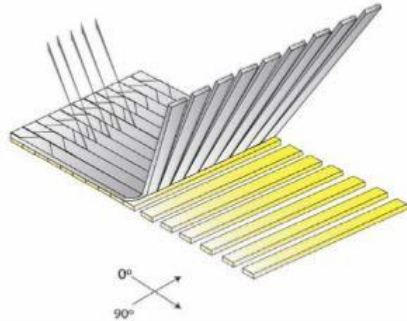
E-LT 3900

Fiber Type: E-Glass
Architecture: 0º/90º Biaxial
Dry Thickness: 0.042 in. / 1.07 mm
Total Weight: 39.70 oz/sq.yd / 1346 g/sq.m

Layer Number	Fiber Type	Fiber Orientation	Linear Density	Fiber Diameter	Sizing	Ends per Inch	Areal Wt.	
			Yield	µm	Weight		oz/yd²	g/m²
1*	E-Glass	0 Degree	113	24	0.55%	7.00	35.68	1210
2**	E-Glass	90 Degree	1800	13	0.55%	10.50	3.36	114
Stitch Yarn	Stitch Type		Fiber Type		Gauge	Fiber Areal Weight:	39.04	1324
	Mod. Tricot 1-0/0-1/2-1/1-2		100% Polyester		7 per inch	Fabric Areal Weight:	39.70	1346

* PPG Hybon 2026
**PPG Hybon 2022 or Hybon 2026

Vectorply Corporation
3500 Lakewood Drive Phenix City, AL 36867
tel. 334-291-7704 fax. 334-291-7743

HEXION

Technical Data Sheet

Issued: August 2006

EPIKOTE™ Resin MGS™ RIMR 135 and
EPIKURE™ Curing Agent MGS™ RIMH 134–RIMH 137

CHARACTERISTICS

Approval	German Lloyd
Application	Specially designed for infusion processes (RMT, SCRIMP/VARI); rotor blades for wind turbines, boat and shipbuilding, sports equipment
Operational Temperature	-60 °C up to +50 °C (-76 °F up to 122 °F) without heat treatment -60 °C bis +80 °C (-76 °F up to 176 °F) after heat treatment
Processing	At temperatures between 10 °C and 50 °C (50-122 °F) due to the very low mixing viscosity especially suited for infusion, injection and pultrusion
Features	Very low viscosity, excellent initial curing properties at room temperature, pot life from approx. 0,5 hours to approx. 4 hours, short curing times at high temperatures
Storage	Shelf life of 24 months in originally sealed containers

APPLICATION

Very low viscosity laminating resin system with different pot lives for processing of glass, carbon and aramide fibers. Due to its good mechanical properties, this system is suitable for the production of components featuring high static and dynamic loadability.

The range of pot lives is between approx. 0,5 hour and 3-4 hours. The parts can be worked and demoulded after curing at room temperature. Curing at higher temperatures (up to approx. 80-100 °C, 176-212 °F) is possible, depending on layer thickness and geometry of the parts to be manufactured. The curing times can be reduced to a few minutes by this.

Adding internal parting agents, such as zinc stearate, etc., has proven useful for pultrusion processes. Profiles with good surface qualities are obtained. Depending on profile geometry, mould temperatures in the range of 180-230 °C (356-446 °F) are possible, thus permitting high drawing speeds.

The mixing viscosity is very low, which is especially advantageous for infusion and injection processes. It may be lowered to approx. 150 mPas by heating the resin mass (see diagram). This means that even complicated molded parts with long flow paths can be easily infused. The temperature rise with hardener RIMH 137 remains very low up to a mold temperature of approx. 30 °C, so that even parts of greater thickness can be produced at elevated temperatures.

The infusion resin system does not contain any unreactive components. The raw materials used feature a

very low vapor pressure. This permits processing of the material under vacuum even at elevated temperatures (VARIM process). Compatibility problems are not to be expected in combination with UP gelcoats, various paints (e.g. PUR-based), etc. However, comprehensive tests are indispensable.

The relevant industrial safety regulations for the handling of epoxy resins and hardeners and our instructions for safe processing are to be observed.

The resin and hardeners can be stored for at least 24 months in their carefully sealed original containers. The resin and hardeners may crystallise at temperatures below +15 °C (59 °F). The crystallisation is visible as a clouding or solidification of the contents of the container. Before processing, the crystallisation must be removed by warming up. Slow warming up to approx. 50-60 °C (122-140 °F) in a water bath or oven and stirring or shaking will clarify the contents of the container without any loss of quality. Use only completely transparent products. Before warming up, open containers slightly to permit equalization of pressure. Caution during warm-up! Do not warm up over an open flame! While stirring up, use safety equipment (gloves, eyeglasses, respirator).

SPECIFICATIONS

		Infusion Resin RIM 135
Density	[g/cm³]	1,13 - 1,17
Viscosity	[mPas]	700 - 1.100
Epoxy equivalent	[g/equivalent]	166 - 185
Epoxy value	[equivalent/100g]	0,54 - 0,60
Refractory index		1,548- 1,552

		Hardener RIMH 134	Hardener RIMH 137
Density	[g/cm³]	0,93 - 1,00	0,93 - 0,98
Viscosity	[mPas]	10 - 80	10 - 50
Amine Value	[mg KOH/g]	550 - 700	400 - 600
Refractory index		1,4900 - 1,5000	1,460 - 1,463

Measuring conditions: measured at 25 °C / 77 °F

EPIKOTE Resin MGS RIMR 135 and EPIKURE Curing Agent MGS RIMH 134–RIMH 137

MECHANICAL DATA

Mechanical Data of Neat Resin		
Density [g/cm³]		1,18 - 1,20
Flexural strength	[N/mm²]	90 - 120
Modulus of elasticity	[kN/mm²]	2,7 - 3,2
Tensile strength	[N/mm²]	60 - 75
Compressive strength	[N/mm²]	80 - 90
Elongation of break	[%]	8 - 16
Impact strength	[KJ/m²]	70 - 80
Water absorption at 23 °C	24 h [%] 7 d [%]	0,10 - 0,20 0,20 - 0,50
Fatigue strength under reversed bending stresses acc. to DLR Brunsw.	10% 90%	exp. $> 1 \times 10^6$ exp. $> 2 \times 10^6$
Curing: 24 h at 23° C (74° F) + 15 h at 60° C (140° F), partly cured/full cure Typical data according to WL 5.3203 Parts 1 and 2 of the GERMAN AVIATION MATERIALS MANUAL		

Advice: Mechanical data are typical for the combination of laminating resin RIMR 135 with hardener RIMH 137. Data can differ in other applications.

3M
Scotch-Weld™
Epoxy Adhesives
DP460 Off-White • DP460 NS

Technical Data	**March, 2004**

Product Description

3M™ Scotch-Weld™ Epoxy Adhesives DP460 Off-White and DP460 NS are high performance, two-part epoxy adhesives offering outstanding shear and peel adhesion, and very high levels of durability.

Features

- High shear strength
- High peel strength
- Outstanding environmental performance
- Easy mixing
- Controlled flow
- 60 minute worklife
- Non sag (Scotch-Weld DP460 NS)

Typical Uncured Physical Properties

Note: The following technical information and data should be considered representative or typical only and should not be used for specification purposes.

Product		Scotch-Weld Epoxy Adhesive DP460 Off-White	Scotch-Weld Epoxy Adhesive DP460 NS
Viscosity (approx.) @ 73°F (23°C)	Base Accelerator	20,000-50,000 cps 8,000-14,000 cps	150,000-275,000 cps 8,000-14,000 cps
Base Resin	Base Accelerator	epoxy amine	epoxy amine
Color	Base Accelerator	white amber	white amber
Net Weight Lbs./Gallon	Base Accelerator	9.3-9.7 8.8-9.2	9.3-9.7 8.8-9.2
Mix Ratio (B:A)	Volume Weight	2:1 2:0.96	2:1 2:0.96
Worklife, 73°F (23°C)	20 g mixed 10 g mixed 5 g mixed	60 minutes 75 minutes 90 minutes	60 minutes 60 minutes 60 minutes

Scotch-Weld™
Epoxy Adhesives
DP460 Off-White • DP460 NS

Typical Cured Thermal Properties

Note: The following technical information and data should be considered representative or typical only and should not be used for specification purposes.

Product		3M™ Scotch-Weld™ Epoxy Adhesive DP460 Off-White	3M™ Scotch-Weld™ Epoxy Adhesive DP460 NS
Physical Color		Opaque, off-white	Off-white
Shore D Hardness		75-80	78-84
Thermal Coefficient of Thermal Expansion (in./in./°C)	Below Tg	59×10^{-6}	74.44×10^{-6}
	Above Tg	159×10^{-6}	166×10^{-6}
Thermal Conductivity (btu - ft./ft.^{2} - hr. - °F) @ 45°C		0.104	0.104
Electrical Dielectric Strength (ASTM D 149)		1100 volts/mil	727 volts/mil
Volume Resistivity (ASTM D 257)		2.4×10^{14} ohm-cm	3.25×10^{15} ohm-cm

Typical Curing Characteristics

Note: The following technical information and data should be considered representative or typical only and should not be used for specification purposes.

Rate of Strength Build-Up
Aluminum, Overlap Shear (7 mil Bondline) (ASTM D 1002-72)
Bonds Tested at 73°F (23°C)
Scotch-Weld Epoxy Adhesive DP460 Off-White

Time in Oven	Cure Temperature		
	73°F (23°C)	120°F[1] (49°C)	140°F[1] (60°C)
30 min.	—	<50	3000/60[2]
60	—	1300	4500/60[2]
90	—	4300/60[2]	—
2 hr.	—	4400/60[2]	4800
3	—	4800/60[2]	—
5	400	—	—
6	1000	—	—
7	3500	—	—
24	4000/60[2]	—	—

Scotch-Weld Epoxy Adhesive DP460 NS

Time in Oven	Cure Temperature		
	73°F (23°C)	120°F[1] (49°C)	160°F[1] (71°C)
15 min.	—	–	4860
30	—	10	5250
60	—	2800	5300
2 hr.	1	5050	5470
4	46	5400	5320
6	970	5570	5140
24	4500	–	5210

[1]This represents the oven temperature to which the bonds were subjected for the prescribed time. The average bondline temperature during the cure time will be somewhat lower than the oven temperature.

[2]The value in the denominator is the expected minimum 73°F (23°C) T-peel strength (piw) measured after the indicated cure cycle.

NOTE: The data in this Technical Data Sheet were generated using the 3M™ EPX™ Applicator System equipped with an EPX static mixer, according to manufacturer's directions. Thorough hand-mixing will afford comparable results.

Scotch-Weld™
Epoxy Adhesives
DP460 Off-White • DP460 NS

Typical Adhesive Performance Characteristics

Note: The following technical information and data should be considered representative or typical only and should not be used for specification purposes.

Substrates and Testing

A. Overlap Shear (ASTM D 1002-72)

Overlap shear (OLS) strengths were measured on 1 in. wide 1/2 in. overlap specimens. These bonds were made individually using 1 in. x 4 in. pieces of substrate except for aluminum. Two panels 0.063 in. thick, 4 in. x 7 in. of 2024T-3 clad aluminum were bonded and cut into 1 in. wide samples after 24 hours. The thickness of the bondline was 0.005-0.008 in. All strengths were measured at 73°F (23°C) except where noted.

The separation rate of the testing jaws was 0.1 in. per minute for metals, 2 in. per minute for plastics and 20 in. per minute for rubbers. The thickness of the substrates were: steel, 0.060 in.; other metals, 0.05-0.064 in.; rubbers, 0.125 in.; plastics, 0.125 in.

B. T-peel (ASTM D 1876-61T)

T-peel strengths were measured on 1 in. wide bonds at 73°F (23°C). The testing jaw separation rate was 20 inches per minute. The substrates were 0.032 in. thick.

C. Bell Peel (ASTM D 3167)

Bell peel strengths were measured on 1/2 in. wide bonds at the temperatures noted. The testing jaw separation rate was 6 in. per minute. The bonds are made with 0.064 in. bonded to 0.025 in. thick adherends.

D. Cure Cycle

With the exception of Rate of Strength Build-Up Tests, all bonds, were cured 7 days at 73°F (23°C) at 50% RH before testing or subjected to further conditioning or environmental aging.

Aluminum, Overlap Shear, at Temperature (PSI)

	3M™ Scotch-Weld™ Epoxy Adhesive DP460 Off-White	3M™ Scotch-Weld™ Epoxy Adhesive DP460 N S
-67°F (-55°C)	4500	4900
73°F (23°C)	4500	4650
180°F (82°C) (15 min.)[1]	700	1360
(30 min.)[1]	1000	1810
(60 min.)[1]	1400	2630
(4 hr.)[1]	2500	2680
250°F (121°C) (15 min.)[1]	220	420

[1]Represents time in test chamber oven before test.

Metals, Overlap Shear, Tested @ 73°F (23°C) (PSI)

		Scotch-Weld Epoxy Adhesive DP460 Off-White	Scotch-Weld Epoxy Adhesive DP460 N S
Aluminum	Etched	4500	4500
	Oakite degrease	3200	2300
	MEK/abrade/MEK	3500	2670
Cold Rolled Steel	Oakite degrease	3500	—
	MEK/abrade/MEK	2800	3600
Copper-	MEK/abrade/MEK	4000	4400
Brass-	MEK/abrade/MEK	—	3400
	CDA 260	4000	—
	Cartridge	4200	—
Stainless Steel	MEK/abrade/MEK	4000	2400
Galvanized Steel-	Oakite degrease		
	Hot dipped	2000	2480
	Electrodeposited	2100	3000

Scotch-Weld™
Epoxy Adhesives
DP460 Off-White • DP460 NS

Typical Adhesive Performance Characteristics (continued)

Note: The following technical information and data should be considered representative or typical only and should not be used for specification purposes.

Substrates and Testing *(continued)*

Aluminum, T-Peel (PIW), at Temperature

Aluminum - etched (17-20 mil bondline)

	3M™ Scotch-Weld™ Epoxy Adhesive DP460 Off-White	3M™ Scotch-Weld™ Epoxy Adhesive DP460 N S
-67°F (-55°C)	5-10	3-5
73°F (23°C)	60	60
180°F (82°C)	3-5	20

Metals, T-Peel, Tested @ 73°F (23°C) (PIW)

		Scotch-Weld Epoxy Adhesive DP460 Off-White	Scotch-Weld Epoxy Adhesive DP460 N S
Aluminum, etched	17-20 mil bondline	60	not tested
	5-8 mil bondline	50	
Cold Rolled Steel	17-20 mil bondline Oakite degreased MEK/abrade/MEK	40 25	not tested

Aluminum Bell Peel (PIW), at Temperature (ASTM D 3167)

	Scotch-Weld Epoxy Adhesive DP460 N S
-67°F (-55°C)	19
73°F (23°C)	77
180°F (82°C)	39

Other Substrates, Overlap Shear Tested @ 73°F (23°C)

Substrate	Surf. Prep. 1		Surf. Prep. 2	
	Scotch-Weld Epoxy Adhesive DP460 Off-White	Scotch-Weld Epoxy Adhesive DP460 N S	Scotch-Weld Epoxy Adhesive DP460 Off-White	Scotch-Weld Epoxy Adhesive DP460 N S
ABS	300	345	575	572
PVC	500	815[3]	350	313[3]
Polycarbonate	400	380	500	390
Polyacrylic	220	210	330	270
Polystryene	450	320	475[3]	490
FRP	800	570	1000[3]	1379[3]
Phenolic	1400[3]	1210[3]	1400[3]	1231[3]
SBR/Steel	150[3]	130	140[3]	239[3]
Neoprene/Steel	100	90	120[3]	114[3]

[1]Isopropyl Alcohol Wipe. See Surface Preparation Section D for additional information.

[2]Isopropyl Alcohol/Abrade/Isopropyl Alcohol: See Surface Preparation Section E for additional information.

[3]Substrate failure.

«FREKOTE®

770-NC™

October 2009

PRODUCT DESCRIPTION

770-NC™ provides the following product characteristics:

Technology	Mold Release
Appearance	Clear, colorless™
Chemical Type	Solvent Based Polymer
Odor	Solvent
Cure	Room temperature cure
Cured Thermal Stability	≤400 °C
Application	Release Coatings
Application Temperature	15 to 60 °C
Specific Benefit	• No contaminating transfer • High gloss finish • High slip • No mold build-up • Low odor

770-NC™ offers excellent release for various molding applications. 770-NC™ can be used for the release of epoxies, polyester resins, vinyl ester resins, thermoplastics, adhesives, and rotationally molded plastics. This product is particulary well suited for tougher to release processes such as filament winding and non gel coated polyester and fiberglass molding.

TYPICAL PROPERTIES OF UNCURED MATERIAL

Specific Gravity @ 25 °C   0.715 to 0.725™

Flash Point - See MSDS

GENERAL INFORMATION

This product is not recommended for use in pure oxygen and/or oxygen rich systems and should not be selected as a sealant for chlorine or other strong oxidizing materials

For safe handling information on this product, consult the Material Safety Data Sheet (MSDS).

Mold Preparation

Cleaning:

Mold surfaces must be thoroughly cleaned and dried. All traces of prior release must be removed. This may be accomplished by using Frekote® PMC or other suitable cleaner. Frekote® 915WB™ or light abrasives can be used for heavy build-up.

Sealing New/Repaired Molds:

Occasionally, green or freshly repaired molds are rushed into service prior to complete cure causing an increased amount of free styrene on the mold surface. Fresh or "production line" repairs, new fiberglass and epoxy molds should be cured per manufacturer's instructions, usually a minimum of 2 -3 weeks at 22°C before starting full-scale production. Fully cured previously unused molds should be sealed before use. This can be accomplished by applying one to two coats of an appropriate Frekote® mold sealer, following the directions for use instructions. Allow full cure of the appropriate Frekote® mold sealer before you apply the first coat of 770-NC™ as outlined in the directions of use.

Directions for use:

1. 770-NC™ can be applied to mold surfaces at room temperature up to 60°C by spraying, brushing or wiping with a clean lint-free, cloth. When spraying ensure a dry air source is used or use an airless spray system. Always use in a well ventilated area.
2. Wipe or spray on a smooth, thin, continuous, wet film. Avoid wiping or spraying over the same area that was just coated until the solvent has evaporated. If spraying, hold nozzle 20 to 30cm from mold surface. It is suggested that small areas be coated, working progressively from one side of the mold to the other.
3. Initially, apply 2 to 3 base coats allowing 5 to 10 minutes between coats for solvent evaporation .
4. Allow the final coat to cure for 5 to 10 minutes at 22°C.
5. Maximum releases will be obtained as the mold surface becomes conditioned to 770-NC™. Performance can be enhanced by re-coating once, after the first few initial pulls.
6. When any release difficulty is experienced, the area in question can be "touched-up" by re-coating the entire mold surface or just those areas where release difficulty is occurring.
7. **NOTE**: 770-NC™ is moisture sensitive, keep container tightly closed when not in use. The product should always be used in a well ventilated area.
8. **Precaution:** Users of closed mold systems(rotomolding) must be certain that solvent evaporation is complete and that all solvent vapors have been ventilated from the mold cavity prior to closing the mold. An oil-free compressed air source can be used to assist in evaporation of solvents and ventilation of the mold cavity.

Mold Touch up

Touch up coats should only be applied to areas where poor release is noticed and should be applied using the same method as base coats. This will reduce the possibility of release agent or polymer build-up. The frequency of touch ups will depend on the polymer type, mold configuration, and abrasion parameters.

Loctite Material Specification™

LMS dated May 29, 2007. Test reports for each batch are available for the indicated properties. LMS test reports include selected QC test parameters considered appropriate to specifications for customer use. Additionally, comprehensive controls are in place to assure product quality and consistency. Special customer specification requirements may be coordinated through Henkel Quality.

(Henkel)

Storage
The product is classified as flammable and must be stored in an appropriate manner in compliance with relevant regulations. Do not store near oxidizing agents or combustible materials. Store product in the unopened container in a dry location. Storage information may also be indicated on the product container labelling.
Optimal Storage: 8 °C to 21 °C. Storage below 8 °C or greater than 28 °C can adversely affect product properties. Material removed from containers may be contaminated during use. Do not return product to the original container. Henkel cannot assume responsibility for product which has been contaminated or stored under conditions other than those previously indicated. If additional information is required, please contact your local Technical Service Center or Customer Service Representive.

Conversions
(°C x 1.8) + 32 = °F
kV/mm x 25.4 = V/mil
mm / 25.4 = inches
μm / 25.4 = mil
N x 0.225 = lb
N/mm x 5.71 = lb/in
N/mm² x 145 = psi
MPa x 145 = psi
N·m x 8.851 = lb·in
N·m x 0.738 = lb·ft
N·mm x 0.142 = oz·in
mPa·s = cP

Note
The data contained herein are furnished for information only and are believed to be reliable. We cannot assume responsibility for the results obtained by others over whose methods we have no control. It is the user's responsibility to determine suitability for the user's purpose of any production methods mentioned herein and to adopt such precautions as may be advisable for the protection of property and of persons against any hazards that may be involved in the handling and use thereof. In light of the foregoing, **Henkel Corporation specifically disclaims all warranties expressed or implied, including warranties of merchantability or fitness for a particular purpose, arising from sale or use of Henkel Corporation's products. Henkel Corporation specifically disclaims any liability for consequential or incidental damages of any kind, including lost profits.** The discussion herein of various processes or compositions is not to be interpreted as representation that they are free from domination of patents owned by others or as a license under any Henkel Corporation patents that may cover such processes or compositions. We recommend that each prospective user test his proposed application before repetitive use, using this data as a guide. This product may be covered by one or more United States or foreign patents or patent applications.

Trademark usage
Except as otherwise noted, all trademarks in this document are trademarks of Henkel Corporation in the U.S. and elsewhere. ® denotes a trademark registered in the U.S. Patent and Trademark Office.

Reference 0.0

Americas
+860.571.5100

Europe
+49.89.320800.1800

Asia
+86.21.2891.8863

For the most direct access to local sales and technical support visit www.henkel.com/industrial

98

AE SENSOR CALIBRATION CERTIFICATE

PHYSICAL ACOUSTICS CORPORATION
A MISTRAS Holdings Company

Sensor Name: WDI-AST
Sensor S/N: CB71
Comment:

Max. Value (dB): -25.89
Peak Freq.(kHz): 551.76

Test Date: 12/26/2012
Tested By: J.G

PAC Certifies that this sensor meets all performance, environmental and physical standards established in applicable PAC specifications. Calibration methodology based on ASTM standard E976- "Guide for Determining the Reproducibility of AE Sensor Response."

APPENDIX B

APPENDIX B: Test Data

ASTM Designation: D 3518/D 3518M – 94[ε1]

Standard Test Method for
In-Plane Shear Response of Polymer Matrix Composite
Materials by Tensile Test of a ±45° Laminate[1]

This standard is issued under the fixed designation D 3518/D 3518M; the number immediately following the designation indicates the year of original adoption or, in the case of revision, the year of last revision. A number in parentheses indicates the year of last reapproval. A superscript epsilon (ε) indicates an editorial change since the last revision or reapproval.

This standard has been approved for use by agencies of the Department of Defense.

ε[1] NOTE—Title changed from "practice" to "test method" in August 1995.

1. Scope

1.1 This test method determines the in-plane shear response of polymer matrix composite materials reinforced by high-modulus fibers. The composite material form is limited to a continuous-fiber reinforced composite ± 45° laminate capable of being tension tested in the laminate χ-direction.

1.2 *This standard does not purport to address all of the safety concerns, if any, associated with its use. It is the responsibility of the user of this standard to establish appropriate safety and health practices and determine the applicability of regulatory limitations prior to use.*

1.3 The values stated in either SI units or inch-pound units are to be regarded separately as standard. Within the text the inch-pound units are shown in brackets. The values stated in each system are not exact equivalents; therefore, each system must be used independently of the other. Combining values from the two systems may result in nonconformance with the standard.

2. Referenced Documents

2.1 *ASTM Standards:*

D 883 Terminology Relating to Plastics[2]

D 3039/D 3039M Test Method for Tensile Properties of Polymer Matrix Composite Materials[3]

D 3878 Terminology of High-Modulus Reinforcing Fibers and Their Composites[3]

E 6 Terminology Relating to Methods of Mechanical Testing[4]

E 111 Test Method for Young's Modulus, Tangent Modulus, and Chord Modulus[4]

E 177 Practice for Use of Terms Precision and Bias in ASTM Test Methods[5]

E 456 Terminology Relating to Quality and Statistics[5]

E 1309 Guide for the Identification of Composite Materials in Computerized Material Property Databases[3]

E 1313 Guide for Recommended Formats for Data Records Used In Computerization of Mechanical Test Data for Metals[6]

E 1434 Guide for Development of Standard Data Records for Computerization of Mechanical Test Data for High-Modulus Fiber-Reinforced Composite Materials[3]

E 1471 Guide for the Identification of Fibers, Fillers, and Core Materials in Computerized Material Property Databases[3]

3. Terminology

3.1 *Definitions*—Terminology D 3878 defines terms relating to high-modulus fibers and their composites. Terminology D 883 defines terms relating to plastics. Terminology E 6 defines terms relating to mechanical testing. Terminology E 456 and Practice E 177 define terms relating to statistics. In the event of a conflict between terms, Terminology D 3878 shall have precedence over the other standards.

3.2 *Definitions of Terms Specific to This Standard:*

NOTE 1—If the term represents a physical quantity, its analytical dimensions are stated immediately following the term (or letter symbol) in fundamental dimension form, using the following ASTM standard symbology for fundamental dimensions, shown within square brackets: [M] for mass, [L] for length, [T] for time, [Θ] for thermodynamic temperature, and [nd] for non-dimensional quantities. Use of these symbols is restricted to analytical dimensions when used with square brackets, as the symbols may have other definitions when used without the brackets.

3.2.1 *±45° laminate*—in *laminated composites,* a balanced, symmetric lay-up composed only of + 45° plies and −45° plies. (See also *ply orientation.*)

3.2.2 *balanced, adj*— in *laminated composites,* having, for every off-axis ply oriented at +θ, another ply oriented at −θ that is of the same material system and form.

3.2.3 *lamina, n—pl. laminae,* in *laminated composites,* a single, thin, uniform layer that is the basic building block of a laminate. (Syn. *ply*).

D 3518/D 3518M

3.2.4 *material coordinate system, n—in laminated composites*, a 123 Cartesian coordinate system describing the principle material coordinate system for a laminated material, where the 1-axis is aligned with the ply principal axis, as illustrated in Fig. 1. (See also *ply orientation, ply principal axis,* and *principal material coordinate system.*)

3.2.5 *nominal value, n—*a value, existing in name only, assigned to a measurable property for the purpose of convenient designation. Tolerances may be applied to a nominal value to define an acceptable range for the property.

3.2.6 *off-axis, adj— in laminated composites*, having a ply orientation that is neither 0 nor 90°.

3.2.7 *ply, n—in laminated composites*, synonym for *lamina.*

3.2.8 *ply orientation, n, θ—in laminated composites*, the angle between a reference direction and the ply principal axis. The angle is expressed in degrees, greater than −90° but less than or equal to +90°, and is shown as a positive quantity when taken from the reference direction to the ply principal axis, following the right-hand-rule.

3.2.8.1 *Discussion—*The reference direction is usually related to a primary load-carrying direction.

3.2.9 *ply principal axis, n— in laminated composites*, the coordinate axis in the plane of each lamina that defines the ply orientation. (See also *ply orientation* and *material coordinate system.*)

3.2.9.1 *Discussion—*The ply principal axis will, in general, be different for each ply of a laminate. The angle that this axis makes relative to a reference axis is given by the ply orientation. The convention is to align the ply principal axis with the direction of maximum stiffness (for example, the fiber direction of unidirectional tape, or the warp direction of fabric reinforced material).

3.2.10 *principal material coordinate system, n—*a coordinate system having axes that are normal to planes of symmetry within the material. (See also *material coordinate system.*)

3.2.10.1 *Discussion—*Common usage, at least for Cartesian coordinate systems (for example, 123 or xyz), aligns the first axis of the principal material coordinate system with the direction of highest property value; for elastic properties, the axis of greatest elastic modulus is aligned with the 1 or x axes.

3.2.11 *symmetric, adj— in laminated composites*, when the constituents, material form, and orientation for the plies located on one side of the laminate midplane are the mirror image of the plies on the other side of the midplane.
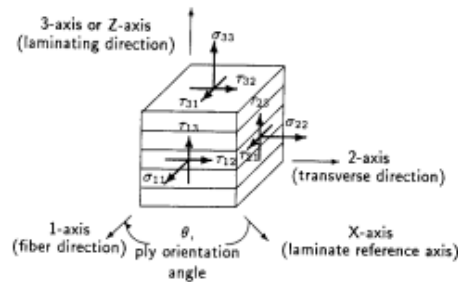
3.2.12 *transition region, n—*a strain region of a stress-strain or strain-strain curve over which a significant change in the slope of the curve occurs within a small strain range.

3.2.12.1 *Discussion—*Many filamentary composite materials exhibit a non-linear stress/strain response during loading, such as seen in plots of either longitudinal stress versus longitudinal strain or transverse strain versus longitudinal strain. In certain cases the non-linear response may be conveniently approximated by a bilinear fit. There are varying physical reasons for the existence of a transition region. Common examples include: matrix cracking under tensile loading and ply delamination.

3.3 *Symbols:*

3.3.1 *A—*cross-sectional area of a coupon.

3.3.2 *CV—*coefficient of variation statistic of a sample population for a given property (in percent).

3.3.3 $F_{12}°$ *(offset)—*the value of the τ_{12} shear stress at the intersection of the shear chord modulus of elasticity and the stress stress curve, when the modulus is offset along the shear strain axis from the origin by the reported strain offset value.

3.3.4 G_{12}—in-plane shear modulus of elasticity.

3.3.4.1 *Discussion—*Indices 1 and 2 indicate the fiber direction and transverse to the fiber direction in the plane of the ply, respectively, as illustrated in Fig. 2.

3.3.5 *n—*number of coupons per sample population.

3.3.6 *P—*load carried by test coupon.

3.3.7 P^m—the load carried by test coupon that is the lesser of the 1) maximum load prior to failure, or 2) load at 5 % shear strain.

3.3.8 s_{n-1}—standard deviation statistic of a sample population for a given property.

3.3.9 x_i—test result for an individual coupon from the sample population for a given property.

3.3.10 $\bar{x}$—mean or average (estimate of mean) of a sample population for a given property.

3.3.11 ϵ—general symbol for strain, whether normal strain or shear strain.

FIG. 1 Material Coordinate System
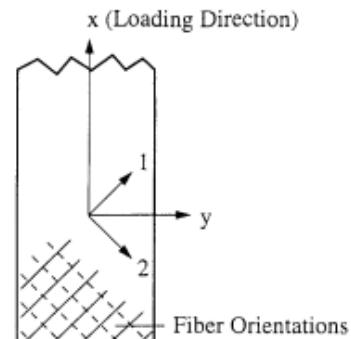
x and *y* represent the Specimen or Reference Axes, while 1 and 2 represent the Material or Local Axes

FIG. 2 Definition of Specimen and Material Axes

3.3.12 ε—indicated normal strain from strain transducer or extensometer.

3.3.13 τ_{12}—shear stress on the plane perpendicular to the 1-axis that acts parallel to the 2-axis.

3.3.14 $\tau_{12}{}^m$—the calculated value of the τ_{12} shear stress taken at the lesser of 1) maximum shear stress prior to failure, or 2) shear stress at 5 % shear strain.

3.3.15 γ_{12}—shear strain on the plane perpendicular to the 1-axis that acts parallel to the 2-axis.

3.3.16 $\gamma_{12}{}^m$—the value of the γ_{12} shear strain at the maximum shear stress prior to failure, or 5 %, whichever is less.

4. Summary of Test Method

4.1 A uniaxial tension test of a ±45° laminate is performed in accordance with Test Method D 3039, although with specific restrictions on stacking sequence and thickness. Use of this test for evaluation of in-plane shear response was originally proposed by Petit[7] and was later improved by Rosen.[8] Using expressions derived from laminated plate theory, the in-plane shear stress in the material coordinate system is directly calculated from the applied axial load, and the related shear stress is determined from longitudinal and transverse normal strain data obtained by transducers. This data is used to create an in-plane shear stress-shear strain curve.

5. Significance and Use

5.1 This test method is designed to produce in-plane shear property data for material specifications, research and development, quality assurance, and structural design and analysis. Factors that influence the shear response and should therefore be reported include the following: material, methods of material preparation and lay-up, specimen stacking sequence and overall thickness, specimen preparation, specimen conditioning, environment of testing, specimen alignment and gripping, speed of testing, time at temperature, void content, and volume percent reinforcement. Properties that may be derived from this test method include the following:

5.1.1 In-plane shear stress versus shear strain response,

5.1.2 In-plane shear chord modulus of elasticity,

5.1.3 Offset shear properties,

5.1.4 Maximum in-plane shear stress for a ±45° laminate, and

5.1.5 Maximum in-plane shear strain for a ±45° laminate.

6. Interferences

6.1 *Impurity of Stress Field*—The material in the gage section of this specimen is not in a state of pure in-plane shear stress, as an in-plane normal stress component is present throughout the gage section and a complex stress field is present close to the free edges of the specimen. Although this test method is believed to provide reliable initial material response and can establish shear stress-shear strain response

well into the nonlinear region, the calculated shear stress values at failure do not represent true material strength values and should only be used with caution. Despite attempts to minimize these effects, the shear stress at failure obtained from this test method, even for otherwise identical materials that differ only in cured ply thickness or fabric areal weight, may have differing failure modes and may not be able to be statistically pooled. The technical basis for the further discussion below is taken from the paper by Kellas et al.[9]

6.1.1 *Effects of In-Plane Normal Stress Field*—Of particular concern is the in-plane stress component normal to the fiber direction. This component of stress is present in all plies and throughout the gage section of the specimen. The effect of this stress on a given ply is minimized by the fiber reinforcement of the neighboring plies. Since the ply constraint is reduced with increasing ply thickness, the thickness of the individual plies is an important parameter that influences both the shear stress-shear strain response and the ultimate failure load of this specimen.[10] Moreover, the surface plies of a given specimen, being constrained by only one neighboring ply (as opposed to interior plies, which are constrained by a ply on each side), represent the weakest link in a ±45° specimen. During the tensile loading of this test coupon, the first ply failures consist primarily of normal stress (or mixed mode) failures, rather than pure shear failures. Because of this, the actual material shear strength cannot be obtained from this test. Except for the case of materials capable of sustaining large axial test coupon strains (greater than about 3.0 %), the shear stress at failure is believed to underestimate the actual material shear strength.

6.1.2 *Total Thickness Effects*—As a result of the failure processes discussed above, the shear stress-shear strain response at higher strain levels depends upon the total number of plies. As the total number of plies in the specimen configuration is increased, the relative contribution of the two weak surface plies to the total load-carrying capacity is decreased. After the surface plies of the laminate fail, their portion of the load is redistributed to the remainder of the intact plies. The higher the total number of plies, the greater the chance that the remaining plies will be able to carry the load without immediate ultimate failure of the coupon. However, with each successive ply matrix failure the number of remaining intact plies diminishes, to the point where the applied load can no longer be carried. Due to this process higher ply count specimens tend to achieve higher failure loads. In order to minimize these effects, this test method requires the use of a homogeneous stacking sequence and requires a fixed number of plies, for which the only repeating plies are the two required for symmetry on opposite sides of the laminate mid-plane.

6.1.3 *Effects of Large Deformation*—Note that extreme fiber scissoring can occur in this specimen for the cases of ductile matrices, weak fiber/matrix interfaces, thick specimens with a

[7] Petit, D. H., "A Simplified Method of Determining the In-plane Shear Stress/Strain Response of Unidirectional Composites," *Composite Materials: Testing and Design, ASTM STP 460*, 1969, pp. 83–93.

[8] Rosen, B. W., "A Simple Procedure for Experimental Determination of the Longitudinal Shear Modulus of Unidirectional Composites," *Journal of Composite Materials*, October 1972, pp. 552–554.

[9] Kellas, S., Morton, J., and Jackson, K. E., "Damage and Failure Mechanisms in Scaled Angled-Ply Laminates," *Fourth Composites Symposium on Fatigue and Fracture, ASTM STP 1156*, W. Stinchcomb and Ashbaugh, N. E., Eds., ASTM, 1993, pp. 257–280.

[10] Repeating plies (adjacent plies at the same ply orientation) have an effect similar to thick plies, therefore this test method prohibits constructions with repeating plies.

D 3518/D 3518M

large number of repeated plies, or a combination of the above. Kellas et al suggest that a general rule of thumb for this specimen is that a fiber rotation of 1° takes place for every 2 % of axial strain (or every 3.5 % shear strain for commonly tested materials). Such fiber scissoring, if left unbounded, would lead to an unacceptable violation of the assumption in this test method of a nominal ±45° laminate. This is the principal rationale for terminating this test at a large strain level, even if load is still increasing on the specimen. This test method terminates data reporting at 5 % calculated shear strain; this limits fiber scissoring to about 1.5°, is approximately the limit of foil strain gage technology (if used), and is also well beyond the strain levels required for common engineering practice. Further details of the effects of stacking sequence, specimen geometry, and, in particular, specimen and ply thickness, are presented in the reference by Kellas et al.

6.1.4 *Effects of Edge Stresses*—Even though interlaminar stresses reach a maximum value near the free edges of this laminate, the effect of interlaminar stresses on the failure process of ±45° laminates is insignificant when compared to the effect of the normal stress component transverse to the fiber direction in the plane of the specimen. Therefore, the effect of specimen width is much less important than stacking sequence and specimen thickness effects.

6.1.5 *Effect of Axial Stress Non-Uniformity*—Both the shear stress and the shear modulus calculations depend upon the uniformity of the applied axial stress. Since the average applied load is used to calculate the shear stress this will not necessarily correspond to the stress in the vicinity of the measured shear strain, unless the axial stress is uniform throughout the volume of the stressed material. Therefore, the greater the degree of material inhomogeneity, such as with coarsely woven fabrics or materials with significant resin-rich regions, the greater the potential for inaccuracies in the measured response.

6.2 *Other*—Additional sources of potential data scatter in testing of composite materials are described in Test Method D 3039.

7. Apparatus

7.1 Apparatus shall be in accordance with Test Method D 3039. However, this test method requires that load-normal strain data be measured in both the longitudinal and transverse directions of the coupon.

8. Sampling and Test Specimens

8.1 *Sampling*—Sampling shall be in accordance with Test Method D 3039.

8.2 *Geometry*—The coupon geometry shall be in accordance with Test Method D 3039, as modified by the following:

8.2.1 The stacking sequence shall be [45/−45]ns, where 4 ≤ n ≤ 6 for unidirectional tape (16, 20, or 24 plies) and 2 ≤ n ≤ 4 for woven fabric (8, 12, or 16 plies). The recommended coupon width is 25 mm [1.0 in.], and the recommended coupon length range is 200–300 mm [8–12 in.], inclusive.

Note 2—Tabs, which are optional for the Test Method D 3039/D 3039M test coupon, are normally not required for successful conduct of this Practice.

8.3 *Specimen Preparation*—Specimen preparation shall be in accordance with Test Method D 3039/D 3039M.

9. Calibration

9.1 Calibration shall be in accordance with Test Method D 3039/D 3039M.

10. Conditioning

10.1 Conditioning shall be in accordance with Test Method D 3039/D 3039M.

11. Procedure

11.1 Perform a tension test on the ±45° laminate coupon in accordance with Test Method D 3039/D 3039M, with normal strain instrumentation in both longitudinal and transverse directions and continuous or nearly continuous load-normal strain data recording. If ultimate failure does not occur within 5 % shear strain, the data shall be truncated to the 5 % shear strain mark (see 6.1.3 for the explanation). When the data is truncated, for the purpose of calculation and reporting, this 5 % shear strain point shall be considered the maximum shear stress. Any truncation of data shall be noted in the report.

12. Calculation

12.1 *Maximum Shear Stress/Shear Stress*— Calculate the maximum in-plane shear stress for the ±45° laminate using Eq 1 and report the results to three significant figures. If the shear modulus is to be calculated, determine the shear stress at each required data point using Eq 2.

$$\tau_{12}^{m} = \frac{P^{m}}{2A} \tag{1}$$

$$\tau_{12i} = \frac{P_i}{2A} \tag{2}$$

where:
τ_{12}^{m} = maximum in-plane shear stress, MPa [psi],
P^{m} = maximum load at or below 5 % shear strain, N [lbf],
τ_{12i} = shear stress at *i*-th data point, MPa [psi],
P_i = load at *i*-th data point, N [lfb], and
A = cross-sectional area in accordance with Test Method D 3039/D 3039M, mm²[in.²].

12.2 *Shear Strain/Maximum Shear Strain*— If shear modulus or maximum shear strain is to be calculated, determine the shear strain at each required data point using Eq 3. The maximum shear strain is determined from Eq 4. Report the results to three significant figures.

$$\gamma_{12i} = \epsilon_{x_i} - \epsilon_{y_i} \tag{3}$$

$$\gamma_{12}^{m} = min\left\{ \begin{matrix} 5\% \\ \gamma_{12 \text{ at maximum shear stress}} \end{matrix} \right. \tag{4}$$

where:
γ_{12i} = shear strain at *i*-th data point, µε,
ϵ_{x_i} = longitudinal normal strain at *i*-th data point, µε, and
ϵ_{y_i} = lateral normal strain at *i*-th data point, µε,
γ_{12}^{m} = maximum shear strain, µε.

12.3 *Shear Modulus of Elasticity*:

12.3.1 *Chord Shear Modulus of Elasticity*— Calculate the chord shear modulus of elasticity using Eq 5, applied over a 4000 ± 200 µε shear strain range, starting with the lower strain point in the range of 1500–2500 µε, inclusive. Report the chord shear modulus of elasticity to three significant figures. Also

D 3518/D 3518M

report the shear strain range used in the calculation. A graphical example of chord shear modulus is shown in Fig. 3.

Note 3—The shear strain range of 2000–6000 με for shear modulus determination was selected, based on the shear response of a ±45° tensile coupon with a Poisson ratio near 1.0, to approximately correspond to the normal strain range of 1000–3000 με used to report the tensile chord modulus of elasticity in Test Method D 3039/D 3039M.

12.3.1.1 A different strain range must be used for materials that fail or exhibit a transition region (a significant change in the slope of the stress-strain curve) prior to 6000 με. In such cases the upper strain range value for the sample population shall be determined after testing; defined as 90 % of the average value of the upper limit of the essentially linear region, rounded downward to the nearest 500 με. Any presence of a transition region shall be reported, along with the strain range used.

$$G_{12}^{chord} = \frac{\Delta\tau_{12}}{\Delta\gamma_{12}} \qquad (5)$$

where:
G^{chord} = shear chord modulus of elasticity, GPa [psi],
$\Delta\tau_{12}$ = difference in applied shear stress between the two shear strain points, MPa [psi], and
$\Delta\gamma_{12}$ = difference between the two shear strain points (nominally 0.004).

12.3.2 *Shear Modulus of Elasticity (Other Definitions)*— Other definitions of elastic modulus may be evaluated and reported at the user's discretion. If such data is generated and reported, report also the definition used, the shear strain range used, and the results to three significant figures. Test Method E 111 provides additional guidance in the determination of Modulus of Elasticity.

Note 4—An example of another modulus definition is the secondary chord modulus of elasticity for materials that exhibit essentially bilinear stress-strain behavior.

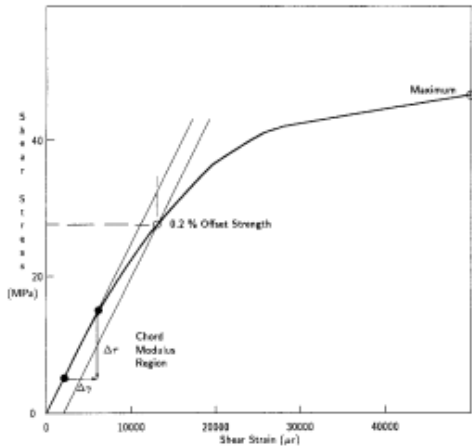12.4 *Offset Shear Strength*—If desired, an offset shear strength may be determined from the shear stress versus shear strain curve. Translate the shear chord modulus of elasticity line along the strain axis from the origin by a fixed strain value, and extend this line until it intersects the stress-strain curve. Determine the shear stress that corresponds to the intersection point and report this value, to three significant digits, as the offset shear strength, along with the value of the offset strain, as in:

$$F_{12}^{\circ} \ (0.2 \text{ % offset}) = 70 \text{ MPa} \qquad (6)$$

A graphical example of offset shear strength is shown in Fig. 3.

Note 5—In the absence of evidence suggesting the use of a more appropriate value, an offset strain value of 0.2 % is recommended.

12.5 *Statistics*—For each series of tests calculate the average value, standard deviation, and coefficient of variation (in percent) for each property determined:

$$\bar{x} = (\sum_{i=1}^{n} x_i)/n \qquad (7)$$

$$s_{n-1} = \sqrt{(\sum_{i=1}^{n} x_i^2 - n\bar{x}^2)/(n-1)} \qquad (8)$$

$$CV = 100 \times s_{n-1}/\bar{x} \qquad (9)$$

where:
$\bar{x}$ = sample mean (average),
s_{n-1} = sample standard deviation,
CV = sample coefficient of variation, in percent,
n = number of specimens, and
x_i = measured or derived property.

13. Report

13.1 The data reported with this test method include mechanical testing data, material identification data, and fiber filler, and core material identification data, and shall be in accordance with Guides E 1434, E 1309, and E 1471, respectively. Each data item discussed is identified as belonging to one of the following categories: (VT) required for reporting of a valid test result, (VM) required for valid material traceability,
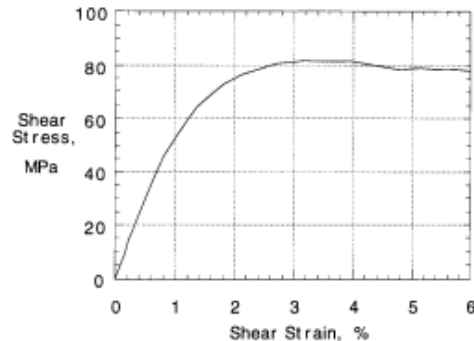

FIG. 3 Illustration of Modulus and Offset Strength Determination

FIG. 4 Typical Shear Stress-Shear Strain Curve for PMC with Low-Ductility Matrix
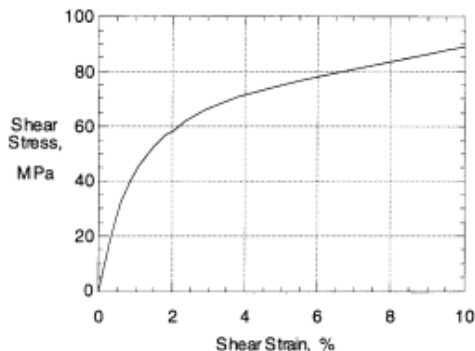
D 3518/D 3518M

FIG. 5 Typical Shear Stress-Shear Strain Curve for PMC with Ductile Matrix

(RT) recommended for maximum test method traceability, (RM) recommended for maximum material traceability, or (O) for optional data items. At a minimum, the report shall include all (VT) category items from Guide E 1434.

13.1.1 *Clarification of E 1434 Responses for This Test Method*:

13.1.1.1 *Field , Test Method*—The response shall be either "D 3518 – 94" or "D 3518M – 94," as appropriate.

13.1.1.2 *Field , Type of Test*—The response shall be "in-plane shear."

13.1.1.3 *Field B2, Specimen Orientation*— The response shall be "0.0"

13.1.1.4 *Block E, Transducer Block*—Used twice; once for each transducer.

13.1.1.5 *Block F, Specimen Geometry Block*— F6 (reinforcement volume) may be actual values, or it may be the average value for a sample. F7 (overall length) and F8 (gage length) may be actual values, or they may be the nominal or average value for the sample. F9 (area) is the actual area in accordance with Test Method D 3039/D 3039M. F10 must also satisfy Test Method D 3039/D 3039M.

13.1.1.6 *H32/K58, Progressive Damage Parameter*—The response shall be "0.2 % offset strength."

13.2 In addition to the data reported in accordance with Test Method D 3039/D 3039M, the report shall include the following information:

13.2.1 The revision level or date of issue of this test method.

13.2.2 Shear strain range used for chord shear modulus determination.

13.2.3 If another definition of shear modulus of elasticity is used in addition to chord shear modulus, describe the method used, the resulting correlation coefficient (if applicable), and the shear strain range used for the evaluation.

13.2.4 Individual values of shear modulus of elasticity, and the average, standard deviation, and coefficient of variation (in percent) values for the population.

13.2.5 Individual values of offset shear strength with the value of the offset strain, along with the average, standard deviation, and coefficient of variation (in percent) values for the population.

13.2.6 Individual maximum shear stresses, and the average, standard deviation, and coefficient of variation (in percent) values for the population. Note any test in which the failure load was less than the maximum load prior to failure.

13.2.7 Individual maximum shear strains, and the average value, standard deviation, and coefficient of variation (in percent) for the population. Note any test that was truncated to 5 % shear strain.

14. Precision and Bias

14.1 *Precision*—The data required for the development of a precision statement is not available for this test method. Committee D-30 is currently planning a round-robin test series for this test method in order to determine precision.

14.2 *Bias*—Bias cannot be determined for this test method as no acceptable reference standard exists.

15. Keywords

15.1 composite materials; shear modulus; shear properties; shear strength

APPENDIX

(Nonmandatory Information)

X1. SIGNIFICANT POINTS OF MAJOR REVISIONS TO THIS TEST METHOD

X1.1 *1991 Revision:*

X1.1.1 Updated the format to conform to 1989 Form and Style for ASTM Standards.

X1.1.2 Changed the Title and clarified the Scope.

X1.1.3 Transformed the document from an inch-pound standard to a dual-units standard.

X1.1.4 Updated the Terminology section.

X1.1.5 Added a new Interferences section.

X1.1.6 Added a new Calibration section.

X1.2 *1994 Revision:*

X1.2.1 Updated the format to conform to current practices of Committee D-30.

X1.2.2 Relaxed the scope to allow usage of this test method on material forms reinforced by woven fabrics.

X1.2.3 Extensively updated the Interferences section to discuss difficulty with this test method in obtaining reliable values for ultimate shear strength, and generally replaced the modifier ultimate with the term maximum throughout the text, as appropriate.

D 3518/D 3518M

X1.2.4 Added to the coupon geometry, limitations on the stacking sequence of the test specimen laminate, and provided recommended values for coupon length and width.

X1.2.5 Indirectly incurred several procedural changes, through changes to Test Method D 3039/D 3039M, including the approach to standard conditioning described by Test Method D 5229/D 5229M.

X1.2.6 Added the determinations and reporting of an offset shear strength.

X1.2.7 Shear modulus reporting now includes, at a minimum, a strain-range based chord shear modulus, and also requires documentation of the strain range used for any other modulus definitions reported.

X1.2.8 Shear stress/shear strain data has been truncated at 5 % shear strain.

X1.2.9 Ultimate shear strength has been removed from this practice, replaced by reporting of maximum shear stress, determinated as the maximum shear stress not exceeding 5 % shear strain.

X1.2.10 New illustrations have been included.

X1.2.11 Data reporting now follows Guide E 1434.

November 15, 2016
Daniel Samborsky, Montana State University

Summary of Vectorply E-LT-3800-10 Fabric Properties

Laminates were constructed using Vectorply E-LT-3800-10 fabric. Fabric construction is shown in Figure 1 and Table 1 details the fiber weights and directions. The laminates were infused with Hexion 135/1366 epoxy resin, cured at 25°C for 24 hours, followed by a 12 hour post-cure at 70°C. Table 2 details the laminates manufactured and Table 3 details the fiber volume fractions and average ply thickness. Following Figures summarize the test results and Table 5 compares the E-LT-3800 fabric with the E-LT-5500 fabric.

| Front | Back | Transmitted |

5 cm
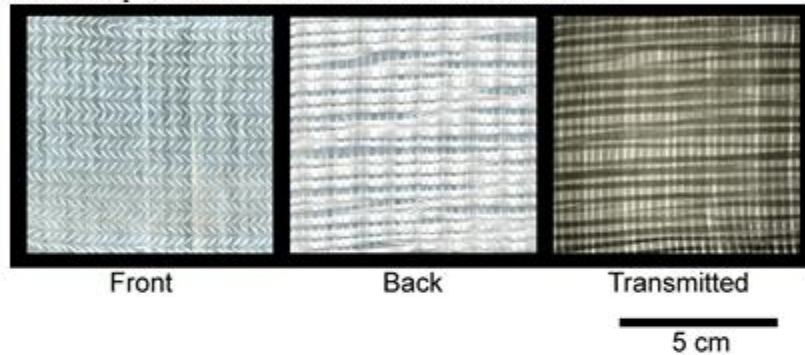
Figure 1. E-LT-3800-10 Fabric, Front Face (0), Back (b) Face and Transmitted Light.

Table 1. Fabric Construction Fiber Weights

Manufacturer and Product Designation	Fiber Areal Weight, g/m²						
	Total	0°	90°	-45°	+45°	mat	stitch
Vectorply E-LT-3800-10	1264	1138	114	0	0	0	12
Percentages	100%	90%	9%	0	0	0	1%
Vectorply E-LT-5500	1875	1728	114	0	0	0	33
Percentages	100%	0.92	6%	0	0	0	2%

Table 2. E-LT-3800-10 Laminates Tested

Layup	Tests
(0)₂	Longitudinal tension
(0)₄	Longitudinal compression
(90)₄	Transverse tension and compression
(+/-45)₂ₛ	Simulated shear

Table 3. Fiber Volume Fraction (ASTM D2584)

Fiber Volume Fraction, V_F		Thickness, Average mm/ply
Average, %	STD	
55.2	0.43	0.874

E-LT-3800, (0/b)(b/0), Hexion 135/1377, 24h at 25°C and 12h at 70°C
ASTM D3039   E calculated over 0.1 - 0.3% range

Coupon	Vf, %	UTS, MPa	%	E, GPa	nu
4072-100	57.3	1174	3.03	40.0	0.268
4072-101	56.9	1146	3.17	40.5	0.272
4072-102	54.7	1119	2.98	40.0	0.282
4072-103	55.3	1093	2.82	40.1	0.281
Average	56.1	1133	3.00	40.2	0.273
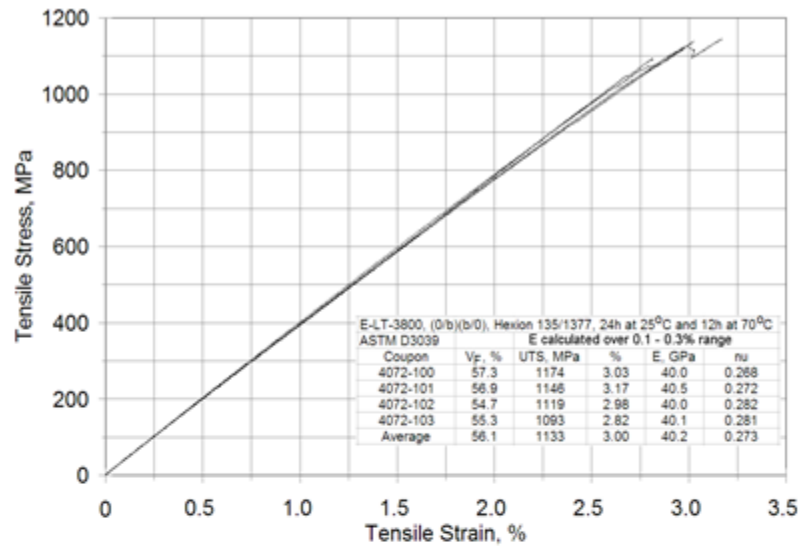
Figure 2. Summary of the Longitudinal Tension Tests.

E-LT-3800, (0/b)2S
Hexion 135/1377, 24h at 25°C and 12h at 70°C
ASTM D3039   E calculated over 0.05 - 0.10%

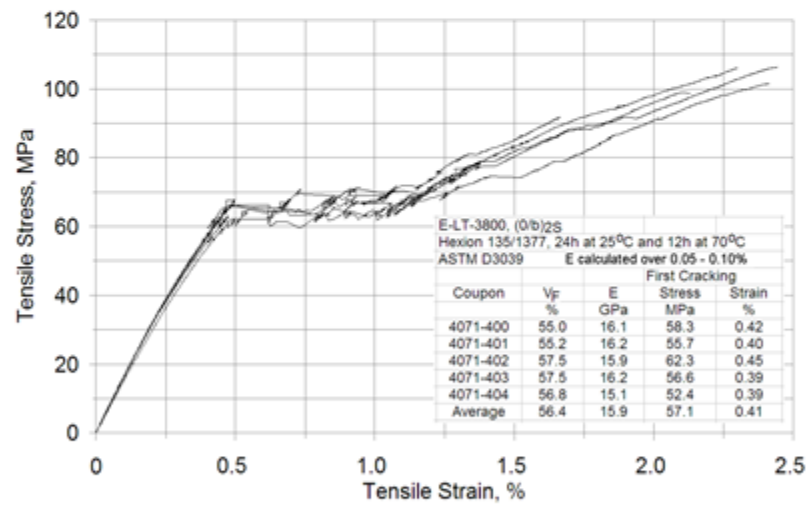| Coupon	Vf %	E GPa	First Cracking Stress MPa	Strain %
4071-400	55.0	16.1	58.3	0.42
4071-401	55.2	16.2	55.7	0.40
4071-402	57.5	15.9	62.3	0.45
4071-403	57.5	16.2	56.6	0.39
4071-404	56.8	15.1	52.4	0.39
Average	56.4	15.9	57.1	0.41

Figure 3. Summary of Transverse Tension Tests.
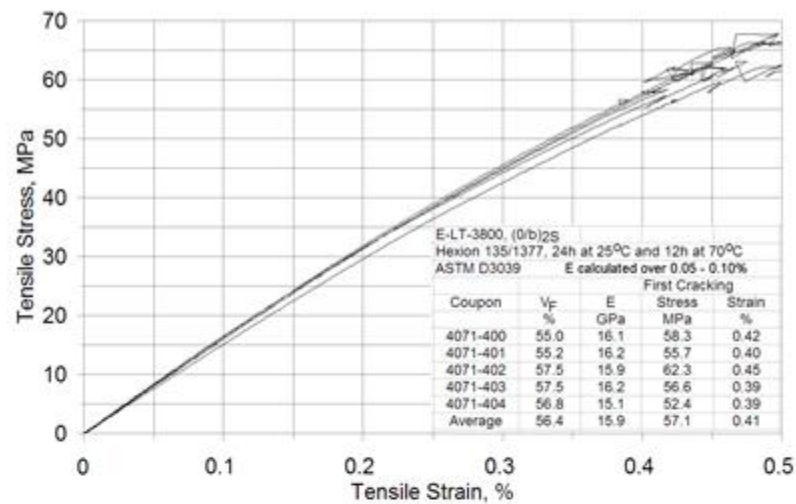
Figure 4. Summary of Transverse Tension Tests to First Matrix Cracking.

E-LT-3800, (0/b)2S
Hexion 135/1377, 24h at 25°C and 12h at 70°C
ASTM D3039   E calculated over 0.05 - 0.10%

Coupon	V_F %	E GPa	First Cracking Stress MPa	First Cracking Strain %
4071-400	55.0	16.1	58.3	0.42
4071-401	55.2	16.2	55.7	0.40
4071-402	57.5	15.9	62.3	0.45
4071-403	57.5	16.2	56.6	0.39
4071-404	56.8	15.1	52.4	0.39
Average	56.4	15.9	57.1	0.41
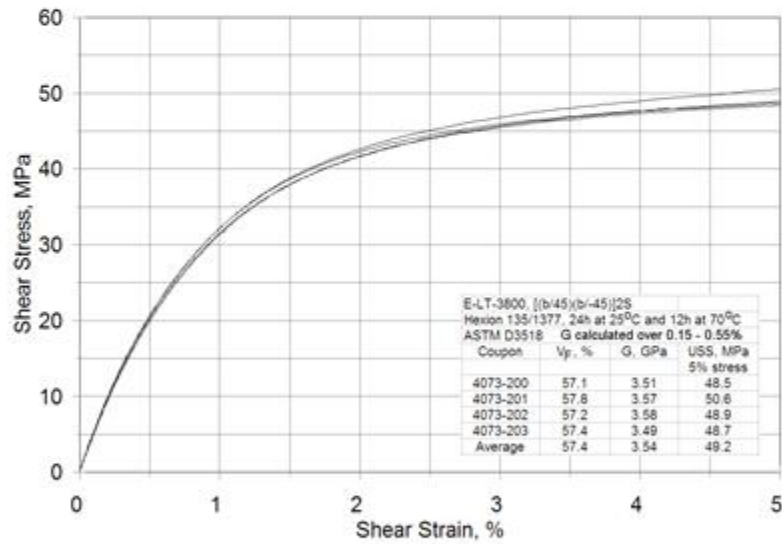
Figure 5. Summary of ASTM D3518 Simulated Shear Tests.

E-LT-3800, [(b/45)(b/-45)]2S
Hexion 135/1377, 24h at 25°C and 12h at 70°C
ASTM D3518   G calculated over 0.15 - 0.55%

Coupon	V_F, %	G, GPa	USS, MPa 5% stress
4073-200	57.1	3.51	48.5
4073-201	57.8	3.57	50.6
4073-202	57.2	3.58	48.9
4073-203	57.4	3.49	48.7
Average	57.4	3.54	49.2

Table 4, Summary of Compression Tests.

Longitudinal Compression, (0/b)2S			
Coupon	Thickness, mm	UCS, MPa	Calc. Strain, %
4071-412	3.40	-667	-1.66
4071-413	3.45	-829	-2.06

4071-414	3.47	-827	-2.06
4071-415	3.53	-689	-1.71
4071-416	3.40	-830	-2.07
	Average	-768	-1.91
Transverse Compression, (90/b)$_{2S}$			
4071-406	3.37	-221	-0.55
4071-407	3.49	-236	-0.59
4071-409	3.39	-245	-0.61
4071-410	3.49	-236	-0.59
4071-411	3.49	-201	-0.50
	Average	-228	-0.57

Table 5. Comparison of Mechanical Properties for E-LT-5500 and E-LT-3800 Fabrics

	E-LT-5500	E-LT-3800
Laminate Elastic Constants[1]	$V_F = 56.8 - 58.2\%$	$V_F = 55.0 -57.5$
Tensile Modulus E_L (GPa)	44.6	40.2
Tensile Modulus E_T (GPa)	17.0	15.9
Poisson Ratio ν_{LT}	0.262	0.273
Shear Modulus G_{LT} (GPa)	3.49	3.54

[1]Tensile and compressive moduli and Poisson's ratios determined from best fit line between 0.1% and 0.3% strain; shear moduli calculated from best fit line between 0.15% and 0.55% shear strain.

Laminate Strength Properties	Stress Direction	E-LT-5500 Strength (MPa) / Strain (%)	E-LT-3800 Strength (MPa) / Strain (%)
Tension	Longitudinal	1240 / 3.00	1133 / 3.00
Tension[2]	Transverse	43.9 / 0.28	57.1 / 0.41
Compression	Longitudinal	-774 / -1.83	-768 / -1.91
Compression	Transverse	-179 / -1.16	-228 / -0.57
Shear[3]	LT	55.8 / 5.00	49.2 / 5.00

[2]Transverse tension properties given for first cracking (knee) stress
[3]Shear values given for 5% strain following ASTM D5379

Table 6. Summary of Neat Resin Properties

Hexion 135/1366 Neat Resin Properties	
Tensile Modulus (GPa)	3.53
Poisson's Ratio	0.347
Compression Modulus (GPa)	2.98
Shear Modulus (GPa)	0.990
0.2% Offset Tensile Yield Stress (MPa)	41.0
Ultimate Tensile Strength (MPa)	76.3
Ultimate Tensile Strain (%)	4.20
0.2% Offset Compressive Yield Stress (MPa)	-64.7
Ultimate Compressive Strength (MPa)	-91.0
Ultimate Compressive Strain (%)	-5.38
0.2% Offset Shear Stress (MPa)	26.1
Shear Stress at 5% Strain (MPa)	37.7